

RAFAEL SILVERIO BARBOSA

Optimization of organic Rankine cycles for offshore waste heat recovery with improved efficiency and temperature control under dynamic conditions

São Paulo

2024



RAFAEL SILVERIO BARBOSA

Optimization of organic Rankine cycles for offshore waste heat recovery with improved efficiency and temperature control under dynamic conditions

VERSÃO CORRIGIDA

Thesis presented to the Postgraduate Program in Mechanical Engineering of the Polytechnic School of the University of São Paulo as part of the requisites required to obtain the title of Doctor of Science in Mechanical Engineering.

Supervisor: Prof. Dr. Jurandir Itizo Yanagihara.

São Paulo


2024

Autorizo a reprodução e divulgação total ou parcial deste trabalho, por qualquer meio convencional ou eletrônico, para fins de estudo e pesquisa, desde que citada a fonte.

Este exemplar foi revisado e corrigido em relação à versão original, sob responsabilidade única do autor e com a anuência de seu orientador.

São Paulo, 03\_de junho de 2024

Assinatura do autor:



Assinatura do orientador:



### Catálogo-na-publicação

Barbosa, Rafael

Optimization of organic Rankine cycles for offshore waste heat recovery with improved efficiency and temperature control under dynamic conditions /

R. Barbosa -- versão corr. -- São Paulo, 2024.

172 p.

Tese (Doutorado) - Escola Politécnica da Universidade de São Paulo.  
Departamento de Engenharia Mecânica.

1.ciclos de Rankine orgânicos 2.otimização 3.design 4.compressor 5.turbina a gás I.Universidade de São Paulo. Escola Politécnica. Departamento de Engenharia Mecânica II.t.

*To my daughter, Leticia. My light and my joy.*

## ACKNOWLEDGEMENTS

First and above all, I would like to thank God Almighty, who allowed me to get this far. My infinite gratitude also needs to be given to my parents, Ana and Umberto, whose support throughout my life, especially for my education, was relentless.

A special thanks must be given to Professor Jurandir Itizo Yanagihara, who provided me an enriching guidance and who was always available to share his wisdom.

I would like to thanks ANP/PRH for the scholarship granted.

Last but not least, I would like to thank USP/Poli/PPGEM for all opportunities and for the honor to be part of its graduate program.

“How much better to acquire wisdom than gold!  
To acquire understanding is more desirable than  
silver.”

Proverbs 16:16

## ABSTRACT

The Pre-salt contribution to oil production in Brazil makes this region and its assets strategic to the country. To achieve this production, FPSOs have been extensively used. However, current environmental goals to reduce greenhouse gas emissions present challenges for designing thermal systems on oil platforms. The low thermal efficiency of gas turbines and the significant amount of wasted heat in the processing plant systems must be addressed in the coming years. In this context, the application of organic Rankine cycles (ORC) on oil platforms has been studied. Given the characteristics of the power plant and processing systems onboard, the ORC design must consider both thermal aspects and operational conditions. This thesis presents an innovative ORC design methodology using the algorithm HORCAT, which combines Fuzzy Logic and particle swarm to maximize ORC electrical power output and minimize equipment volume. This method is employed in the ORC design to recover waste heat from the exhaust gas of a GE LM2500+ gas turbine, with a model developed and calibrated specifically for this application based on the performance of equipment operating in an FPSO in the Brazilian Pre-salt region. Additionally, a novel application of ORCs is proposed for temperature control at the discharge of large compression units. These applications consider steady-state, full-load conditions, as well as off-design and dynamic conditions. HORCAT's capability to handle complex objective functions was verified using test functions from the literature commonly used to assess multi-objective optimization algorithms. The results obtained were comparable or superior to those in the references. The computational model of the gas turbine simulated typical operational load demands observed in FPSOs, such as sudden load decreases and increases. Calibration against real-life operational data led to the development of a robust simulator for the GE LM2500+ used in FPSOs. For the recovery of gas turbine waste heat, HORCAT generated 16 designs evaluated under part load and dynamic conditions. The electrical power range at full load was from 489 kW to 1.97 MW. Under dynamic conditions, the number of feasible solutions decreased from 16 to 12, aligning with the power output response to the exhaust temperature of the gas turbine, controlled by a simple proportional mass flow rate regulator for the working fluid. For the compressor temperature control application, the innovative approach facilitated by HORCAT, along with dynamic conditions validation and an optimized PID controller, led to designs with significant power output and suitable volume for potential real-world implementation. The response of these designs under transient conditions was notable, with a 50% reduction in the number of valid designs during intense transient simulations. Applying PID controllers to manage transient



conditions revealed performance nuances, including minor overshoots in larger ORCs. This emphasized that steady-state conditions alone are inadequate for assessing equipment suitability. However, despite an efficiency drop from 18% at full load to 7% at minimum load, temperature control improved power generation.

Keywords: organic Rankine cycle, optimization, design, dynamic simulation, compressor, gas turbine

## RESUMO

A contribuição do Pré-Sal para a produção de petróleo no Brasil torna essa região e seus ativos estratégicos para o país. Para alcançar essa produção, FPSOs têm sido amplamente utilizados. No entanto, as metas de redução de emissões de gases de efeito estufa apresentam desafios para o design de sistemas térmicos. A baixa eficiência térmica das turbinas a gás e a significativa quantidade de calor desperdiçado na planta de processamento precisam ser abordadas nos próximos anos. Nesse contexto, a aplicação de ciclos orgânicos de Rankine (ORC) em plataformas tem sido estudada. Dadas as características dos módulos de potência e dos sistemas de processamento a bordo, o design do ORC deve considerar tanto os aspectos térmicos quanto operacionais. Esta tese apresenta uma metodologia inovadora de design de ORC utilizando o algoritmo HORCAT, que combina Lógica Fuzzy e enxame de partículas para maximizar a produção de energia elétrica do ORC e minimizar o volume dos equipamentos. Este método é aplicado para a recuperação de calor da exaustão de uma turbina a gás GE LM2500+, com um modelo computacional calibrado especificamente para esta aplicação com base no desempenho de equipamentos operando no Pré-Sal. Adicionalmente, uma aplicação inovadora de ORCs é proposta para o controle de temperatura na descarga de módulos de compressão. Regime permanente, condições fora do ponto de projeto e dinâmicas são aplicadas. Funções objetivo complexas, tipicamente usadas na literatura para teste de algoritmos de otimização multiobjetivo foram utilizadas para a avaliação do HORCAT, com resultados comparáveis ou superiores aos das referências. O modelo da turbina a gás simulou demandas típicas observadas em FPSOs, como tomadas e rejeições de carga. A calibração contra dados operacionais reais levou ao desenvolvimento de um simulador robusto para a GE LM2500+. Para a recuperação do calor residual da turbina a gás, o HORCAT gerou 16 designs, avaliados sob condições de carga parcial e dinâmica. A faixa de potência elétrica variou de 489 kW a 1,97 MW. Em condições dinâmicas, o número de soluções viáveis diminuiu de 16 para 12, alinhando-se com a resposta de potência à temperatura de exaustão da turbina a gás, que utilizou um controlador proporcional simples de vazão mássica para o fluido de trabalho. Para a aplicação de controle de temperatura do compressor, a abordagem inovadora viabilizada pelo HORCAT, juntamente com a avaliação das condições dinâmicas e de um controlador PID otimizado, levou a designs com significativa produção de energia e com volume adequado para potencial implementação no mundo real. A resposta desses designs em condições transitórias levou a uma redução de 50% no número de designs válidos durante simulações transitórias. A aplicação de controladores PID para gerenciar condições transitórias revelou nuances de

desempenho, incluindo pequenos sobre-sinais em ORCs de maior volume. Isso enfatizou que condições de regime permanente, por si só, são inadequadas para avaliar este tipo de aplicação. No entanto, apesar de uma queda de eficiência de 18% em carga total para 7% em carga mínima, o controle de temperatura incrementou a geração de energia.

Palavras-chave: ciclos de Rankine orgânicos, otimização, design, simulação dinâmica, compressor, turbina a gás.

## LIST OF FIGURES

Figure 1 – Brazilian offshore oil and gas production.....	23
Figure 2 – Brazilian primary energy production.....	24
Figure 3 - Heat recovery system layout. ....	28
Figure 4 - Net power output as function of heat transfer area for the different working fluids. ....	29
Figure 5 - Compressor share of total power consumption versus FPSO gas-load.....	33
Figure 6 - Combined cycle layout including the Siemens SGT-500 twin spool gas turbine, the intermediate loop, and the organic Rankine cycle. ....	35
Figure 7 - Structure of the multi-objective optimization algorithm. ....	36
Figure 8 - Pareto fronts obtained for the ORC designs.....	37
Figure 9 - Architecture of the DYNDES design tool. ....	39
Figure 10 - Pareto fronts of the three waste heat recovery technologies. CO <sub>2</sub> emissions and net present value are presented as concurrent objective functions for the three waste heat recovery options. ....	40
Figure 11 - Object diagram of the entire combined cycle system. It can be noted the temperature control adopted for the steam turbine regulating valve.....	44
Figure 12 - (a) Multi-objective optimization results, Pareto front showing the relation between the objective functions - ORC system net power and the volume of the heat transfer equipment. (b) Results of the dynamic test, the light gray line represents the load variation. ....	45
Figure 13 - Overall optimization results per ORC proposed.....	46
Figure 14 – Overview of the multi-objective optimization algorithm. ....	47
Figure 15 – Pareto front for the steady-state optimization scenario.....	48
Figure 16 – Petrobras 74 FPSO.....	51
Figure 17 – An overview on the topside modules and its main functions. ....	53
Figure 18 – HISEP: the subsea separation technology to be applied in the exploration of a reservoir in Brazil (Mero) with a high-CO <sub>2</sub> content produced fluid.....	54
Figure 19 – Gas processing plant modules. Colors indicate the fluid being processed: purple - crude; yellow – gases; red – CO <sub>2</sub> rich gas.....	55
Figure 20 – The basic components of the gas compression system. ....	56
Figure 21 – The Siemens SGT-A35 (former Rolls-Royce RB211) gas turbine and its offshore container.....	57
Figure 22 – Power consumption time series of an oil platform located in the North Sea. ....	58
Figure 23 – T-s plot of typically used organic fluids and water.....	59
Figure 24 – Flow diagram for a typical real-life ORC.....	60
Figure 25 – ORC equipment from Turboden. Plants from this company generates up to 10 MW in WHR applications. ....	61
Figure 26 – Temperature limits of the organic fluids commonly used in commercial projects.....	61
Figure 27 – Modeling and development flowchart applied to thermal systems simulation and ORC design. The steps here presented are not necessarily performed in sequence and the process admits an iterative development. ....	65
Figure 28 – The compressor map and beta lines tabulating method. ....	66
Figure 29 – Beta lines plot over a mass flow rate map. ....	67
Figure 30 – Effect on the compressor map caused by the geometry change in the IGV (a) and the working line caused by the air bleeding (b). ....	68
Figure 31 – The turbine map.....	69
Figure 32 – The GE LM2500 cut view. ....	71

Figure 33 – LM2500+ components coupling model. The streams codes and the components names are the same used throughout the equations.....	72
Figure 34 – LM2500+ compressor maps ( $N = N1T1N1DPT1DP$ ).....	73
Figure 35 – The control feedback defined for the gas turbine simulation. The output signal $w(t)$ is the calculated load, which is compared with the setpoint $r(t)$ . ....	78
Figure 36 - Compressor characteristics used for the simulation LM 2500+. ....	80
Figure 37 - Computational model of the gas turbine - view on the workflow for each timestep. In some cases, the block modules comprise the naming component and other minor components, e.g., Splitter 1 and the Plenum 1 are included in the Compressor Block; Plenum 2 and Mixer 2 are included in the CT block.....	82
Figure 38 - Load maneuver from 100% to 90% load. The steady-state results at 90% load are taken in $t = 2$ s.....	83
Figure 39 – Multi-component model of the ORC evaporator. ....	85
Figure 40 - Model of the heat exchanger in a modular and causal approach. This technique improves the reusability and reconfiguration, but the mathematical model imposes an extra simplification to allow simultaneous solution of the DAE system.....	86
Figure 41 - ORC equipment arrangement for gas turbine waste heat recovery. ....	89
Figure 42 - ORC arrangement proposed for the heat recovery and temperature control of the compression train. ....	90
Figure 43 - Mass flow control at the steam turbine inlet, defined as a function of the gas turbine exhaust temperature. ....	95
Figure 44 - Process and instrumentation diagram for the heat exchanger - hot stream temperature control. ....	96
Figure 45 – Conjugate gradient convergence tracking.....	99
Figure 46 – BFGS convergence tracking. ....	100
Figure 47 – Nelder-Mead simplex convergence tracking. ....	101
Figure 48 – Powell’s method convergence tracking. ....	102
Figure 49 – Search representation in terms of vector composition per iteration.....	103
Figure 50 – The particle swarm convergence tracking for the reference function. Here it is presented the best element found ( $\pi G$ ) in each iteration. The search was conducted by using the Python pyswarm library. ....	104
Figure 51 – Map of the optimization applications in this thesis.....	105
Figure 52 - General process of design, optimization, and evaluating the ORC design.....	107
Figure 53 - Optimization process implemented in HORCAT.....	110
Figure 54 - Generic representation of a Fuzzy System. ....	113
Figure 55 - Decision-making process during HORCAT search.....	114
Figure 56 - Dynamic load maneuver used to evaluate the ORC designs. ....	115
Figure 57 – Process implemented for the evaluation of ORC designs generated for the waste heat recovery from the gas turbine exhaust. ....	116
Figure 58 – Compressor data used for the calibration of the PID parameters. ....	117
Figure 59 – Compressor data used for the validation of the PID parameters.....	118
Figure 60 – Compressor dataset used for the simulation of the ORC for temperature control. ....	120
Figure 61 – Optimization process applied to the calibration of PID parameters. ....	121
Figure 62 – First subsystem of the calibration algorithm, where the Ziegler-Nichols parameters are optimized for each ORC design. ....	122
Figure 63 – Second subsystem, where the validation and intense transient simulation are performed for each ORC design.....	123

Figure 64 – Selected dry air conditions for the verification of the thermodynamic properties methodology.....	124
Figure 65 – Verification of the thermodynamic properties calculation – deviation between the calculated values and the reference. ....	125
Figure 66 - Modelica model, which employs the Thermopower library. This model is used as a reference for the verification of the combustor model implemented for the simulation of the GE LM2500+.....	126
Figure 67 - Normalized air pressure and temperature selected for the verification. ....	126
Figure 68 - Comparison between the combustor exhaust temperature calculated through a Modelica/Thermopower model and the model presented in Section 4.2.5. ....	127
Figure 69 - Results for the compressor outlet pressure at the selected loads. ....	127
Figure 70 - Results for the compressor outlet temperature at the selected loads. ....	128
Figure 71 - Results for the gas generator shaft speed at the selected loads.....	128
Figure 72 - Results for the gas generator outlet temperature at the selected loads. ....	129
Figure 73 - Results for the gas generator outlet temperature at the selected loads. ....	130
Figure 74 – Deviation between the simulated and reference values. ....	131
Figure 75 - Dynamic response to a load increase, from load = 0.4 to 0.79.....	132
Figure 76 - Dynamic response to a load decrease, from load = 0.79 to 0.47. ....	132
Figure 77 – Results of the dynamic simulation of the critical performance parameters under typical operational demand. The results are normalized for all parameters.....	133
Figure 78 – Pareto fronts for the minimization of functions F1 and F2 (Binh & Korn). ....	137
Figure 79 – Pareto fronts for the minimization of functions F1 and F2 (ZDT $\tau_1$ ).....	137
Figure 80 – Pareto fronts for the minimization of functions F1 and F2 (ZDT $\tau_3$ ).....	138
Figure 81 – Optimization results for the ORC design considering only the gas turbine at full load: scenario (A): after 3 iterations performed by HORCAT.....	139
Figure 82 – Optimization results for the ORC design considering only the gas turbine at full load: scenario (B): after 30 iterations performed by HORCAT.....	139
Figure 83 – Pareto fronts for the scenario (A) proposed designs under the gas turbine loads of 50%, 75% and 100%. ....	141
Figure 84 – Thermal efficiencies for each valid design under part load conditions - scenario (A). ...	142
Figure 85 – Pareto fronts for the scenario (B) proposed designs under the gas turbine loads of 50%, 75% and 100%. ....	143
Figure 86 – Thermal efficiencies for each valid design at part load conditions - scenario (B).....	143
Figure 87 – Transient response of the dynamic maneuver of the ORC, given the gas turbine. ....	144
Figure 88 – Optimization results for the ORC design for the heat recovery at the compressor discharge. ....	147
Figure 89 – ORC thermal efficiency for the design cases generated for the compressor waste heat recovery.....	148
Figure 90 – The outputs of the objective function defined for the PID calibration. The function gives the cumulative error of the difference between the setpoint and simulated discharge temperatures. .	149
Figure 91 – Case 1: transient response and temperature control results. ....	151
Figure 92 – Case 6: transient response and temperature control results. ....	152
Figure 93 – Case 8: transient response and temperature control results. ....	153
Figure 94 – Case 9: transient response and temperature control results. ....	154
Figure 95 – Case 11: transient response and temperature control results. ....	155
Figure 96 – Case 12: transient response and temperature control results. ....	156
Figure 97 – ORC normalized load as a result of the transient input from the compressor. In this chart, the load is normalized against the maximum output power observed during this specific maneuver. ....	157

Figure 98 – Controlled temperature at the discharge of the first stage of the compressor. ....	158
Figure 99 – Controlled temperature at the discharge of the second stage of the compressor. ....	158
Figure 100 – Pressure enthalpy diagram at design point – cases 10 (failed) and 11 (successful). The saturation lines of the working fluid (R123) are shown in blue. ....	159

## LISTA OF TABLES

Table 1 – Overview of the works on thermal efficiency and energetic optimization in offshore systems. .....	34
Table 2 – Summary of the works concerning the studies on ORC applied to waste heat recovery. ....	42
Table 3 – Summary of the works concerning the design of ORC through multi-objective optimization. .....	49
Table 4 – ORC power systems in operation and its main characteristics. ....	59
Table 5 – GE LM2500+ performance data at design point. ....	79
Table 6 – Natural gas composition used for the calculation of the properties of the compressor working fluid. ....	93
Table 7 – Organic fluids database used for the ORC optimization. ....	94
Table 8 – Compressor train design point parameters. ....	117
Table 9 – Parameters obtained for the gas turbine PID controller. ....	131
Table 10 – Test cases and references used for the verification of HORCAT. ....	134
Table 11 – Initial parameters of the PSO defined for each of the packs of HORCAT. ....	135
Table 12 – General configuration of the algorithm for the optimization defined for each test function. .....	136
Table 13 – Main thermodynamic parameters of the ORC design with the biggest power output – Scenario B. ....	144
Table 14 – Main thermodynamic parameters of the ORC design with the biggest power output – Compressor. ....	146
Table 15 – Results obtained for the PID parameters after the calibration. ....	149



## LIST OF ABBREVIATIONS AND ACRONYMS

<i>FPSO</i>	Float Production Storage and Offloading
<i>HORCAT</i>	Hunting ORCs with Asa-de-Telha
<i>IGV</i>	Inlet Guide Vanes
<i>ORC</i>	Organic Rankine Cycle
<i>PID</i>	Proportional Integral Derivative
<i>PSO</i>	Particle Swarm Optimization
<i>WHR</i>	Waste Heat Recovery
<i>WHRU</i>	Waste Heat Recovery Unit

## LIST OF SYMBOLS

### Lowercase

$a$	Ziegler-Nichols parameter
$a$	speed of sound (m/s)
$c$	particle swarm acceleration parameter
$ce$	cumulative error
$f$	generic function
$g$	generic function
$h$	specific enthalpy (J/kg)
$\hbar$	generic function
$k$	heat capacity ratio
$\dot{m}$	mass flow rate (kg/s)
$p$	pressure (Pa)
$r$	random number
$t$	time (s)
$u$	generic vector / specific internal energy(J/kg)
$v$	particle velocity / generic vector
$x$	generic variable
$y$	air ratio

### Uppercase

$A$	area (m <sup>2</sup> )
$C$	heat capacity (J/K)
$E$	Elite (Pareto front)
$ER$	expansion ratio
$FAR$	fuel to air ratio
$K$	control model constant
$LHV$	lower heating value (J/kg)
$\mathcal{L}$	heat exchanger tube length (m)

$M$	mass
$PR$	pressure ratio
$\dot{Q}$	heat transfer rate (W)
$T$	temperature (K)
$U$	global heat transfer coefficient (W/m <sup>2</sup> K)
$\mathcal{V}$	volume(m <sup>3</sup> )
$\dot{W}$	power (W)

### Greek symbols

$\alpha$	constant
$\beta$	constant
$\kappa$	control model constant (gain)
$\pi$	particle swarm pack best solution found
$\rho$	density (kg/m <sup>3</sup> )
$\nu$	controlled variable
$\Phi$	generic function
$\omega$	particle swarm inertia weight parameter

### Subscripts:

$A$	air
$C$	cold side
$d$	derivative
$DP$	design point
$F$	fuel
$G$	global
$H$	hot side
$i$	inlet / integral
$is$	isentropic conditions
$o$	outlet
$p$	proportional

*sp* setpoint  
*w* metal

Equipment:

*AMB* ambient  
*IN* inlet  
*C* compressor / condenser  
*CC* combustion chamber  
*CO* condenser  
*CT* combustion turbine  
*HX* heat exchanger  
*M* mixer  
*OUT* outlet  
*P* pump  
*PL* plenum  
*PT* power turbine  
*SP* splitter  
*ST* steam turbine

## CONTENTS

1.	INTRODUCTION .....	23
1.1	Motivation .....	23
1.2	Objectives .....	25
1.3	Manuscript Outline .....	25
2.	LITERATURE REVIEW .....	27
2.1	Thermal efficiency optimization at FPSOs .....	27
2.2	ORC for waste heat recovery .....	35
2.3	Design of ORCs through multi-objective optimization.....	43
2.4	Final remarks .....	50
3.	AN OVERVIEW ON FPSO PROCESSES AND ORC.....	51
3.1	Topside process plants.....	51
3.2	The gas compression modules.....	54
3.3	Power plant.....	56
3.4	Organic Rankine Cycles .....	58
4.	MODELING AND SIMULATION .....	63
4.1	Computational modeling of thermal systems .....	63
4.2	Gas turbine model.....	66
4.2.1	Overview and main techniques of modeling Brayton cycle-based plants .....	66
4.2.2	Mathematical model .....	70
4.2.3	Control system .....	77
4.2.4	LM2500+: performance data selection and constructive information.....	79
4.2.5	The gas turbine computational model.....	80
4.2.6	Calibration methodology applied to simulate the FPSO gas turbine.....	83
4.3	Modeling Organic Rankine cycles .....	84

4.3.1	Overview of techniques applied to modeling Rankine cycle-based plants.....	84
4.3.2	The ORC model .....	88
4.3.3	Fluid models .....	93
4.4	The ORC control model .....	94
4.4.1	Control method for the ORC used for waste heat recovery in the gas turbine exhaust	94
4.4.2	Temperature control at the compressor discharge .....	96
4.5	Optimization methods .....	97
4.6	Optimization applications throughout the thesis .....	104
5.	THE ORC DESIGN SYSTEM.....	106
5.1	The design process .....	106
5.2	The optimization algorithm: HORCAT.....	108
5.3	Decision-making during the optimization process .....	111
5.4	Demonstrating performance in real-world applications .....	114
5.4.1	Gas turbine loads and transient maneuver .....	114
5.4.2	The compressor dataset.....	116
6.	RESULTS .....	124
6.1	Gas turbine model – calibration, verification and validation .....	124
6.1.1	Thermodynamic properties – verification of the weighted calculation .....	124
6.1.2	Combustion chamber .....	125
6.1.3	Calibration at the design point and steady-state simulation .....	127
6.1.4	Control calibration and dynamic simulation.....	131
6.2	HORCAT verification .....	133
6.3	ORC design applied for gas turbine waste heat recovery.....	138
6.3.1	Gas turbine in steady state .....	138
6.3.2	Gas turbine dynamics.....	144
6.4	ORC design applied for the compressor train temperature control .....	146

6.4.1	Compressor at steady-state – ORC designs .....	146
6.4.2	Compressor dynamics .....	148
7.	CONCLUSION AND RECOMMENDATIONS .....	161
7.1	Conclusion .....	161
7.2	Recommendations for future works .....	162
	BIBLIOGRAPHY .....	164



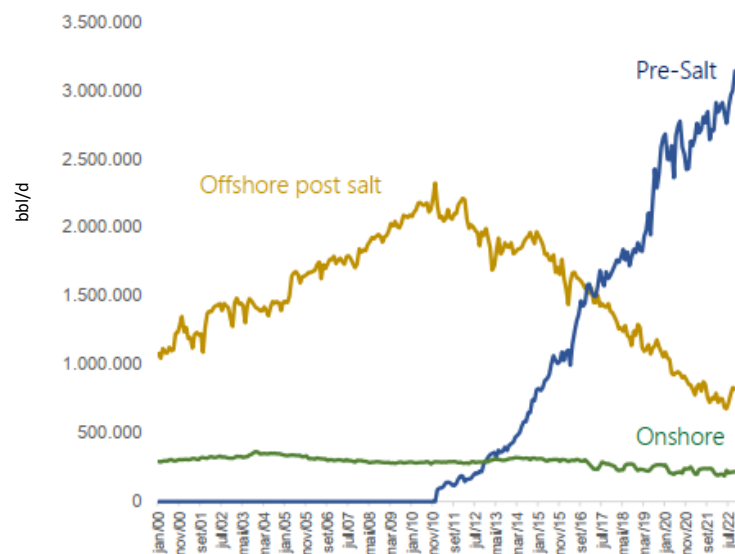


## 1. INTRODUCTION

### 1.1 Motivation

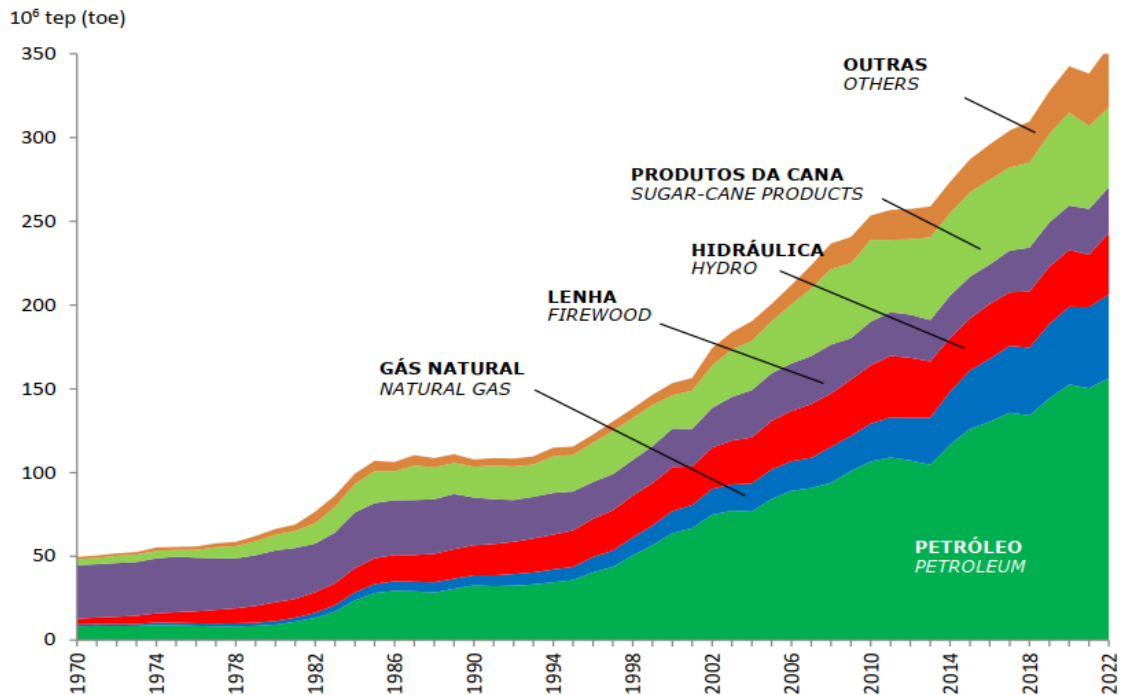
Brazilian Pre-salt has become in the recent years the main and most profitable crude oil source for the country and have recently achieved recently 76% of the national oil production (AGÊNCIA NACIONAL DO PETRÓLEO, 2023). This remarkable milestone became feasible as several challenges were overcome, including the distance between the platforms and the shore, the peculiar fluid composition, and the ultra-deepwater conditions (MORAIS, 2013). The importance of Pre-salt in the oil and gas production can be observed in Figure 1. Production in Pre-salt has been substantially increased and post-salt production is severely decreased throughout the years, while the overall oil and gas production is increasing, as Figure 2 shows.

Figure 1 – Brazilian offshore oil and gas production.



Source: Saboia (2023).

Figure 2 – Brazilian primary energy production.



Source: Empresa de Pesquisa Energética (2023).

In terms of fluid composition, particularly, the high concentration of CO<sub>2</sub>, H<sub>2</sub>S and other gases in the crude makes the FPSO process and power plants quite singular. The requirement of having all the CO<sub>2</sub> and eventually the produced natural gas reinjected demands a complex and highly power demanding gas compression system<sup>1</sup>, achieving up to 50% of the total power demand (ALLAHYARZADEH-BIDGOLI et al., 2018). Additionally, the presence of such contaminants in the gas injection stream may induce faults into the subsea and surface equipment. Stress corrosion cracking (SCC) for example, can be triggered by the gas in a specific thermodynamic state and into a certain temperature range, which may therefore reduce the useful life of equipment (SANDANA, 2016).

Furthermore, the typical operational conditions of the power module and the power demand strategy adopted onboard requires a large variation on the load supplied – which leads to a low thermal efficiency for the gas turbines (SVALHEIM, KING, 2003) (PIEROBON et al., 2014). Although this concern has been studied from a technical and economic perspective, today the solution to this problem has become mandatory, given its social and environmental impacts (INTERNATIONAL ENERGY AGENCY, 2021) (ALLAHYARZADEH-BIDGOLI,

<sup>1</sup> Throughout this manuscript, the term ‘system’ follows the definition given under the concept of Systems Engineering, i.e., a construct or collection of different elements that together produce results not obtainable by the elements alone (NATIONAL AERONAUTICS AND SPACE ADMINISTRATION, 2017).

YANAGIHARA, 2023). Even with such drawbacks, this condition also creates an opportunity for waste heat recovery.

Given this context, two opportunities become clear on the FPSO topside: (i) the need to increase the energy efficiency; and (ii) the improvement of the temperature control in the CO<sub>2</sub>-rich fluids to avoid catastrophic failure modes on the surface and subsea equipment. Both problems can be solved through the adoption of a single solution: organic Rankine cycles (ORCs). These systems can be used for a broad range of heat source temperatures and coupled to several types of topping equipment or plant (NONDY, GOGOI, 2021). Furthermore, its smaller footprint and high flexibility in terms of design and working fluids are consistent with the need to increase the efficiency and reduce the footprint of the power plant.

### *1.2 Objectives*

Considering the challenges in designing and applying ORC to real-life offshore conditions, this thesis presents a new ORC design methodology based on a multi-objective optimization performed by a fuzzy-PSO algorithm. Therefore, the objectives of the thesis are:

- (i) The development of an optimization algorithm, a tailor-made implementation specifically for the ORC design, harnessing the effectiveness of PSO in non-linear landscapes alongside the fuzzy logic systems capability to take decisions to improve the search performance during its execution.
- (ii) The design of ORCs for waste heat recovery from a GE LM2500+ gas turbine with the typical configuration found in Brazilian FPSOs. Furthermore, the analysis is made considering not only the gas turbine full load condition but also its part load and dynamic conditions.
- (iii) While recovering waste heat is valuable, this work goes further, showcasing the ORC capability to control compressor discharge temperatures, a crucial and novel application for ORCs in oil platform operations.

### *1.3 Manuscript Outline*

This thesis is structured into seven chapters, which are organized as follows.

- **Chapter 1:** introducing the context in which the thesis is motivated and its objectives.
- **Chapter 2:** presenting a global literature review on the subjects directly linked to the thesis development: the thermal efficiency optimization in FPSOs; the application of

ORCs for the heat recovery and power generation; and the design of these systems by using multi-objective optimization.

- **Chapter 3:** describing the two main energy processes and associated plants analyzed in this thesis: the FPSO topside plants and the ORC plant;
- **Chapter 4:** showing the foundations of the thermal systems modeling and optimization, including the mathematical models of the gas turbine and ORC related equipment.
- **Chapter 5:** depicting HORCAT, the multi-objective optimization algorithm developed for the ORC optimization.
- **Chapter 6:** presenting and discussing the results.
- **Chapter 7:** discussing the research conclusions.

## 2. LITERATURE REVIEW

### 2.1 *Thermal efficiency optimization at FPSOs*

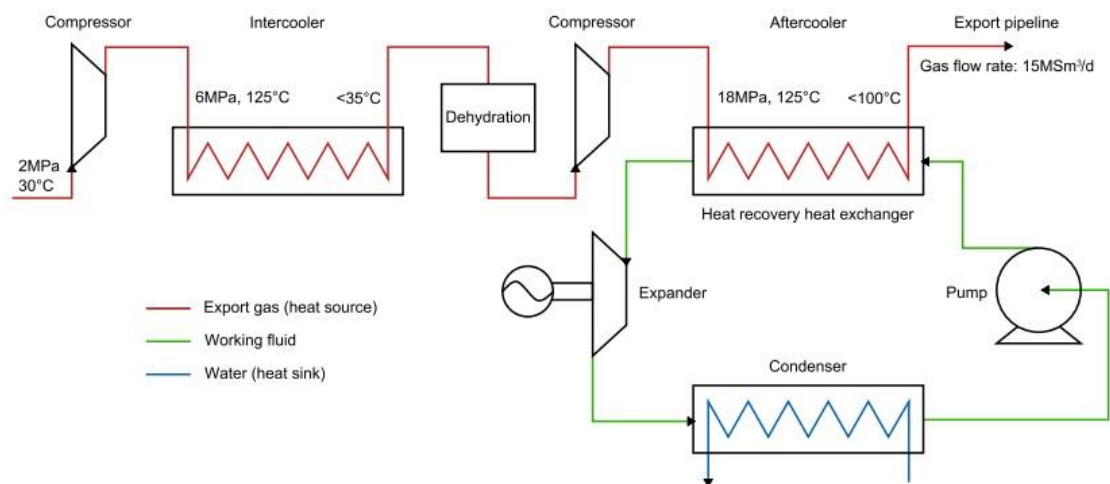
Environmental regulatory issues and cost concerns have led to several research works on the thermal efficiency analysis and improvement on oil platforms. Oliveira Junior and Van Hombeeck (1997) presents a detailed description of the process aboard an oil platform and performs an exergetic analysis of the plant. The plant simulations were performed, focused on the processes of separation, compression, and pumping, by using the software HYSIM and the thermodynamic properties of the fluids were calculated by applying the Peng-Robinson equation of state. The main findings of this analysis are: the largest exergy consumers of the plant are heating and compression; the separation module (then furnace-based) had the lowest exergetic efficiency of the plant; and the low exergetic efficiency (below 30%) of the internal combustion engine has a great contribution to the overall plant exergetic efficiency of the plant (9.7%).

The work of Svalheim and King (2003) presents a study on the energy performance of three oil platforms from BP operating ant the Norwegian Continental Shelf. The authors present an in-house developed tool to calculate the energy performance over the field life and to identify the optimal energetic condition. Additionally, an energy metric is proposed by the calculation of the ratio between the energy consumed and the oil and gas exported, both measured in barrels of oil equivalent. The tool identified the key consumption processes and the design parameters that influence the energy consumption. Furthermore, a dedicated model (Best in Class, BiC) is presented, which defines the optimal power consumption. It was observed that in a production facility where water injection is used instead of gas injection, which would supposedly lead to a lower power consumption, the energy efficiency is lower than expected, with an energy performance 33% higher than the BiC. This is explained as a result of the need to offload oil production and, to cope with this, gas turbines operate at full load only during this operation, leading to low performance of this equipment in the most part of the operating time. In addition to this, the pumps and compressors operate at fixed speed, which does not allow the most efficient power control. However, for another platform, even with the gas injection recovery strategy, the energy performance was only of 5% above BiC. This was observed because gas turbines operate near the base load and pumps and compressors are quite fit to the load demanded throughout the field lifecycle. The author also highlighted that facilities without gas turbines mechanically driving the compressor and pumps and operating with electric motors

have the best energy performance. As general aspects that justify the good performance of the facilities, it can be listed: no flaring allowed; the use of a combined cycle power plant and the use of high-performance gas turbines such as the GE LM2500.

Rohde et al. (2013) identify in their work that the huge amount of heat wasted in the compressor intercoolers in the export gas system has a potential to be recovered and presents alternatives to generate more power aboard, improve the energy efficiency and reduce CO<sub>2</sub> emissions. With this objective in mind, it is proposed the use of a Rankine cycle instead of regular intercooling heat exchangers, as Figure 3 shows.

Figure 3 - Heat recovery system layout.

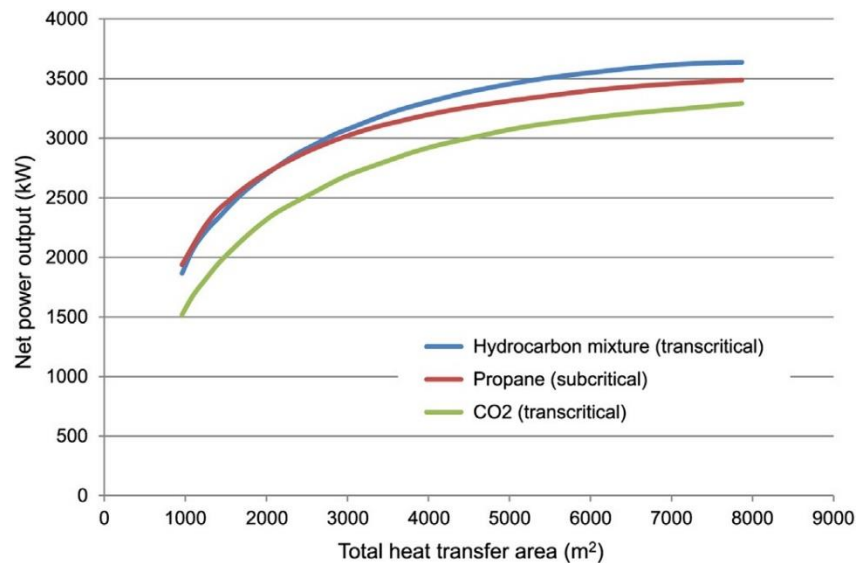


Source: Rohde et al. (2013).

A computational program for thermal calculations, implemented in MS Excel/VBA, and the thermodynamic properties were obtained through REFPROP. The modeling focus was given to the heat exchangers implemented for the heat recovery and the condensers. Given a detailed geometry input, the model calculates other design parameters, such as hydraulic diameter, perimeter, and cross-sectional area. After that, the fluid outlet conditions are calculated through integration of the fluid passes and iteration on the wall temperature profile. A real-life case was selected for the application of the methodology, and three working fluids were considered for the Rankine cycle and consequent heat exchanger design: (i) a hydrocarbon mixture - propane and ethane at transcritical conditions (60/ 40% mole fraction, respectively); (ii) propane at subcritical conditions; and (iii) CO<sub>2</sub> at transcritical conditions. These fluids were selected because they are already processed in the plant and therefore no additional safety measures would be needed for the adoption of these substances as working fluids. Figure 4

presents the results of the Rankine cycle power generation versus the total heat transfer area per type of working fluid. The maximum power generation is above 3.5 MW for the hydrocarbon mixture. Two relevant aspects are highlighted as the conclusion: (i) the need of proper optimization of the plant size and (ii) the need to include the transient behavior in the analysis to have a robust and reliable solution.

Figure 4 - Net power output as function of heat transfer area for the different working fluids.



Source: Rohde et al. (2013).

An exergetic and thermodynamic assessment of oil platforms in the North Sea is presented by Nguyen et al. (2013). The work was developed accordingly to three main steps: validation of a generic model of an oil platform; simulation of cases typically found in real life; exergetic and energetic analyses. The crude oil was considered a mixture of 83 chemical compounds and the composition of the cases studied was defined accordingly with the reservoir to be analyzed. The modeling and simulation were carried out using the software Aspen Plus, except for the power plant, which was simulated using the software DNA (Dynamic Network Analysis), developed at the Technical University of Denmark. It was identified that the compressor train is the major electricity consumer, demanding up to 56% of the produced power. The water injection pumping system also represents the top consumer with a demand of 23%. Concerning exergy analysis, the total exergy destruction in the processing plant can reach up to 32 MW. However, the greatest exergy destruction occurs in the gas turbines combustion chambers, reaching up to 50% of the overall exergy destruction in the platform. The crude composition has a major impact in the energetic and exergetic performance, and, therefore, it

is mandatory to take the composition into consideration when comparing processing plants located in different offshore producing regions of the world, such as North Sea, Gulf of Mexico and Brazilian basins. As recommendations arising from the study, as options to increase the plant performance, it is suggested the adoption of a bottoming cycle to be used with gas turbines; the proper selection of gas turbines with a focus on energy performance can also lead to a better exergetic efficiency.

Nguyen et al. (2016) presented a work in which seven technologies were evaluated to be applied to improve thermal efficiency in offshore plants: (i) the installation of multiple pressure levels in production manifolds; (ii) implementation of multiphase expanders instead of expansion valves; (iii) limitation of gas recirculation for anti-surge control in compressors; (iv) promotion of energy and process integration; (v) heat recovery from low-temperature sources in the gas cooling system; (vi) downsizing or replacement of the existing gas turbines; and (vii) waste heat recovery from the power plant. With this aim, four platforms then operating in the North and Norwegian Seas were evaluated. Different strategies are suggested to improve the energy performance of oil and gas facilities, but it can be summarized into two categories: to reduce the energy demand of the processing plant, by increasing the efficiency of the most energy intensive processes, and redesigning the power generation systems, e.g., replacing the existing gas turbines, improving the cogeneration, and importing electricity. All analyzes were performed by using the software Aspen Plus to simulate the systems of interest and evaluate its energetic behavior.

Concerning (i) the installation of multiple pressure levels in production manifolds, the proposal is to add a high-pressure stage at the production manifold to allow the gas processing in higher pressures, reducing the power demanded by the compressor trains. It is proposed a multi-objective optimization through genetic algorithms having as objectives the minimization of the total power consumption and the maximization of the oil and gas recoveries. The decision variables are the pressure values at each level of the production manifolds. The results lead to a maximum reduction of 17 MW in compressor power consumption, still maintaining a high recovery of crude oil.

If (ii) the multiphase expanders are replaced by expansion valves, the aim is to recover power from the high-energy content crude streams by using two-phase helico-axial expanders, which have expansion efficiencies in the range 30 – 70% and can boost the power production in the platform. However, the authors list a series of challenges that may limit the employment of this technology, such as the fluid flow rate variation during the field lifetime and the associated impurities and contaminants.



The option of (iii) reducing the anti-surge circulation in compressors aims to minimize the power and cooling demands due to the anti-surge system in the compressors. The given proposal is to replace the current compressor operating at high efficiencies only at design point conditions for a train of smaller ones that can withstand high efficiencies at partial loads and eliminate the anti-surge control. The results show a maximum reduction of 20 % in compressor power demand.

The alternative (iv) energy integration is the optimization of the natural 'cold' and 'hot' streams mixing to explore possibilities for cogeneration and to minimize the demand of external cooling and heating and the associated power consumption. A pinch analysis was performed on each system of interest and it showed that the heating demand is much smaller than the cooling demand. The main conclusion is that the feasibility of such a technological alternative is low due to operational and layout reasons.

The (v) waste heat recovery in the process plant is evaluated considering the addition of organic and steam Rankine bottoming cycles, both to be applied to the compressor intercoolers. It is identified a potential harvest of 3.5 MW in electrical power. However, it is also highlighted the need for a detailed design and robust control system, given the challenging off-design conditions during regular operation.

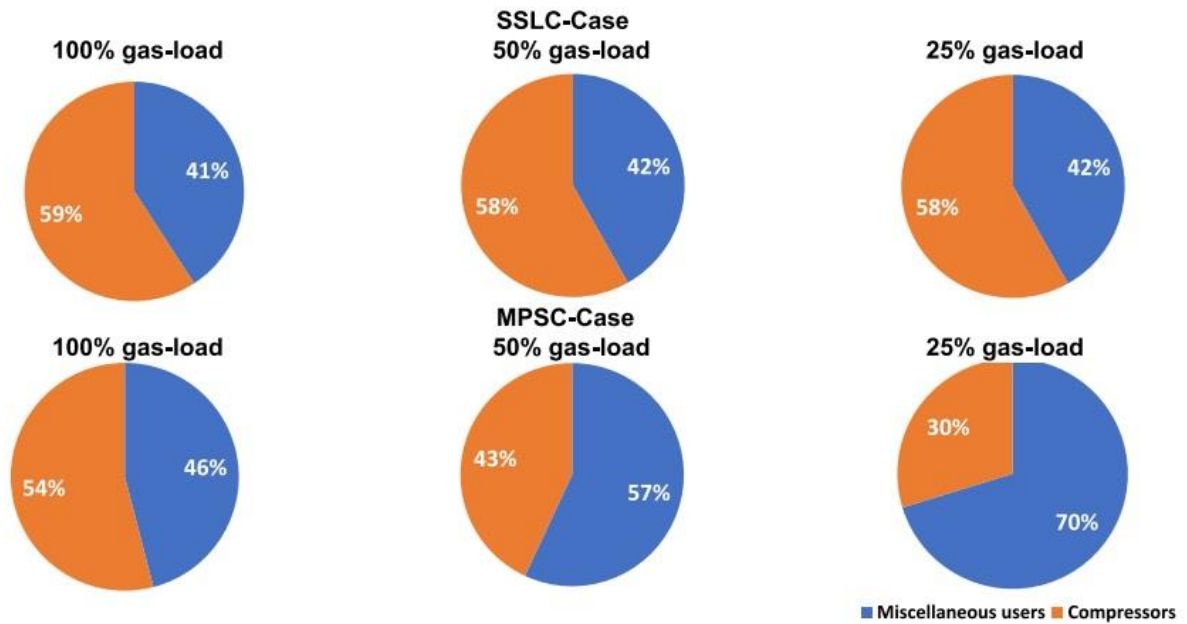
Regarding the downsizing of the gas turbines (vi), since this equipment operates far from its optimal point for a long period of the field lifetime, operating in a load range of 60-70%, some alternatives to improve the overall thermal efficiency are suggested: the change of the engines by smaller ones to be turned on and off accordingly with the power demand but always operating near the full power conditions; the removal of one the gas turbines and the addition of a bottoming cycle; and downsize the gas turbines and add a bottoming cycle. Only the first option is detailed and it seems to be feasible in a thermodynamic, economic and environmental perspective - the energy savings result in greater gas production and smaller CO<sub>2</sub> emissions.

Finally, study (vii) on the waste heat recovery from the power plant using steam Rankine cycles and defining a combined cycle returns the best thermal efficiency amongst all alternatives, although its implementation is difficult due to lack of space aboard and due to the fit of the fluid and heat streams in the facility. This approach is particularly interesting when the platform is equipped with larger gas turbines, such as the LM2500, which provide higher mass flow rates and temperatures in its exhaust. In one of the evaluated platforms, the steam cycle would lead to an increase of 4.5 MW for each gas turbine, and also increasing the average thermal efficiency from 23 to 32%.

A complete exergetic analysis of the process and power plant of an FPSO at the Pre-salt was carried out by Allahyarzadeh-Bidgoli et al. (2018), with the aim of applying a multi-objective optimization to define the best operating conditions by minimizing total fuel consumption without adding any new technology or equipment. The design variables defined for the optimization are: the discharge pressure of the first stage of separation, discharge pressure on the first heat exchanger; discharge pressure of the second heat exchanger; discharge pressure of the first separator of the second stage of the separation train; discharge pressure of the second stage of the separation train; discharge pressure of the third stage of the separation train and discharge pressure of the main compressor. Specifically for the power plant, a GateCycle model to simulate the Rolls-Royce RB211G62 gas turbine, and, for the process plant, Aspen HYSYS was used. The optimization method is carried out by coupling the models to a genetic algorithm (in the platform modeFRONTIER) and performing steady-state simulations so that the objective function could return the value of the total fuel consumption, given the above-mentioned design parameters as inputs. The then current FPSO operational scenario was used as the baseline for the analysis and reference to compare the results. The optimization led to a reduction of the fuel consumption of 4.6% and a decrease in power demand of 6.3%, when compared with a baseline case, resulting in a decrease in CO<sub>2</sub> emissions.

Cruz, Araujo and de Medeiros (2020) addresses the problem of the low thermal and exergetic efficiencies at FPSOs by revisiting the compressor train arrangements. Though the research focus is given over the compressors systems, the waste of heat at the gas turbine exhaust is also analyzed. At the base case evaluated, 21% of the available exergy is lost due to the absence of further heat recovery – even considering the use of WHRU. The problem in the single-shaft large centrifugal compressors (SSLC) – used in the studied oil platform - consists in the anti-surge recycles at lower loads, therefore its performance is compared with a Multiple-Paralleled Smaller Compressors (MPSC) arrangement with respect to the following indicators: (i) exergy efficiency; (ii) power demand, fuel consumption and CO<sub>2</sub> emissions per equivalent oil barrel produced; and (iii) FCI/footprint. The comparison was carried out by considering two reference environment and three load conditions: 25, 50 and 100 %, which are representative of the typical Pre-salt FPSO operating loads in a total of six simulation cases. MPSC were simulated at Aspen HYSYS by replacing SSLC compressors by sets of smaller compressors with no anti-surge control, aiming to mitigate exergy destruction. A summary of the impact of the compressor scheme changing is given in Figure 5. A significant impact on power consumption can be noted, mainly at lower loads, where the anti-surge recycles is activated.

Figure 5 - Compressor share of total power consumption versus FPSO gas-load.



Source: Cruz, Araujo and de Medeiros (2020).

The work of Pereira and Yanagihara (2022) aims to optimize the main processing units of a typical FPSO operating in the Brazilian Pre-salt with a high CO<sub>2</sub> content and reduce its dry weight and footprint. Sensitivity analysis is applied with the focus on the processing plant. The analysis is made by integrating machine learning with optimization, where the simulation models were developed in MATLAB. The use of commercial software is discarded for this case since these suites do not contain models for all equipment in the FPSO and the interface between the commercial simulation system with the optimization is not trivial. Therefore, a superstructure optimization is applied with three flowsheets generated. The results show that there is a variation in the power demand of 31%, considering the worst and the best cases.

Table 1 presents a summary of recent work on thermal efficiency in offshore systems.

Table 1 – Overview of the works on thermal efficiency and energetic optimization in offshore systems.

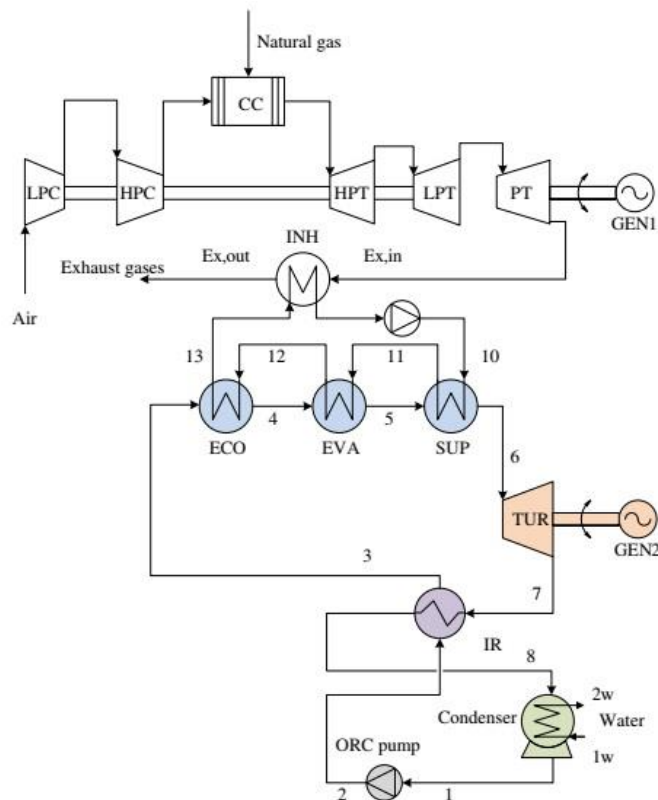
<b>AUTHOR</b>	<b>YEAR</b>	<b>MAIN SUBJECT</b>	<b>RELEVANT ADVANCES</b>
Nguyen et al.	2013	Thermal efficiency at FPSOs	Proper selection of gas turbines and the use of bottoming cycles can improve overall exergetic efficiency.
Nguyen et al.	2016	Energetic optimization at FPSOs	ORCs are feasible for WHR, but more research needs to be applied on their control strategy. The use of genetic algorithms for the multi-objective optimization leads to efficiency improvement and reduction on the fuel consumption.
Allahyarzadeh-Bidgoli et al.	2018	Energetic optimization at FPSOs	

Source: Author.

## 2.2 ORC for waste heat recovery

The application of ORCs for waste heat recovery in oil platforms has been the subject of some relevant scientific works. In particular, a research group from the Technical University of Denmark, Delft University of Technology and Politecnico di Milano has been publishing some relevant works concerning the main target of this thesis. Pierobon et al. (2013) evaluated ORCs for heat recovery at the Siemens SGT-500 exhaust, in a platform operating in the North Sea. A multi-objective optimization methodology was developed which has as objective functions the thermal efficiency, the total volume of the ORC, and the net present value. The work gives a major focus on the shell and tube heat exchanger geometry, calculating the detailed dimensioning, and considering both the heat transfer coefficients and the pressure drops on the shell and tube sides. The layout shown in Figure 6 is applied for modeling and simulation at steady-state conditions. An intermediate fluid is used for the exhaust gases of the heat exchange between the gas turbine and the organic fluid. Dowtherm Q is selected as an intermediate heat carrier.

Figure 6 - Combined cycle layout including the Siemens SGT-500 twin spool gas turbine, the intermediate loop, and the organic Rankine cycle.

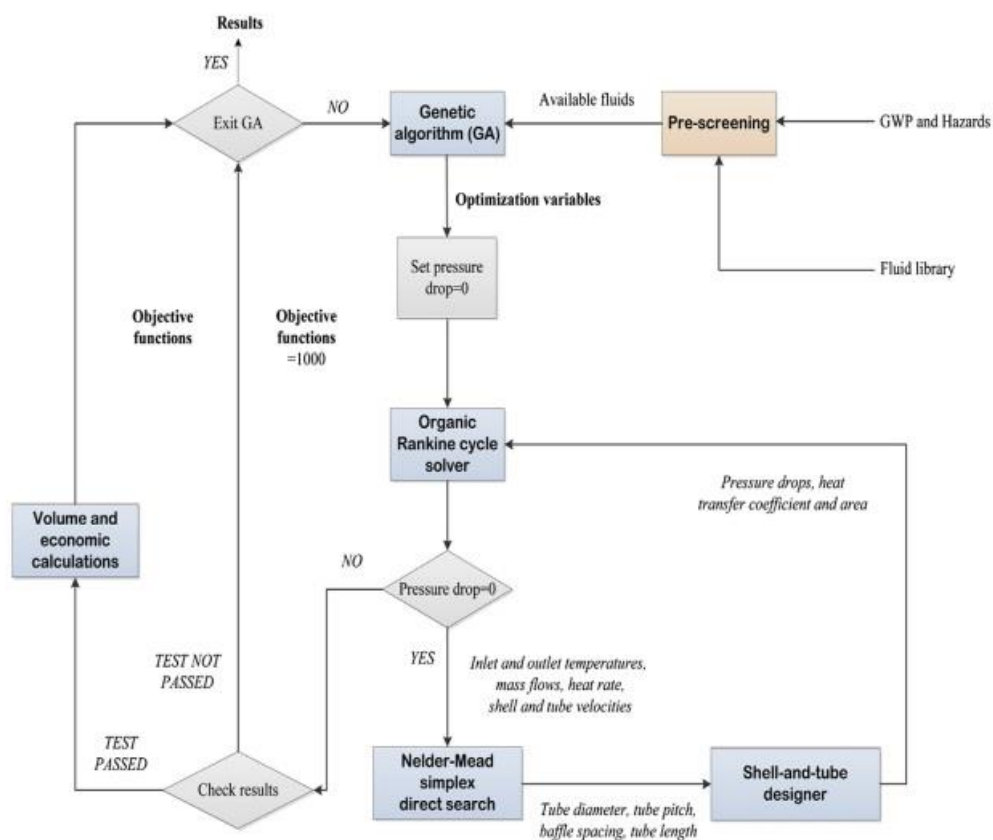


Source: Pierobon et al. (2013).

Concerning the computational program, it was developed in MATLAB and the thermodynamic properties were calculated using REFPROP. Genetic algorithms were used for optimization to avoid the calculation of derivatives and enhance the probability of finding the global optima. The structure of the program is shown in Figure 7 and the design variables are:

- ORC working fluid – 109 options considered.
- Condenser outlet temperature.
- Condenser pinch point (located in the saturated vapor state).
- Internal recuperator pinch point.
- Minimum temperature difference (pinch point) in the economizer or vaporizer.
- Turbine inlet pressure.
- Superheating temperature difference.
- Target velocities in the tubes and on the shell side for each heat exchanger.

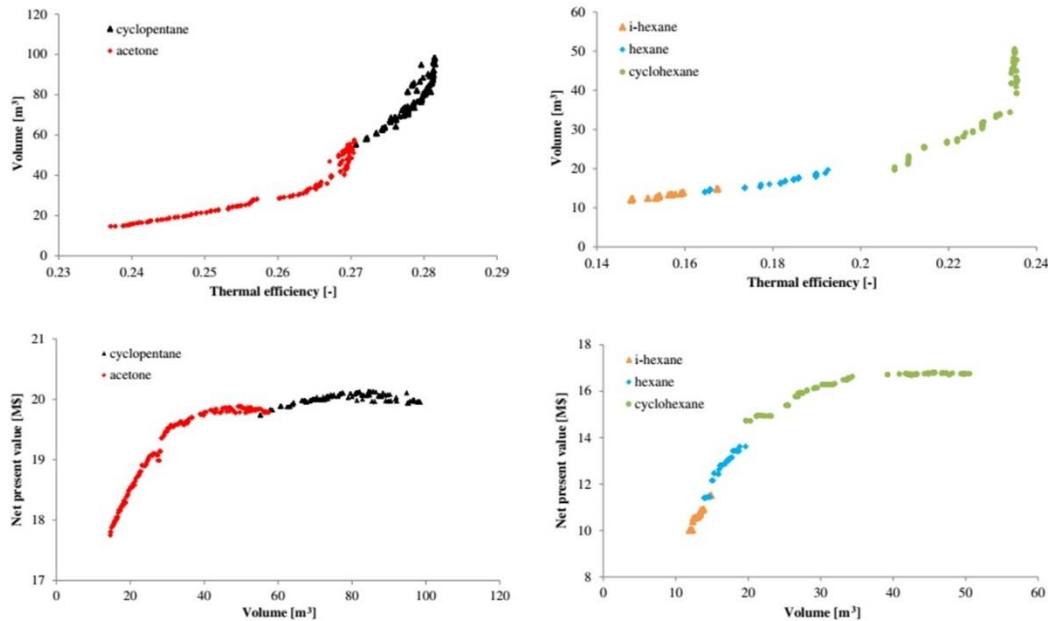
Figure 7 - Structure of the multi-objective optimization algorithm.



Source: Pierobon et al. (2013).

The results are given through a three-dimensional Pareto front composed of 350 points. The results show that, in general, cyclopentane leads to the highest efficiency, but at the cost of higher total volumes and investment. However, in terms of the net present value, cyclopentane is the best choice. The results are summarized in Figure 8.

Figure 8 - Pareto fronts obtained for the ORC designs.



Source: Pierobon et al. (2013).

Pierobon et al. (2014) applied a multi-objective optimization to evaluate three different heat recovery technologies to be implemented at the gas turbine exhaust - in that case, also the Siemens SGT-500 – then operating on an oil platform in the Norwegian Sea. The technologies to be compared were the ORC, the steam Rankine cycle, and the closed-loop air Brayton cycle. The objective functions to be used in the optimization are the average daily CO<sub>2</sub> emissions, the overall plant weight, and the economic revenue. The platform strategy for power supply considers that the full load is shared between two gas turbines, the third is kept in standby or is enrolled into maintenance procedures. In this way, the engines run at low loads - a maximum of 50% - in order to decrease the risk of failure of the system and ensure a power reserve and the safe operation of the engines. On the other hand, this approach led to low thermal performance and a huge amount of heat being wasted in the turbine exhaust. Therefore, the assumption of the need of a heat recovery system is valid, considering its compactness, weight, and reliability. All the equipment operating in the proposed cycles are modeled with emphasis given to the heat exchanger design, and the geometric quantities (e.g. tube length and tube

diameter) are included among the optimization design variables. This design follows the steps defined in standardized procedures to define the overall heat transfer area by iteratively calculating the overall heat transfer coefficient, and this approach is applied for all the heat exchangers considered in each of the three solutions.

For the steam Rankine cycle and the ORC, it is considered a once-through boiler with finned tubes. The pressure drop is considered to happen at the heat exchanger inlet and is split into three components, a static, kinematic, and a contribution of the viscous friction. For the same technologies, the condenser and the recuperator are considered shell-and-tube heat exchangers. The latter is also designed with finned tubes to enhance the heat transfer coefficient on the shell side (superheated steam). The gas turbine models were developed by using interpolating functions applied over the data provided by the manufacturer of the operation range from 10 to 100 % load. For the modeling of the compressor, the characteristics maps are taken from a commercial software, containing tables presenting the values of the corrected mass flow rate, pressure ratio, isentropic efficiency, and shaft speed. The equipment does not have IGVs, so the only control applied is over the fuel flow, with a direct impact on the exhaust temperature. The turbine is considered to follow the Stodola cone law, which means that the pressure ratio is a function of the inlet mass flow rate and temperature. This model is applied to gas turbines and also to those used for the Rankine cycles.

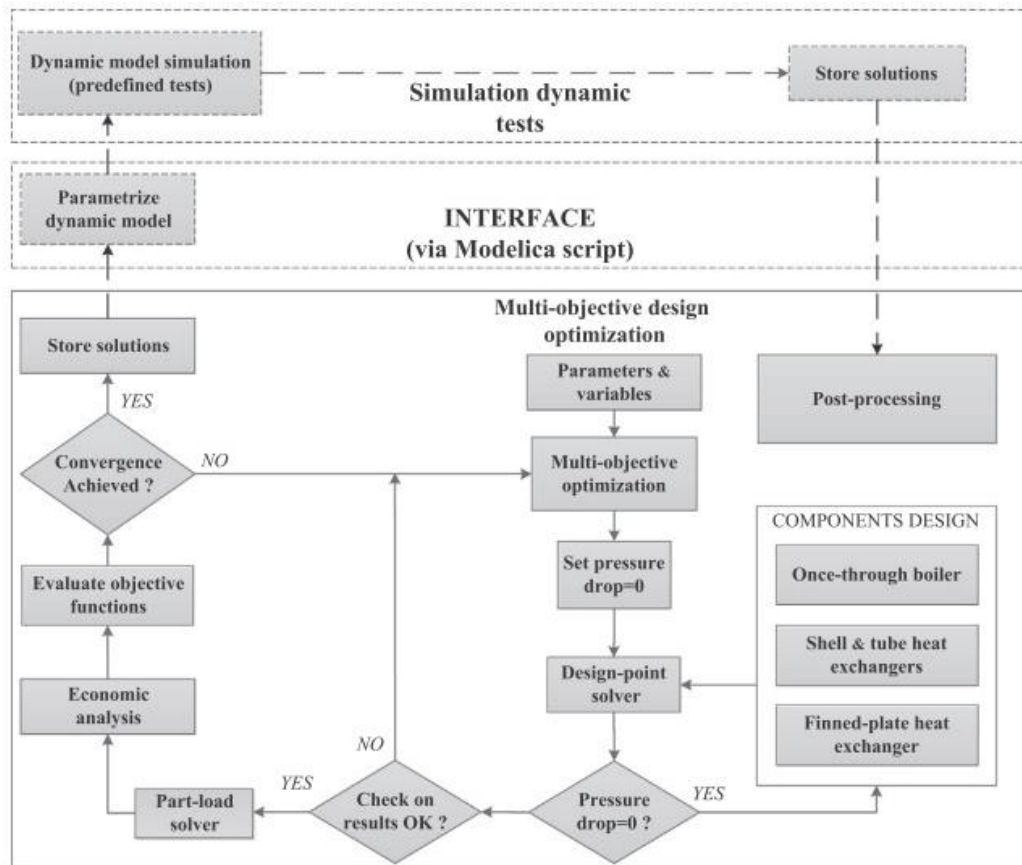
The simulation allows analysis of the steady state and part load performance. Furthermore, some other important premises and methodologies applied for the modeling, simulation and optimization:

- The ORC and steam Rankine operate in a similar range of power.
- Only steady-state simulations are performed.
- Fluid properties are calculated through CoolProp.

The computational program DYNDES was applied to perform the thermodynamic calculations, run the economic analysis and perform the multi-objective optimization. The optimization tool is based on a genetic algorithm that runs until the average change in the spread of the Pareto front is lower than the specified tolerance. The genetic algorithm was chosen over deterministic methods once it is less prone to get stuck in local minima, even though it requires a large computational effort. Its computational flowchart is presented in Figure 9.



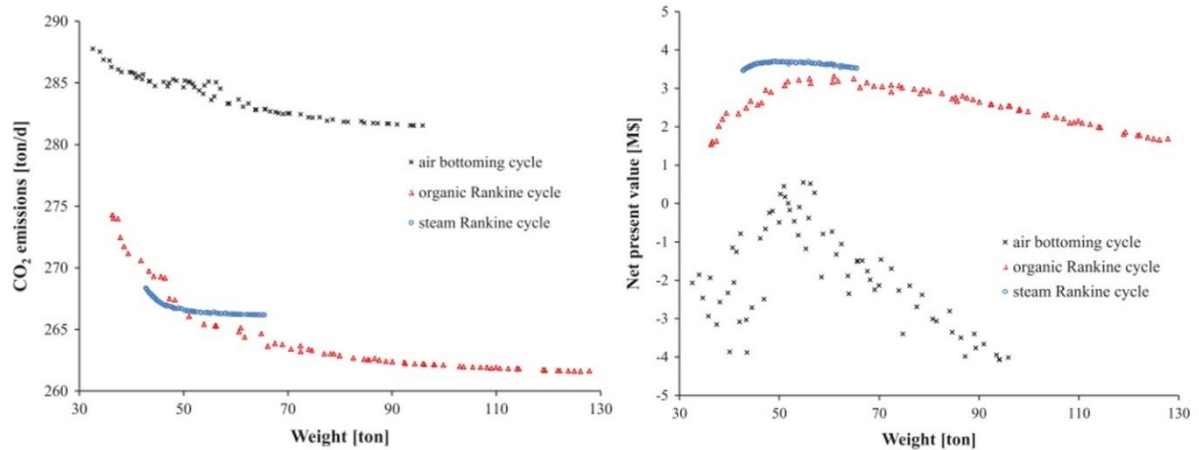
Figure 9 - Architecture of the DYNDES design tool.



Source: Pierobon et al. (2014).

The results show that the closed loop Brayton air cycle presents the highest CO<sub>2</sub> emissions while enabling to achieve the lowest possible weight. The Rankine cycles units compete in terms of weight and efficiency, while the ORC unit is superior in terms of performance compared to both the steam Rankine and air bottoming technology cycles. Regarding the economic analysis, the implementation of the air bottoming cycle unit does not appear to be attractive. Therefore, the waste heat recovery technology which allows to achieve the highest net present value is the steam Rankine cycle. Figure 10 summarizes these results in terms of Pareto fronts.

Figure 10 - Pareto fronts of the three waste heat recovery technologies. CO<sub>2</sub> emissions and net present value are presented as concurrent objective functions for the three waste heat recovery options.



Source: Pierobon et al. (2014).

Reis, Guillen and Gallo (2019) present an analysis on the use of ORCs for heat recovery at the gas turbines exhaust applied over a typical configuration seen in Brazilian FPSOs. The study is based on an FPSO operating on the Pre-salt basin, equipped with four GE LM2500+ gas turbines, being one of them kept in standby mode. It is proposed the removal of one gas turbine from the power plant and consider an ORC as bottoming cycle, recovering heat from the remaining two gas turbines. In addition, the ORC also recovers the heat from a GE LM2000 mechanically coupled to a compressor train. Furthermore, the variation of the power demand throughout the platform lifecycle is considered for the analysis. These arrangements provide power through the ORC and hot water to be consumed in plant processes. Furthermore, the ORC is considered in two configurations: simple and a regenerative. The Thermoflex software is used for the simulation of gas turbines at steady state condition in a load range of 50 to 100%. The simulation results were used to develop fitting polynomial functions to calculate the exhaust conditions (mass flow rate, temperature, and composition) as function of the load and ambient conditions. These polynomials were used to simulate the heat source to be used as input for the ORC and heating models. On the basis of a literature survey, toluene was used as working fluid in ORC. The model is implemented in MATLAB, whose genetic algorithm package is also used to perform a single-objective optimization, with the aim of minimizing an objective function defined to match the electrical demand throughout the platform lifecycle to the power generated power. The results show that the ORC can provide up to 20% of the total power demand and the overall thermal efficiency can reach 47%.

It is worth mentioning other waste heat recovery approaches performed in recent works. de Oliveira Neto, Sotomonte and Coronado (2021) applied ORCs for power generation by recovering waste heat from internal combustion engines. Firstly, the equipment was designed by applying a thermodynamic model, optimized by genetic algorithm to reach the maximum power output, given the heat source parameters. The detailed design was carried out considering equipment standards, with meticulous details implemented for the heat exchanger, steam turbine, and pump. With the parameter established, an off-design and economic analysis could be carried out. The results showed an increase in the increase of up to 10% in power production, with the ORC efficiency reaching 15%.

Shi et al. (2023) discusses the nature of the control system applied to ORCs in waste heat recovery applications. A specific small-scale ORC, operating with R245fa as a working fluid, was used as reference for the analysis. A dynamic model was developed and implemented in MATLAB, and the thermodynamic properties are calculated using REFPROP. Different approaches were evaluated in control models. The potential disturbances in the heat source as a major point of complexity for the control model need to be considered.

In Table 2, the main works concerning the ORC application for waste heat recovery and its most relevant findings can be found.

Table 2 – Summary of the works concerning the studies on ORC applied to waste heat recovery.

<b>AUTHOR</b>	<b>YEAR</b>	<b>MAIN SUBJECT</b>	<b>RELEVANT ADVANCES</b>
Pierobon et al.	2013	ORC as bottoming cycle coupled to gas turbines	ORC is feasible for oil platforms, even though the volume occupied by the equipment is a concern.
Pierobon et al.	2014	WHR alternatives for oil platforms	ORC is superior in terms of performance compared to both the steam Rankine and air bottoming technology cycles.
Shi et al.	2023	ORC control strategy	The ORC control strategy plays an important role in its performance.

---

Source: Author.

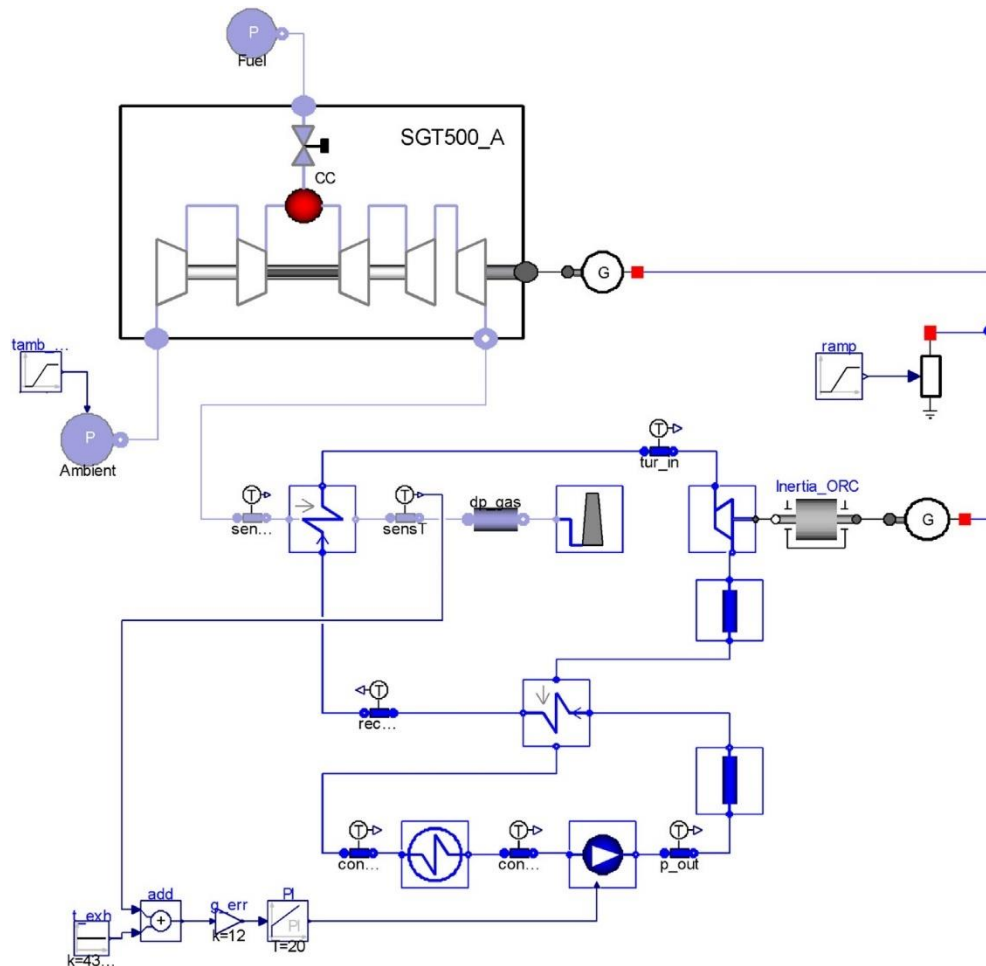
### *2.3 Design of ORCs through multi-objective optimization*

The application of multi-objective optimization to the ORC design is a powerful approach that has been evaluated throughout the years. Pierobon et al. (2014) present an ORC design tool that accounts for the dynamic behavior, to be applied in the heat recovery at the gas turbines exhaust. The turbines were then located in an oil platform in the Norwegian Sea. The design algorithm is implemented in MATLAB. The fluid conditions at the gas turbine exhaust are taken as inputs for the design, thus, the mass flow rate, temperature, and gas composition need to be calculated. Then, the components of the ORC are selected, and the conservation equations are applied to define the inlet and outlet thermodynamic conditions for each equipment. After that, detailed design parameters are calculated, such as the number, length, and diameter of the tubes in the heat exchangers, the turbine flow coefficient. Finally, a multi-objective optimization is carried out to explore the best configurations.

The power plant to be analyzed consists of three Siemens SGT-500 gas turbines, where two operate at a 50% load and other is kept in standby or maintenance. It is considered one ORC per gas turbine. Since the temperature of the exhaust gases is relatively low (380 °C), no intermediary fluid is considered to transfer the heat from the hot source to the organic fluid – cyclopentane – selected based on preliminary studies performed by the main author.

The mathematical model focuses on the heat exchanger models. The Modelica language was selected for the thermal system modeling, being the Thermopower library used for the gas turbine modeling, and the ORC library for the other components. It is worth presenting the object diagram of the thermal system, presented in Figure 11. It can be seen in the gas turbine model diagram, the fuel control block diagram (there is no IGV in the equipment), the shaft speed control for the power turbine (fixed electric frequency) and the inertial models for the shafts. The overall arrangement is simple and does not require minor component blocks to account for heat losses and other phenomena. For the ORC model, the pump mass flow rate control; the electric connection between the generators and also the simple arrangement for the heat exchangers can be highlighted, despite the model complexity. Additionally, several regulating devices for temperature control can be seen.

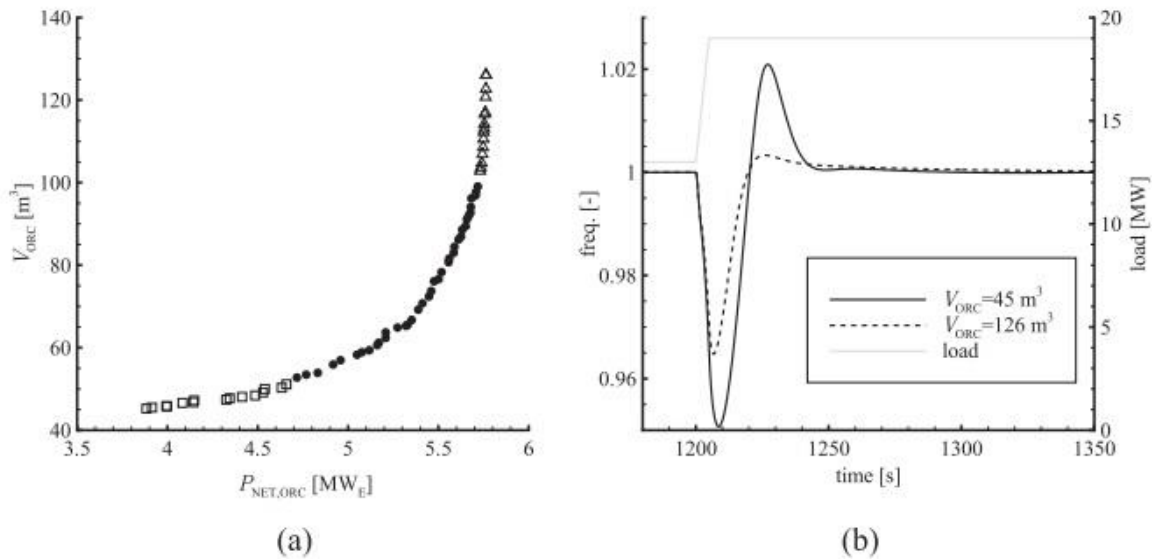
Figure 11 - Object diagram of the entire combined cycle system. It can be noted the temperature control adopted for the steam turbine regulating valve.



Source: Pierobon et al. (2014).

The DYNDES tool is used to couple steady state and dynamic software models and the optimization is performed by using genetic algorithms, having as objectives the minimization of the heat exchangers volume and the maximization of the ORC power output. Transient cases selected for calibration and validation involve sudden load changes, load rejections, or unit trips. The optimization results can be seen in Figure 12. The left-hand side (a) shows the Pareto front, where the feasible designs are represented by the circles. The results plotted with squares and triangles generated unstable designs. On the right side (b), for the minimum and maximum feasible heat exchanger volumes, the transient response of the system is evaluated.

Figure 12 - (a) Multi-objective optimization results, Pareto front showing the relation between the objective functions - ORC system net power and the volume of the heat transfer equipment. (b) Results of the dynamic test, the light gray line represents the load variation.



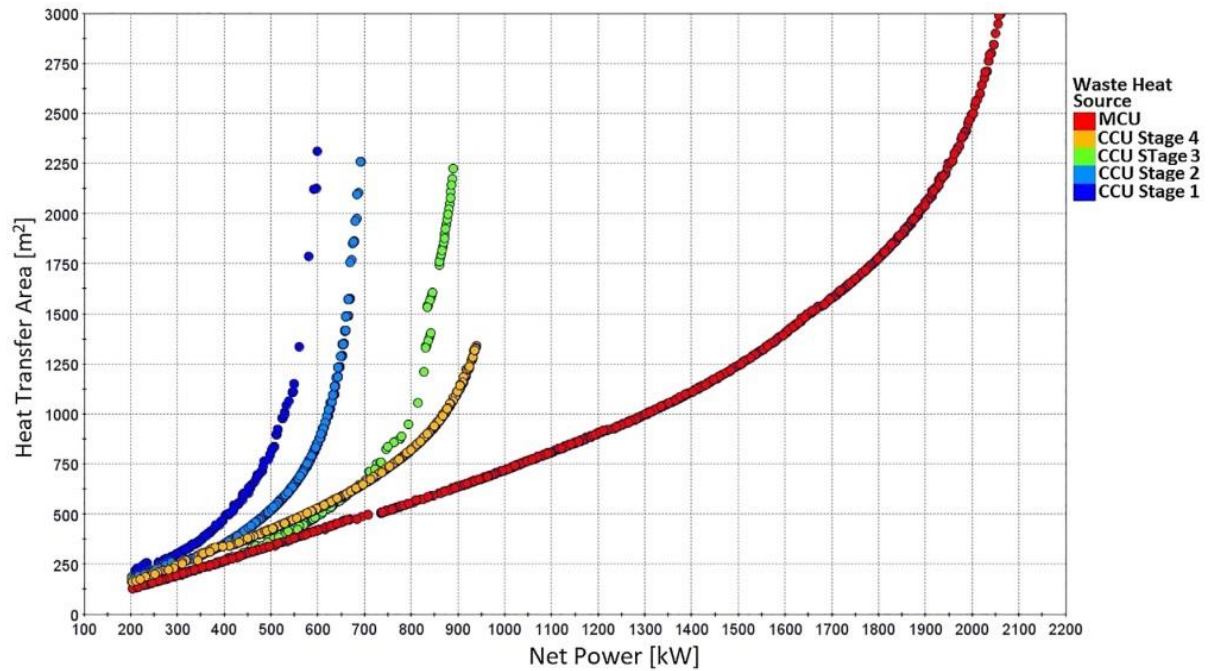
Source: Pierobon et al. (2014).

The proposed methodology was able to generate feasible designs for offshore applications, and the test cases demonstrate the importance of the dynamic analysis, which enabled the proper to exclusion of those system configurations which, although potentially more efficient or compact, may lead to unacceptable frequency fluctuations or increase the risk of decomposition of the working fluid.

Veloso et al. (2018) present a methodology for the quantitative identification of sources of waste heat recovery in an FPSO operating in Brazil. Furthermore, a computational tool to optimize the ORC design was developed. The focus of the investigation, once the main potential heat sources, were identified, was the CO<sub>2</sub> compression unit (CCU) and the main compression unit (MCU), where a significant amount of heat is wasted in the gas cooling heat exchangers. Both systems were modeled using the Aspen-HYSYS software through mass, energy, and exergy balances for each process and equipment. Therefore, the model was used to calculate the energy potential of each source/stream as a function of its chemical composition, pressure, temperature, and molar flow rate. Additionally, a computational model was developed in MATLAB to calculate the performance of each component and to design the ORC on the selected sources/streams. Thermodynamic properties were calculated by using REFPROP. The authors applied a multi-objective optimization through the NSGA-II method over the ORC to minimize the total area occupied by the equipment and to maximize the power generation where the optimal solutions were classified accordingly with the Pareto dominance.

The global results are presented in Figure 13. The working fluids defined for each application were: CCU Stage 1 - R245fa; CCU Stage 2 and Stage 3 - R236fa; CCU Stage 4 - RC318; and MCU – R245CB2.

Figure 13 - Overall optimization results per ORC proposed.



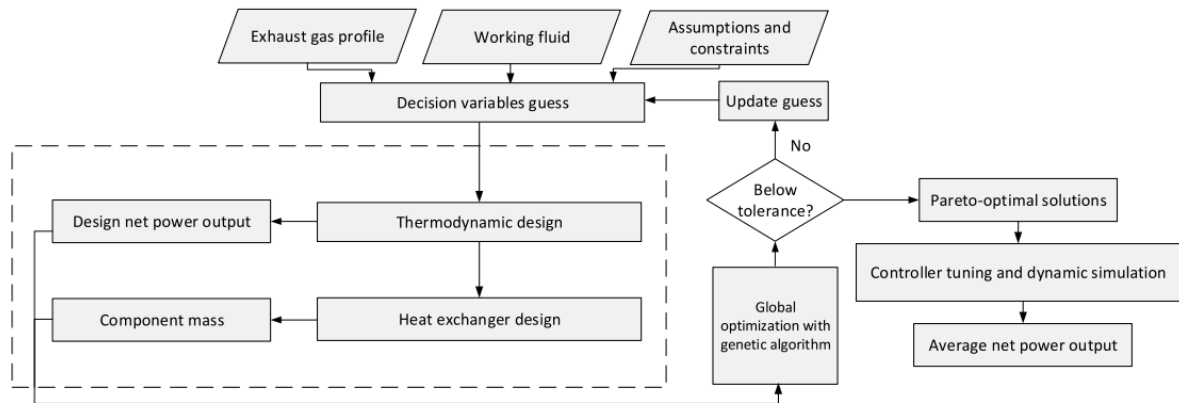
Source: Veloso et al. (2018).

There are other works with relevant applications outside of the oil and gas industry. The work of Wang, Bu, and Li (2020) sheds light on the need of evaluating the off-design performance of ORCs. A parametrized model is presented to evaluate the system performance under off-design conditions. Again, optimization using a genetic algorithm from the MATLAB toolbox is applied to define designs with maximum efficiency and minimum costs.

Pili, Jørgensen and Haglind (2022) evaluate the role of off-design and dynamic conditions in the ORC design. The profile dataset of a 450 HP diesel engine for heavy trucks containing 45 minutes of real operational data is used for the analysis. A multi-objective optimization is applied, by using a genetic algorithm from the MATLAB global optimization toolbox. The thermodynamic model is also implemented in MATLAB and the working fluid properties are obtained via REFPROP. Again, it is identified the important role that off-design and dynamic conditions play in eliminating unfeasible solutions, initially identified for the full-load case. The algorithm implemented is shown in Figure 14.



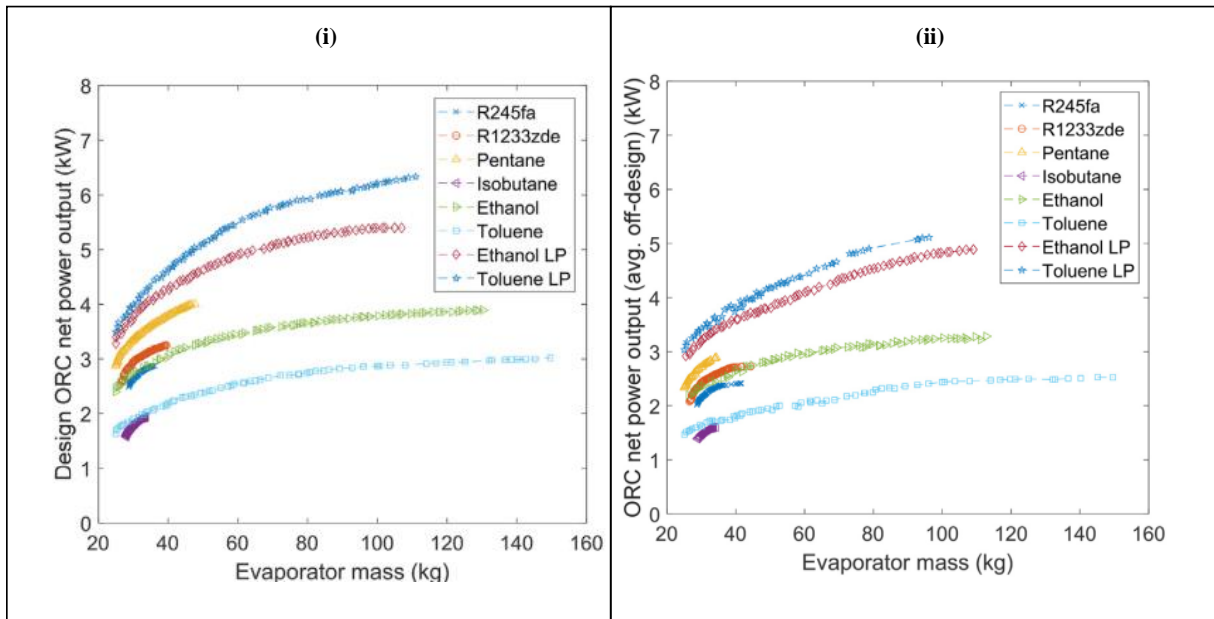
Figure 14 – Overview of the multi-objective optimization algorithm.



Source: Pili, Jørgensen and Haglind (2022).

A comparative analysis is performed among the proposed designs considering (i) the steady-state conditions and (ii) a scenario where the dynamic conditions are taken into account. For case (i), 8 working fluids are considered for selection during the multi-objective optimization. Then a dynamic simulation (ii) is performed to evaluate the proposed designs. Some of the solutions did not converge in this case. Figure 15 shows the results of the optimization that have as objectives the power output and the mass of the evaporator. It can be noted that the representative decrease of valid solutions and the suitability of designs that have toluene as a working fluid to dynamic conditions.

Figure 15 – Pareto front for the steady-state optimization scenario.



Source: Pili, Jørgensen and Haglind (2022).

The impact of the load conditions on the ORC design is the main concern of the work developed by Ping et al. (2023). The ORC is applied for the recovery from the waste heat of automotive internal combustion engines, taking into account its transient response depending on the conditions of the road. The engine behavior is simulated by a model. Then, the data generated by the simulation is used to train a neural network model, which is coupled to a non-dominated Sorting Genetic Algorithm III (NSGA-III), used for the optimization. The results, accounted for by the typical dynamic behavior of the automotive engine, show a thermal efficiency of 4.3%.

Table 3 presents an overview of the main works on multi-objective optimization for the design of ORCS.

Table 3 – Summary of the works concerning the design of ORC through multi-objective optimization.

<b>AUTHOR</b>	<b>YEAR</b>	<b>MAIN SUBJECT</b>	<b>RELEVANT ADVANCES</b>
Pierobon et al.	2014	Design of ORCs for WHR in the gas turbine exhaust.	ORC conception by taking into account the dynamic conditions lead to more accurate designs.
Veloso et al.	2018	Design of ORCs for WHR in compressor trains.	The interstage WHR offers an interesting environment for ORC applications.
Pili et al.	2022	ORC design considering off-design conditions.	Off-design conditions reveal the actual feasible designs.

Source: Author.

## *2.4 Final remarks*

The low thermal efficiency is an important issue in the FPSO processes and in its power plants. Several alternatives have been evaluated to solve or minimize this problem over the years. The works discussed in this chapter point out alternatives where the waste heat recovery can be applied in oil platforms. It is evident from these studies that the gas turbine exhaust and the compressor trains interstage offer a good opportunity for recovery strategies.

The organic Rankine cycle has been distinguished among these potential alternatives. This technology has evolved greatly in the last years with a broad portfolio of real-life applications for low-temperature heat sources and a relatively small volume of its equipment. The pros of ORC are also highlighted in recent works, especially (i) for the possibility of controlling the temperature of the heat source fluid; (ii) its simplicity in terms of operation and maintenance; (iii) its capacity to be used in several applications; and (iv) its capacity to recover heat from very low temperature (from 70 °C) and provide significant power output.

Within this context, ORC design through advanced multi-objective optimization methods have also been also studied. The design of ORCs to be applied in the complex environment of oil platforms requires the development of robust algorithms and the application of heuristic optimization methods. Furthermore, the consideration of off-design and dynamic conditions is recognized as of major importance in the generation of feasible designs.

From the analysis of the literature works, it becomes evident that there is a lack to be explored in the optimization algorithm, mainly when considering dynamic conditions. In addition, it becomes clear that the application of ORC for temperature control is, in fact, an important contribution which reaches further in the application of these solutions in offshore installations. Most importantly, it is clear that the optimization algorithm developed in this thesis proposes an innovative approach for ORC design.

### 3. AN OVERVIEW ON FPSO PROCESSES AND ORC

#### 3.1 Topside process plants

Considering the assortment of types and technologies regarding oil rigs, this chapter focuses on the class of platforms that have been the reference choice for the Brazilian scenario in the projects developed in the last years: the floating production, storage and offloading (FPSO). FPSOs are platforms that can be built from an existing oil tanker or fully designed and built as an oil production and storage facility. These platforms have been largely employed in the Brazilian Pre-salt area, mainly due to the lower project capital expenditures, once no pipelines to the coast need to be installed,<sup>2</sup> whereas the produced is stored until the offloading to a tanker vessel. Figure 16 shows the Petrobras 74 FPSO, now operating at Búzios Field.

Figure 16 – Petrobras 74 FPSO.



Source: Petrobras (2023).

---

<sup>2</sup> Oil can be stored in the FPSO, but natural gas is usually reinjected in the well as part of the pressurization and production strategy (MORAIS, 2013). If the natural gas is exported, the proper pipeline needs to be installed.

Compared with semi-submersible platforms – which was a common solution for Brazilian post-salt fields – FPSOs have a larger deck area and can withstand greater mechanical loads. The topside consists of a major industrial facility whose main objectives can be described as:

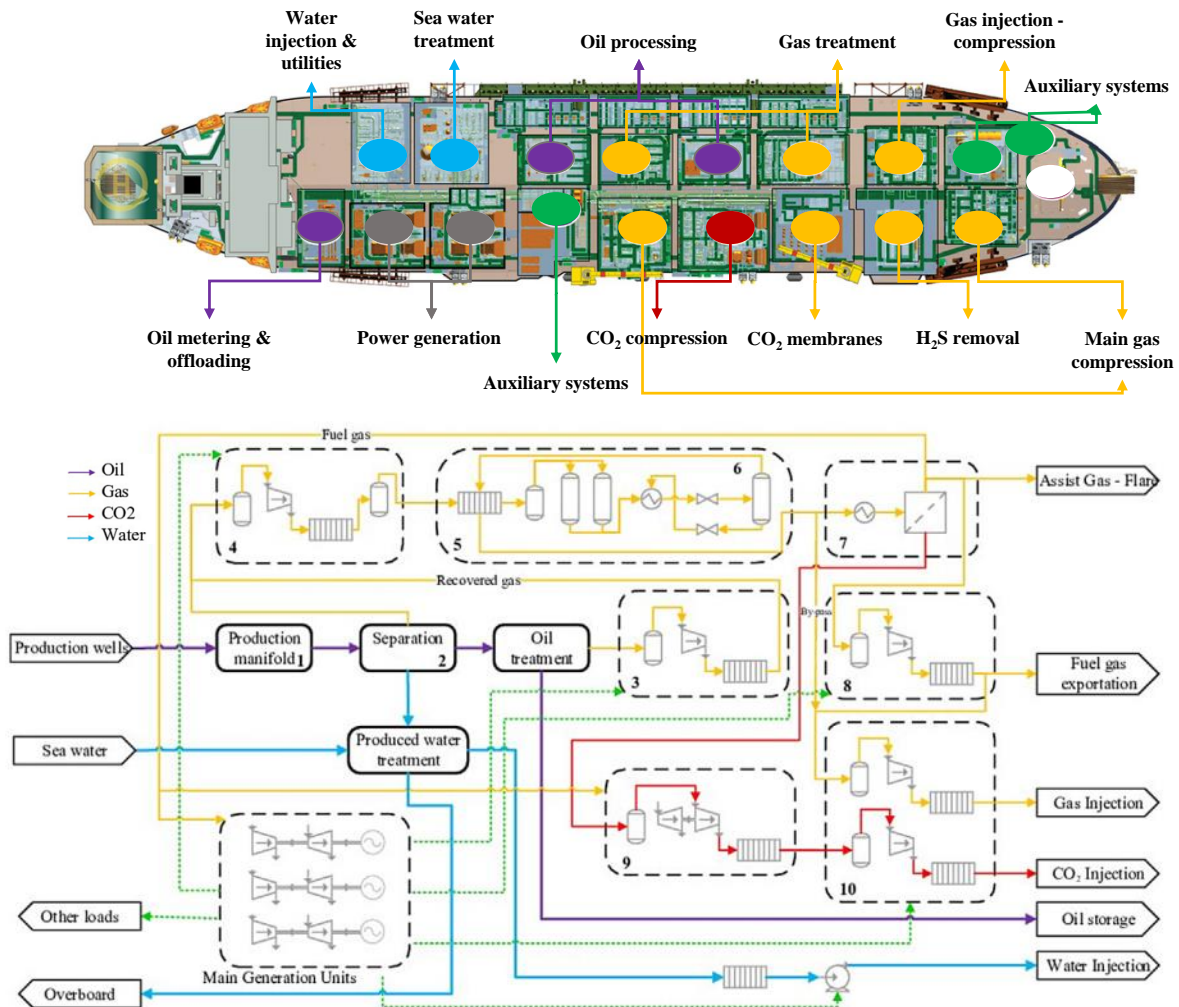
- Separate the components of the fluid coming from the well, typically oil, gas, and water.
- Perform the oil treatment.
- Clear the associated water so that it can be safely discarded.
- Prepare the gases to be reinjected.
- Prepare the natural gas to be used as fuel or exported.

It is worth mentioning that even though some of these objectives can be common to oil rigs operating in post-salt fields, there are some particular characteristics on the oil produced in Pre-salt fields that make the topside facilities diverse from its counterparts operating in other Brazilian regions. Most specifically, the fluid coming from the well has a high gas-to-oil ratio (GOR) and a high concentration of contaminants such as CO<sub>2</sub> and H<sub>2</sub>S, which demands specific equipment for separation and compression (ANDRADE et al., 2015). A summarized description of the topside of the FPSO is given in Figure 17. The fluid coming from the wells is delivered in the FPSO by the risers, and the multiple streams are joined in the production manifold; then it is directed to the separation process by gravity, which is performed in different stages to disassociate the gas, liquid, and solid phases. The separated oil, hence, has to be treated in order to ensure that the oil match the operator quality requirements before storage. In platforms, the treatment is made electrostatically for the demulsification of the mixture. In addition, water is injected to remove salt. After being properly treated, the crude oil goes to storage tanks before being offloaded. The gas phase dissociated after the separation (high pressure) and oil treatment stages (intermediate and low pressures) must be handled to meet the requirements, mainly composition and pressure, related to its final destination (GALLO et al., 2017):

- Fuel gas export and gas lift: If the gas is to be exported, the condensate (through scrubbers) and CO<sub>2</sub> (through membranes) need to be removed and the export/gas lift pressure need to be met after the compression trains.
- Gas injection: In this case, the CO<sub>2</sub> rich gas or even the whole gas stream, if the exportation is not performed, is pressurized to be reinjected in the well.

For environmental and regulatory impositions, the flare is not used as a regular routine and the separated CO<sub>2</sub> is not released into the atmosphere.

Figure 17 – An overview on the topside modules and its main functions.



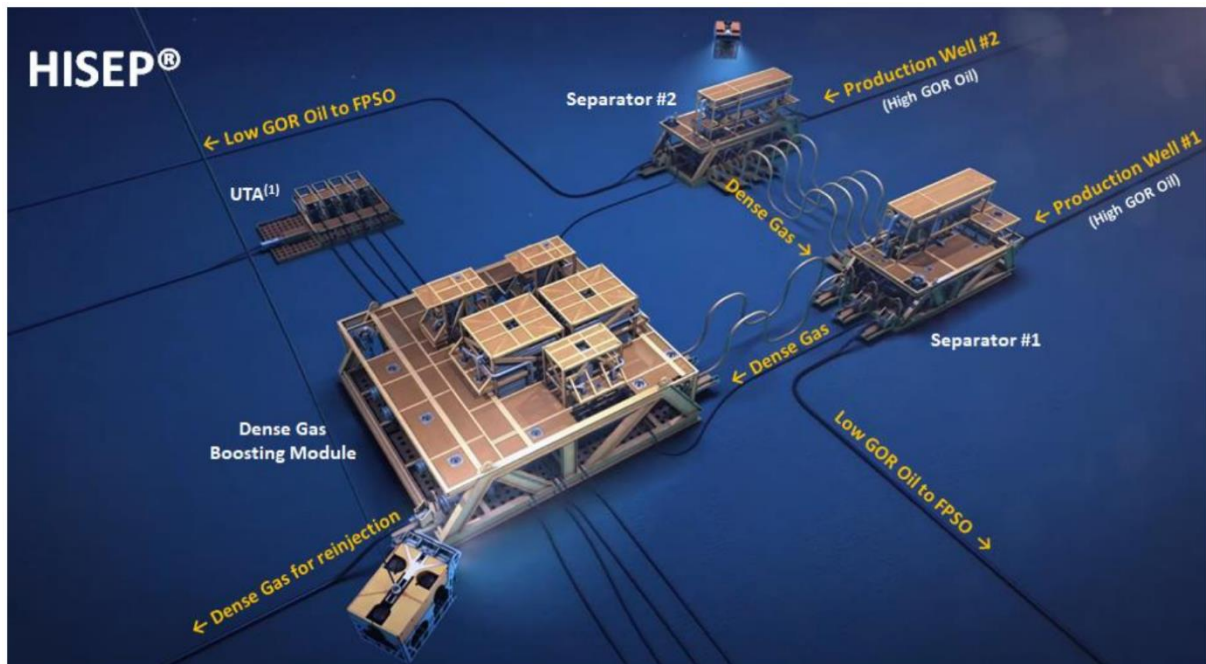
Source: Adapted from SBM Offshore (2016) and Gallo et al. (2017).

Given the purpose of this work, a description on the gas processing plant, focused on the compression systems dedicated for the gas injection is given in the next section. Once the gas turbine operating in the power generation modules and also those mechanically coupled to gas compressors play an important role in the overall plant thermal efficiency, a description of these modules is also given in this chapter.

Before moving forward, it is important to emphasize that recent cutting-edge improvements in subsea process plants seen in HISEP technology (MENEZES PASSARELLI et al. 2019) or those seen for all-electric FPSOs (CORREIA, 2023) still keep the same issues in

temperature control and waste heat. However, these initiatives are obviously a step further in efficiency and reduction of greenhouse gas emissions reduction and a clear evidence of the industry efforts to pursue better efficiency and decarbonization. Figure 18 presents an overview of the subsea arrangement of HISEP.

Figure 18 – HISEP: the subsea separation technology to be applied in the exploration of a reservoir in Brazil (Mero) with a high-CO<sub>2</sub> content produced fluid.



Source: (de OLIVEIRA, 2022).

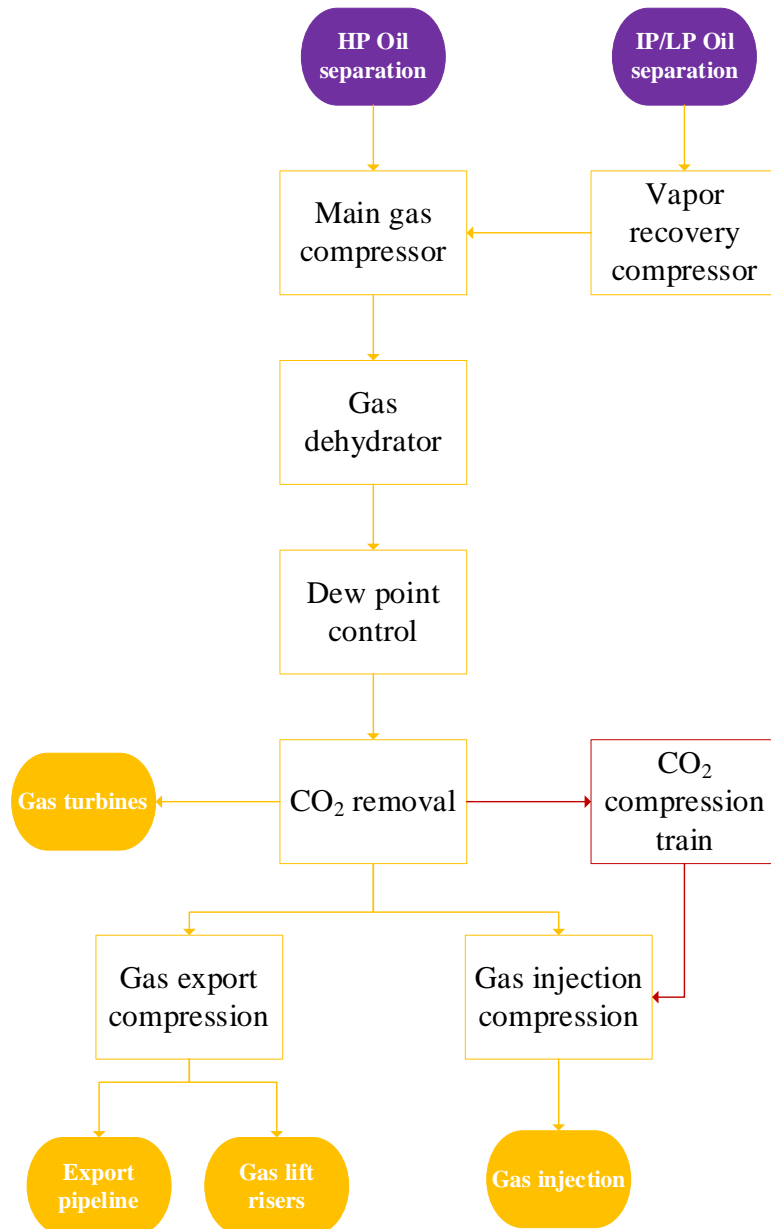
### 3.2 The gas compression modules

The gas processing plant is an important facility on the Pre-salt FPSOs that can take up to 60% of the total plant area due to the high GOR in crude produced in this region (TOUMA, et al. 2019). As presented in Figure 19, the high-pressure gas coming from the oil processing module enters the main gas compressor module, while the other separated streams at lower pressures go to the vapor recovery compressor module to match the entry pressure of the former module. After that, the gas is dehydrated to reduce its water content to the quality standard required by the operator, and then the stream passes through the dew point control. Therefore, the stream enters the CO<sub>2</sub> separation by membranes and the CO<sub>2</sub>-rich gas is sent to its compression system, while the extracted natural gas is sent to be used as fuel to the gas turbines. Finally, the last compression modules are used accordingly with the destination of the gases. Natural gas can be compressed to be exported or injected in the well as a gas lift strategy. If



such operations are not performed, the natural gas is mixed again with the CO<sub>2</sub>-rich gas and the stream is compressed to be used as enhanced oil recovery by gas injection (ALLAHYARZADEH-BIDGOLI et al., 2018) (CRUZ, ARAUJO, de MEDEIROS, 2018).

Figure 19 – Gas processing plant modules. Colors indicate the fluid being processed: purple - crude; yellow – gases; red – CO<sub>2</sub> rich gas.

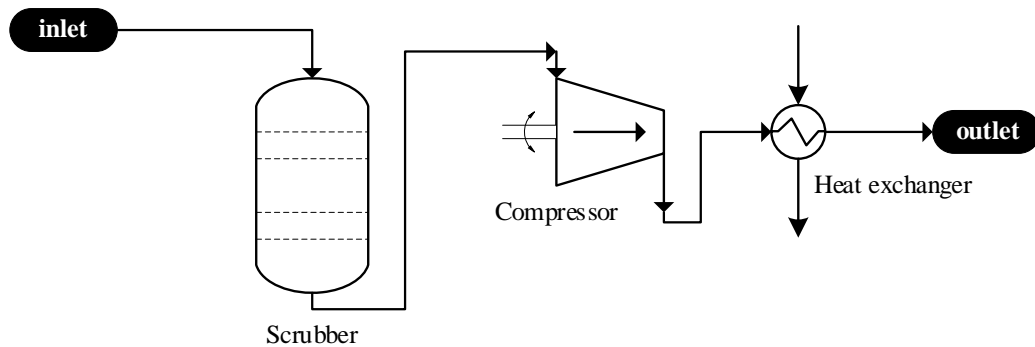


Source: Author.

Even though the gas composition, its mass flow rate, pressure and temperature can be diverse among all compression modules, the equipment that compose the compression systems is typically the same as Figure 20 shows. First, the gas enters the scrubber, equipment used to

remove the liquids and condensate from the stream, and then goes to the compressor. Once the compression process increases the temperature, seawater is used in the heat exchanger to reduce the gas temperature and increase the efficiency in the next compression train.

Figure 20 – The basic components of the gas compression system.



Source: Author.

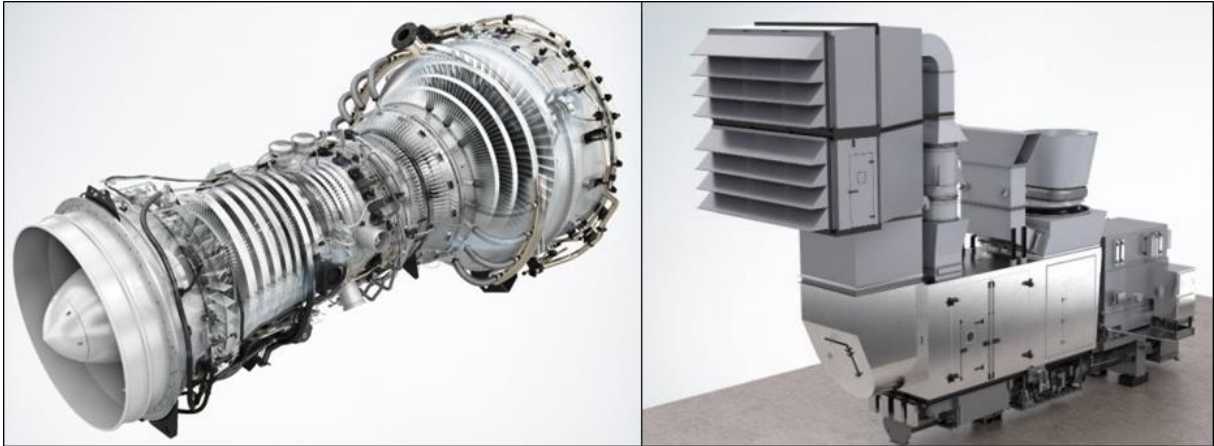
In the gas injection stream, particularly, the massive concentration of CO<sub>2</sub> is well known to induce stress corrosion cracking in flooded-annulus flexible pipes (AGÊNCIA NACIONAL DO PETRÓLEO, 2017). The occurrence of this phenomenon depends, among other factors, on the fluid temperature (FELLET, NYBORG, 2018) and, therefore, if this variable can be controlled before the fluid enters the riser, the failure mode may not be activated. Furthermore, even considering the cooling at the compression train outlet, this gas stream has a massive amount of available exergy that could be converted into useful power. These conditions are prone to the adoption of an ORC to control the temperature and generate power simultaneously.

### 3.3 Power plant

The power generation modules are responsible for the supply of all the FPSO electrical power demand. The module is usually composed of 3 or 4 gas turbines running at partial load to operate with high availability and to safely comply with the power demand peaks imposed by the plant. The gas turbines that commonly operate in the most recent Brazilian FPSOs are aeroderivative as long as its aeronautical heritage gives them high power/volume ratio, low weight, and high reliability when compared with the industrial heavy duty gas turbines. Some gas turbine models used onboard are continuously evolving and have a track record of decades

operating offshore, e.g. the Rolls-Royce RB211 family, now Siemens SGT-A35, shown in Figure 21.

Figure 21 – The Siemens SGT-A35 (former Rolls-Royce RB211) gas turbine and its offshore container.

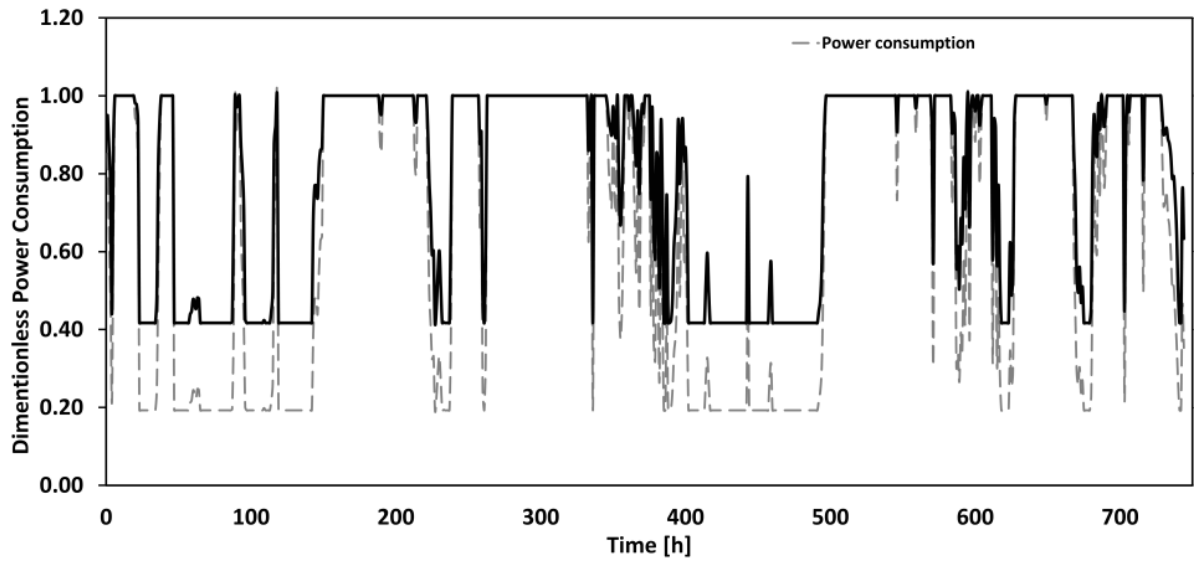


Source: Siemens Energy (2020).

The gas turbine modeled in this work is the GE LM2500+, as it has a large fleet operating in Brazil for both electric and shaft power applications. This machine has been used offshore since the 1970s (SPECTOR, CIMINO, 1990) and has been continuously updated to follow advances in materials and aerodynamics and to comply with environmental regulatory standards. In FPSOs, cutting-edge replicants delivered for the Búzios Field have its power plants equipped with this gas turbine (OFFSHORE MAGAZINE, 2013) (GENERAL ELECTRIC, 2014).

These plants are subjected to challenging operational conditions, due to transitory power demand and the typical operation at partial loads. These characteristics demand extremely robust power generation equipment. Figure 22 presents a time series of the power demand of an oil platform located in the North Sea. The frequent load changes are seen, leading to the need for a comprehensive maintenance and reliability plan for such facilities. Moreover, the demand for lower loads induces low efficiency in gas turbines, which is also an opportunity for waste heat recovery approaches.

Figure 22 – Power consumption time series of an oil platform located in the North Sea.



Source: Adapted from Eyni et al. (2022).

FPSO power plants are not typically equipped with steam bottoming cycles due to the area required for their installation; therefore, the heat recovery at the gas turbine exhaust is performed by WHRU (waste heat recovery unit). These systems are equipment dedicated to transfer heat from gas turbine exhaust gases to an intermediate fluid that provides heating in other parts of the plant. Once again, ORCs can be evaluated to recover heat (even downstream the WHRU) and increase the global thermal efficiency of the plant.

### 3.4 Organic Rankine Cycles

The organic Rankine cycle was idealized in the 19<sup>th</sup> century, but in the second half of the 20<sup>th</sup> century it was further developed, mainly after the oil crisis in the 1970s. During the 2000s, technology saw a major development, thanks to environmental policies related to CO<sub>2</sub> abatement in developed countries. Since then, the ORC has been mostly applied on geothermal and solar power, cogeneration, and waste heat recovery. Table 4 shows some examples of ORC installed around the world, the power generated, and the working fluid.

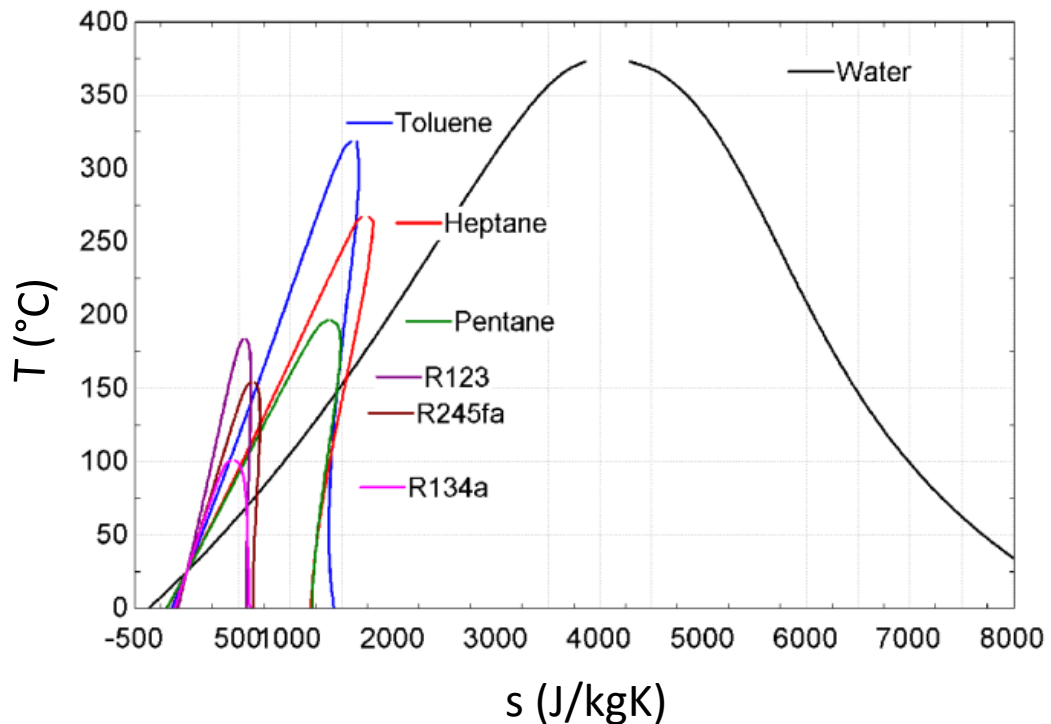
Table 4 – ORC power systems in operation and its main characteristics.

MANUFACTURER	PLANT LOCATION	POWER (kWe)	WORKING FLUID	APPLICATION
Ormat	Mali	0.6	dichlorobenzene	Solar
ElectraTherm	USA	110	R-245fa	WHR
Triogen	England	160	toluene	Biomass
Ormat	USA	1000	n-pentane	Solar
Atlas copco	Canada	2100	R134a	WHR
GE	Canada	17000	Cyclo-pentane	WHR
Exergy	Turkey	22500	n-Butane	Geothermal

Source: Adapted from Casati (2014) and Macchi and Astolfi (2017).

The ORC is based on the same principle and equipment of the classic steam Rankine cycle, however, its working fluid is organic, refrigerants, siloxanes and hydrocarbons, which allows it to work efficiently with temperatures departing from 70 °C. The T-s diagram shown in Figure 23 presents an overview of the most common fluids used in ORC its phase diagrams compared with water.

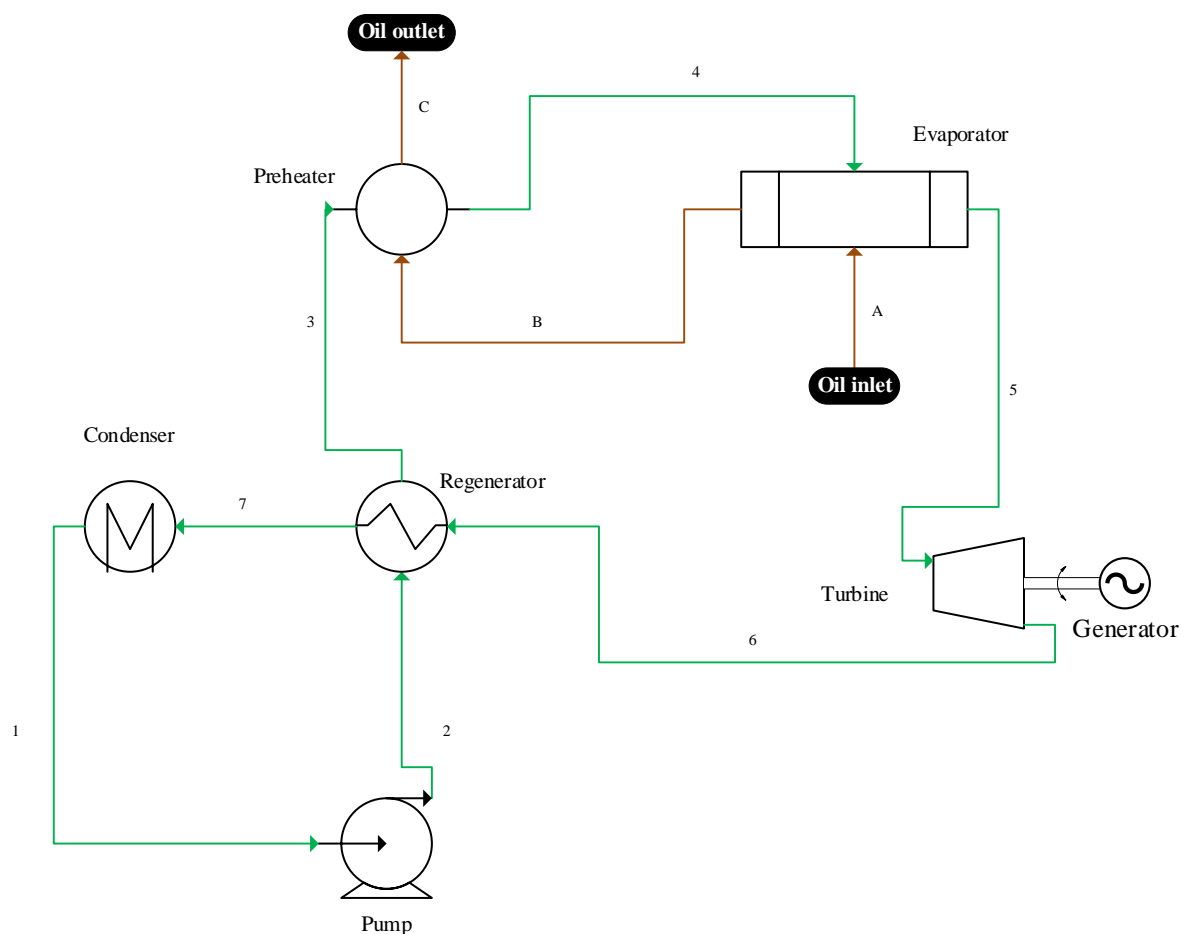
Figure 23 – T-s plot of typically used organic fluids and water.



Source: Quoilin (2011).

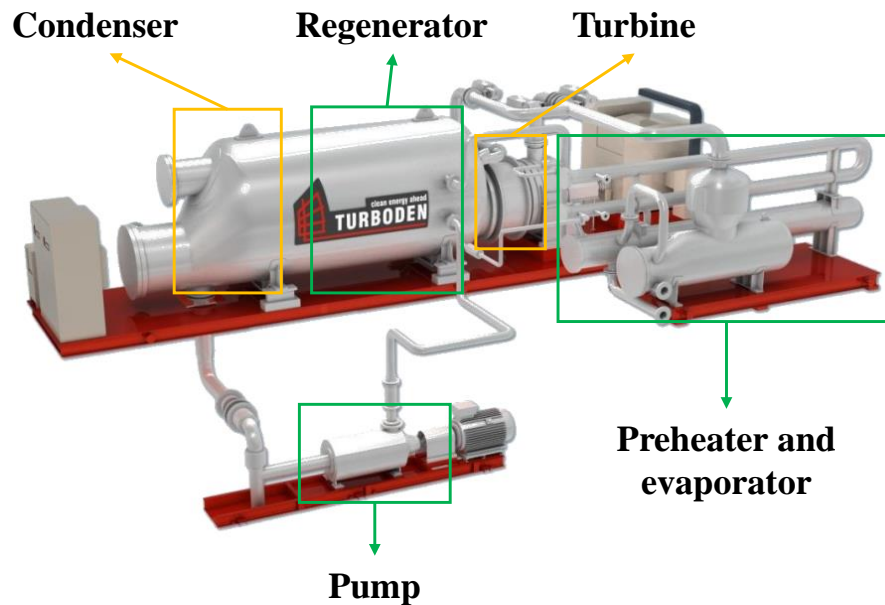
The operating principle of the ORC is very similar to that of its steam counterparts. However, there are some technological features that are intrinsic to the former, mainly regarding the characteristics of the organic fluid and the heat source. Figure 24 presents a typical configuration found in real-life ORC plants, featuring an intermediary fluid, preheating, and regeneration. The liquid organic fluid enters the pump to be compressed and follows to the regenerator, where its temperature increases while receiving heat, in this case, from a diathermic oil and not directly from the heat source. From the regenerator, the fluid goes to the preheater and then to evaporator, where the fluid sees a phase change into gas and becomes superheated. The expansion in steam turbine usually keeps the fluid in its gas phase at the exhaust, which implies lower capital expenditures once no droplets are formed and the turbines have no risk of erosion. The fluid therefore passes through the regenerator and then to the condenser to be liquified (MARCHANDISE, 2014). A real-life ORC equipment is shown in Figure 25.

Figure 24 – Flow diagram for a typical real-life ORC.



Source: Author.

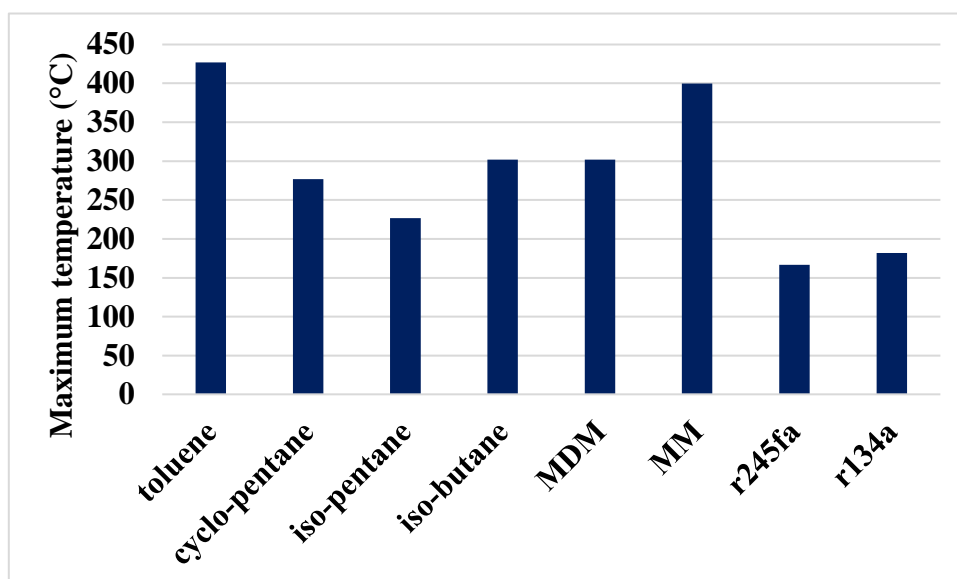
Figure 25 – ORC equipment from Turboden. Plants from this company generates up to 10 MW in WHR applications.



Source: Adapted from Foresti and Archetti (2020).

The working fluid is selected accordingly with the hot source temperature, specific volume, and thermal stability (WANG et al., 2020). From the most common organic fluids used in commercial equipment (CASATI, 2014), its maximum operating temperature is presented in Figure 26 its maximum operation temperature.

Figure 26 – Temperature limits of the organic fluids commonly used in commercial projects.



Source: Author.

Another information to be considered in the fluid selection is how the fluid could be harmful to the environment. Some indicators can be used to estimate the environmental impact of using a specific fluid, such as the global warming potential (GWP), the carbon footprint (CFP), and the greenhouse gas (GHG) emissions.

ORCs are robust, reliable, and well-developed technologies that have been used in several projects for improving energy efficiency in facilities of distinct industries. These characteristics and additionally its relatively low volume make it suitable for offshore applications.



## 4. MODELING AND SIMULATION

### 4.1 Computational modeling of thermal systems

Thermal systems models have been developed throughout the years. This subject has been extensively studied since the flourishing of the computer science and programming languages in the decade of 1950 and the combined evolution of hardware, software, and algorithms has allowed the analysis of systems more and more complex. Today, with the digital transformation popularized by Industry 4.0 concepts, the models have been extensively used as ‘Digital Twins’.

The possibility to simulate the entire plant behavior or a single component, in steady-state and transient conditions, is a powerful tool to reduce costs in engineering, design, and operation (ELMEGAARD, 1999). These models are applied today as a central resource for plant design, operational support, plant operator training, and control systems design and tuning. The current surge in the digital twins popularization led to the spreading of the application of such models across several industries (SLEITI, KAPAT, VESELY, 2022).

The development of such systems implies the development of complex mathematical models with several levels of solving complexity. Lumped parameter models are commonly used, since they provide sufficient accuracy to describe the real-life system behavior. Even with the simplification provided by the lumped parameter approach, the generated mathematical model, in the cases where transient conditions are being accommodated, requires to solve a dynamic-algebraic equation system. There are several techniques that can be applied to solve this problem, to a deep connection with the numerical and computational arrangement to be applied. The choice of a modular or simultaneous solution or even a combination of both approaches is also the subject of several studies (COLONNA, PUTTEN, 2007).

The ORC design methodology developed in this work is based on the modeling and simulation of the Rankine thermal cycle and its adjacent systems to determine the constructive parameters of the equipment. Specifically, for the application studied in this project, the dynamic simulation of equipment that operates coupled aero and thermodynamically demands the solution of differential and constitutive equations and the correct matching throughout the components, which basically requires:

- Knowledge about equipment configuration, constructive information, and the control system.
- The correct construction of the mathematical model.

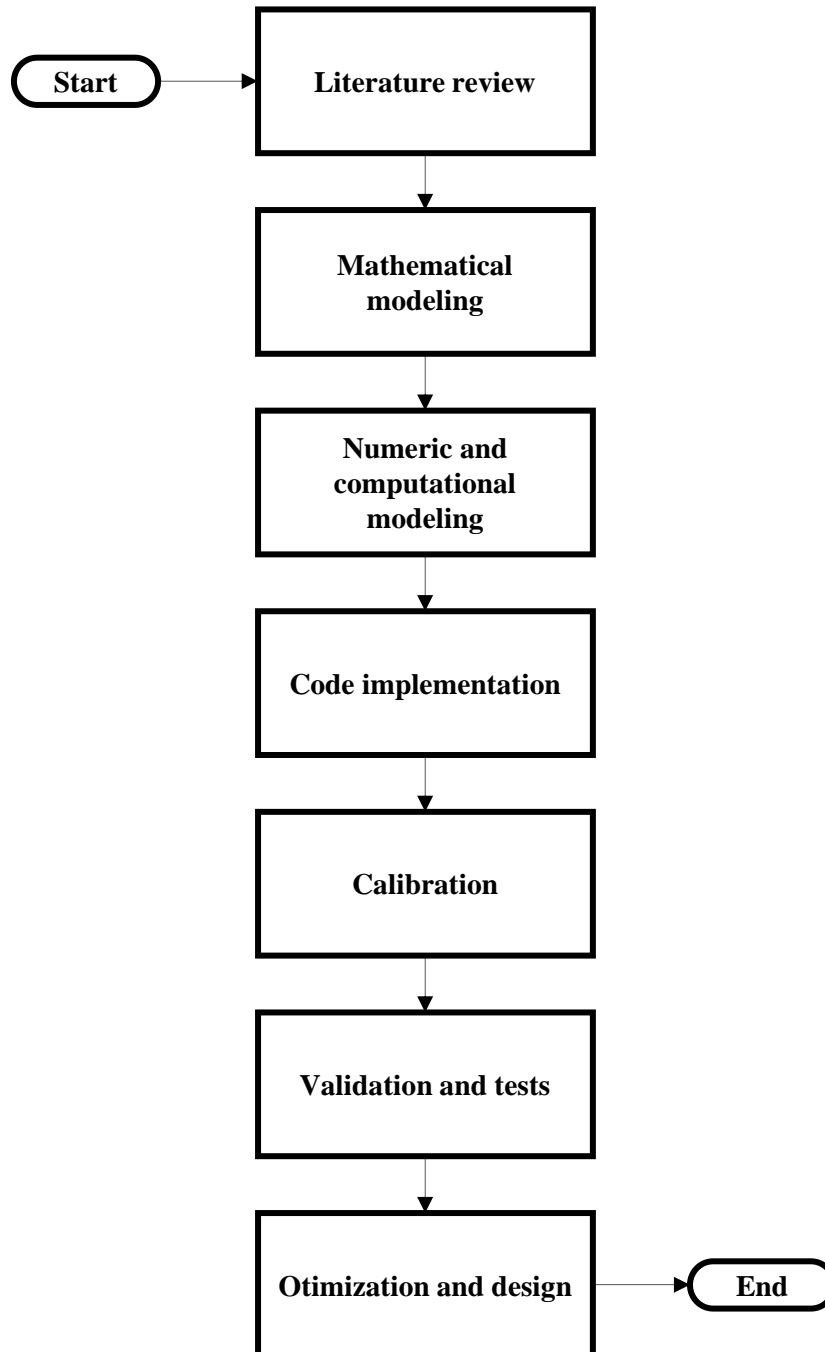
- An efficient and robust numeric arrangement.

The flowchart presented in Figure 27 summarizes the process of developing this nature of systems. Initially, a broad literature review is executed and relevant knowledge is gathered on similar models, applicable equations, and which numeric and computational arrangements were adopted. In addition, it is important to define during this phase how much work needs to be implemented and how much is already available in libraries, software, and other resources ready to be used in the project. The next step is the development of the mathematical model, which takes into consideration, among other aspects, the adopted premises, the available data, the modeling objectives, degrees of freedom and type of problem (lumped, distributed, steady-state, dynamic). Once the problem mathematical basis is built, the computational architecture to be applied need to be evaluated and the analysis about what numerical methods are required need to be carried out. Then, the code can be implemented, taking into consideration good practices such as code reuse and performance improvement. The calibration consists in fitting the model parameter to better represent the simulated phenomena. It can be made using data available in the literature, databases, experiments, field measurements, and other software and models so that the results can fit the desired deviation margin<sup>3</sup>. At this stage, it is fundamental for modeling success to have access to operational data, datasheets, equipment assembly details, and modeling good practices. The validation is carried out to verify whether the system is able to reproduce situations that differ from those used in calibration and to check if the model can accurately simulate all situations of interest. Finally, once the system has demonstrated robustness and accuracy, the ORC design can be done. In this step, several optimization scenarios are evaluated to determine the best solution. The system developed in this work was implemented in Python and uses as much as possible its scientific computing and optimization libraries.

---

<sup>3</sup> When using algorithms such as neural networks, regression/autoregression for instance, this step consists in the training phase.

Figure 27 – Modeling and development flowchart applied to thermal systems simulation and ORC design. The steps here presented are not necessarily performed in sequence and the process admits an iterative development.



Source: Author.

For the purposes of this thesis, the mathematical models of the gas turbine and of the ORC are vital for the successful design. In the next sections, the modeling and features of the model of these two thermal systems are presented and discussed.

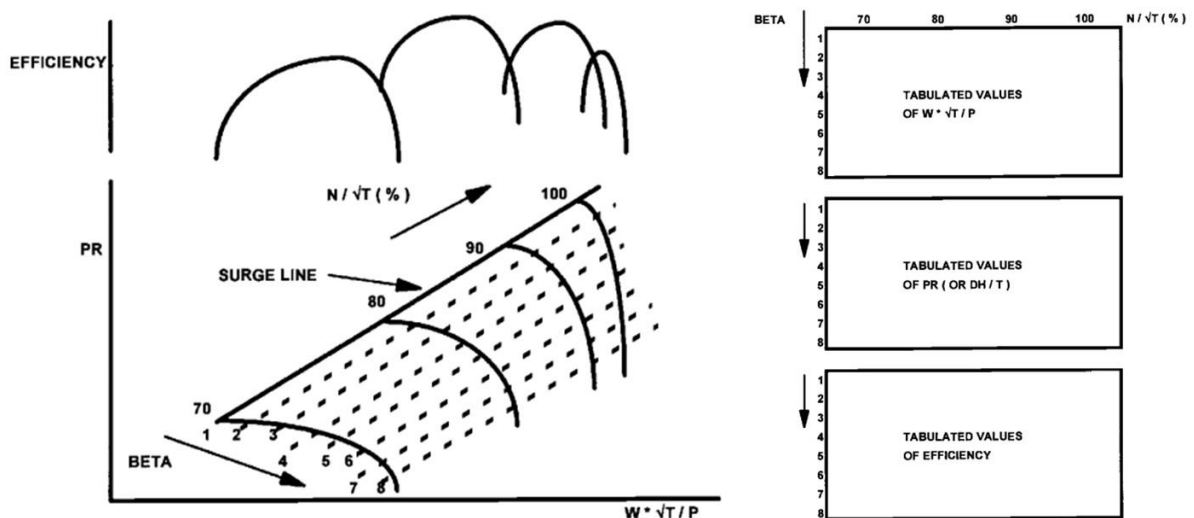
## 4.2 Gas turbine model

### 4.2.1 Overview and main techniques of modeling Brayton cycle-based plants

Gas turbine models have been developed for decades to be applied both for power generation and propulsion. Much before the coining of the term ‘digital twin’, gas turbine models have been operating in model-based control systems, online fault diagnostic systems, full-scope training simulators, and embedded systems (BOYCE, 2006).

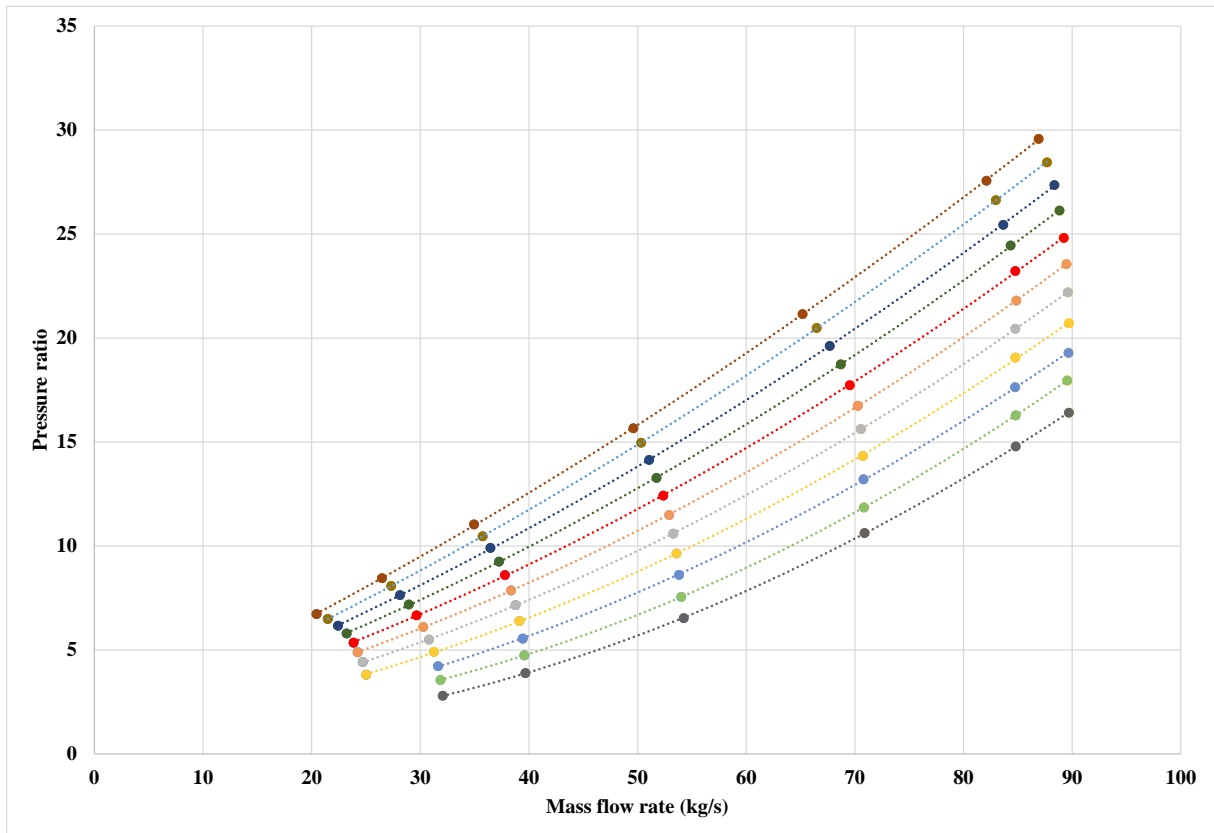
A vast description on the fundamentals of gas turbine dynamic modeling is given by (WALSH, FLETCHER, 2004) in their handbook, with rules to be followed for the simulation of the engine behavior in design, off-design, and transient conditions, including mathematical models and algorithms to predict the gas turbine performance. Some techniques discussed in the handbook are worth mentioning. The compressor modeling is an important component of the overall gas turbine models and relies in the suitable selection and use of the compressor maps. Converting the maps to data to be understood by the simulating algorithm requires the use of tables and tabulating schemes. One option is to use the beta lines, arbitrary lines parallel to the surge line. The points where the beta lines cross the lines of the maps define the arrays and tables, as illustrated in Figure 28. The beta lines plot on a GE LM2500+ map (HAGLIND, ELMEGAARD, 2009) is given in Figure 29.

Figure 28 – The compressor map and beta lines tabulating method.



Source: Walsh and Fletcher (2004).

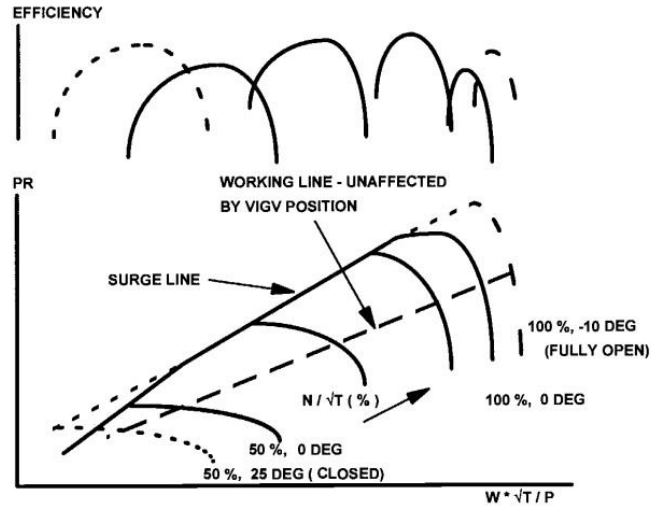
Figure 29 – Beta lines plot over a mass flow rate map.



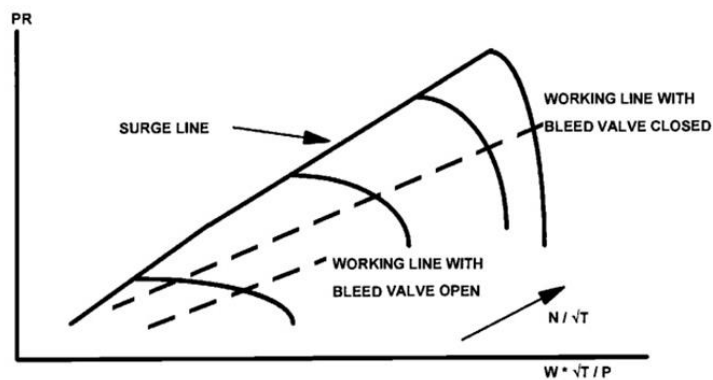
Source: Adapted from Haglind and Elmegaard (2009).

In addition, IGVs and bleed valves play an important role in machine surge, power, and temperature control and cause a change in flow rate and aerodynamics. Changes in IGV or bleed valves position lead to changes in the compressor maps, which means that the compressor map is unique for a fixed value of inlet flow angle and bleed valve position. If available, one way to account for these geometry and flow pattern changes is to use working lines, as shown in Figure 30.

Figure 30 – Effect on the compressor map caused by the geometry change in the IGV (a) and the working line caused by the air bleeding (b).



(a)

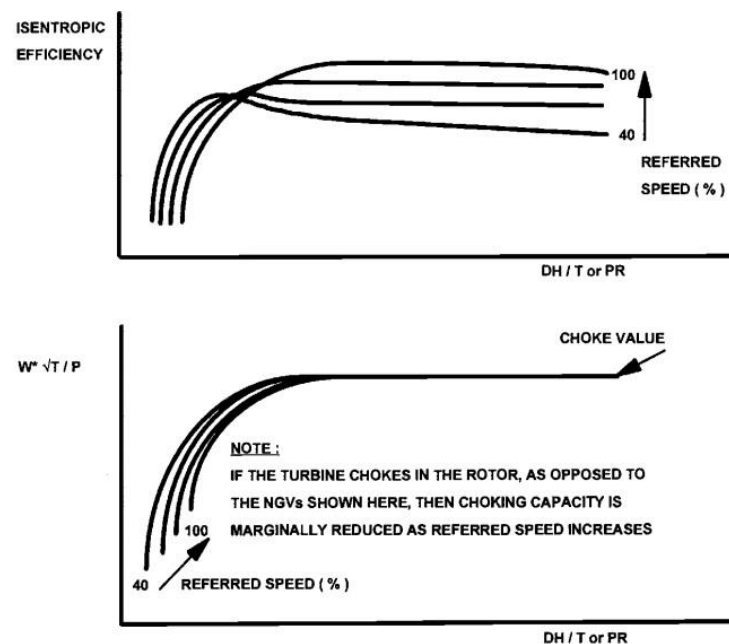


(b)

Source: Walsh and Fletcher (2004).

The turbine (expander) can also be modeled with the support of maps, mainly if low loads are considered to be evaluated. Figure 31 shows a typical turbine map. An important point to be noted is that, for a fixed shaft speed, the values of the corrected mass flow rate and efficiency are constant for higher pressure ratios.

Figure 31 – The turbine map.



Source: Walsh and Fletcher (2004).

One of the challenges in modeling a gas turbine is computational matching among the aerodynamic and mechanically coupled components. Adjusting the thermodynamic operating point of all components simultaneously requires a well-posed algorithm and a robust solver. When considering the transient performance, this task grows in complexity since the control system particularities must be taken into account.

Other relevant modeling considerations are presented in the work of Camporeale, Fortunato and Mastrovito (2006), mainly related with lumped models for dynamic simulation of gas turbines. Specific details on the model and the components organization are given below.

- Compressors and turbines can be modeled as volumeless elements; a plenum is introduced between these elements to take into account the gas dynamics.
- The algebraic equations are arranged in such a way that the output values can be obtained from the input variables without iterative calculations.
- The compressor maps can be taken from the literature, even with the available map refers to an old model of the equipment. The aerodynamics of the equipment tends to be very similar.
- The burner (combustor) can be represented as a pure energy accumulator, neglecting the mass balance that is instead attributed to the upstream plenum block.

- For the turbine, the inlet flow is considered to be choked and then, the inlet corrected mass flow and the isentropic efficiency is considered constant.

#### 4.2.2 Mathematical model

Considering the abovementioned elements and the proposed scope of this work, a gas turbine model that can reproduce the real machine dynamic behavior is important once it: (i) plays a major role in FPSO thermal efficiency; (ii) it is required to change loads constantly; the dynamic conditions are of major interest; (iii) the model can be used to test the ORC design in several situations of interest. Gas turbine models have been described in the literature throughout the years, being applied to dynamic and steady state problems, and being introduced into commercial and scientific software. The model selection, evaluation, and implementation demand the observation of the following criteria:

- The goal of the simulation, e.g.: performance evaluation, model-based control, operator training, etc.
- The availability of data concerning the specific equipment to be modeled.
- The accuracy level to be achieved for specific variables.
- The gas turbine type and application.

Another relevant aspect to be taken into consideration to properly define the model is how the gas turbine components are matched. The LM2500+ has a 17 stage axial compressor mechanically coupled to a two-stage turbine and both components compound the gas generator. The power turbine is coupled to a gearbox, and the latter is coupled to the electric generator<sup>4</sup>. Air enters into the compressor and, after being compressed, enters the combustion chamber. Then, the hot gases enter the gas generator turbine and are expanded to provide enough power for compression. After leaving the gas generator, the gases enter the power turbine and are expanded to provide shaft and then electrical power. The inlet guide vanes and the fuel valve are tuned by the control system as a function of electrical power and the power turbine exhaust gas temperature<sup>5</sup>. A global view of the LM2500+ is shown in Figure 32.

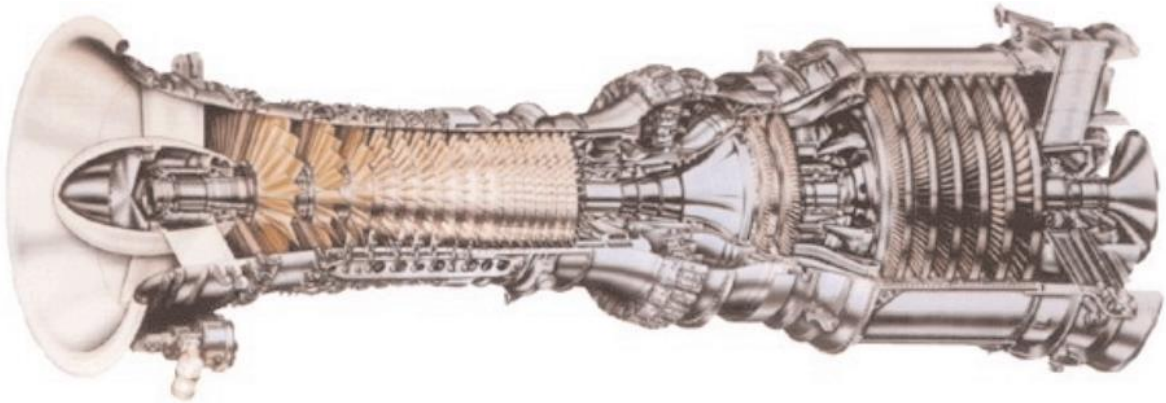
---

<sup>4</sup>The case study of this work is the application of the GE LM2500+ for power generation. This equipment is also widely used for mechanical driving.

<sup>5</sup> The exhaust temperature control is of major importance in the case of combined cycles, where the global thermal efficiency is maximized, even if the Brayton cycle efficiency diminishes. The robust PID control model described in section 4.2.3 enables a substantial reduction in the complexity of the ORC control model to be presented in section 4.4.1.



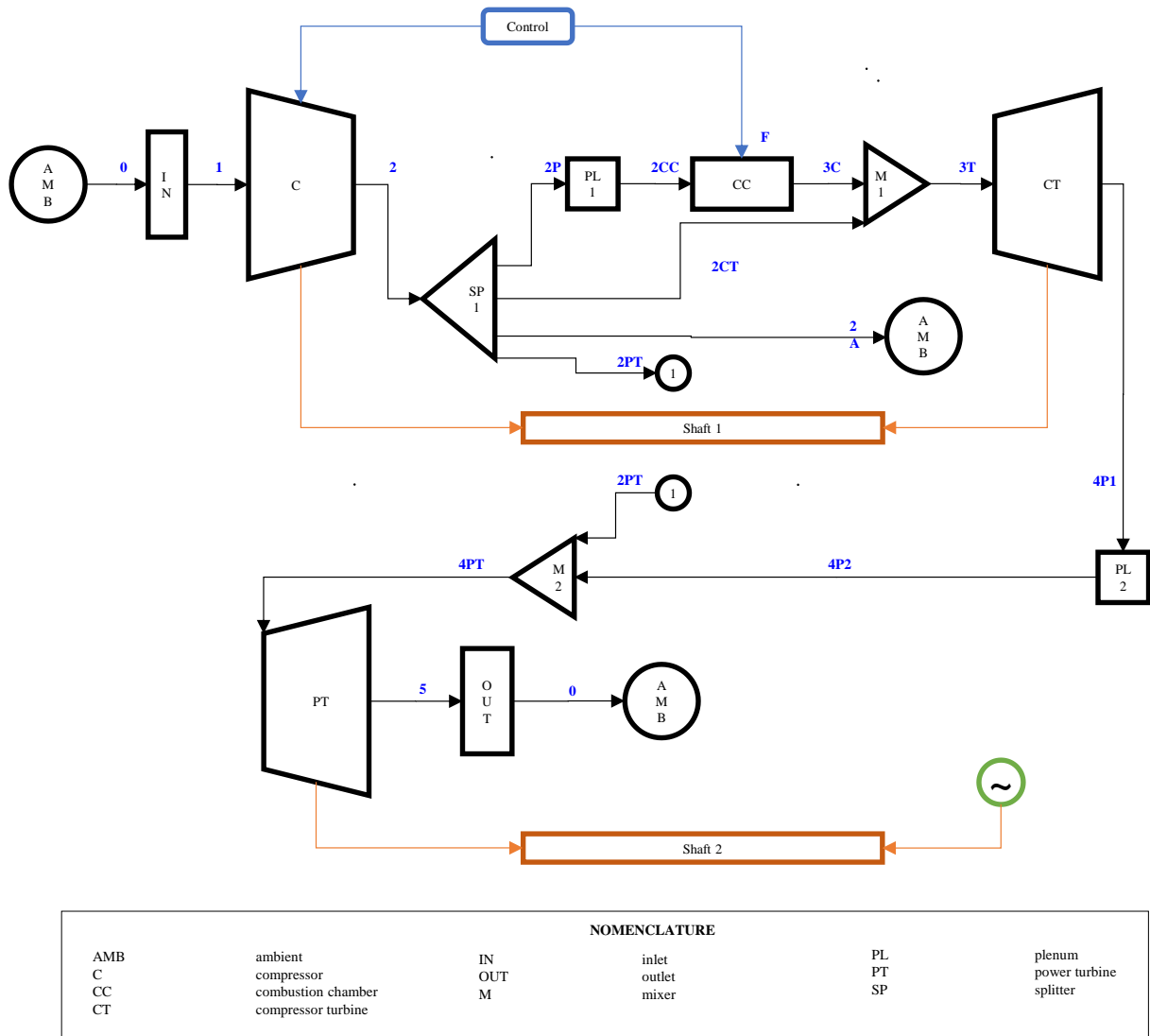
Figure 32 – The GE LM2500 cut view.



Source: Badeer (2000).

The mathematical model here presented is based on classic works regarding gas turbine modeling (COHEN, ROGERS, SARAVANAMUTTOO, 1996) (WALSH, FLETCHER, 2004) (KURZ, 2005) and specific works on models representing the LM2500 performance (CAMPOREALE, FORTUNATO, MASTROVITO, 2006) (HAGLIND, ELMEGAARD, 2009) (MEYER et al., 2014). The components arrangement defined for the model used in this work is shown in Figure 33. Each component and its modeling are going to be discussed in details.

Figure 33 – LM2500+ components coupling model. The streams codes and the components names are the same used throughout the equations.



Source: Author.

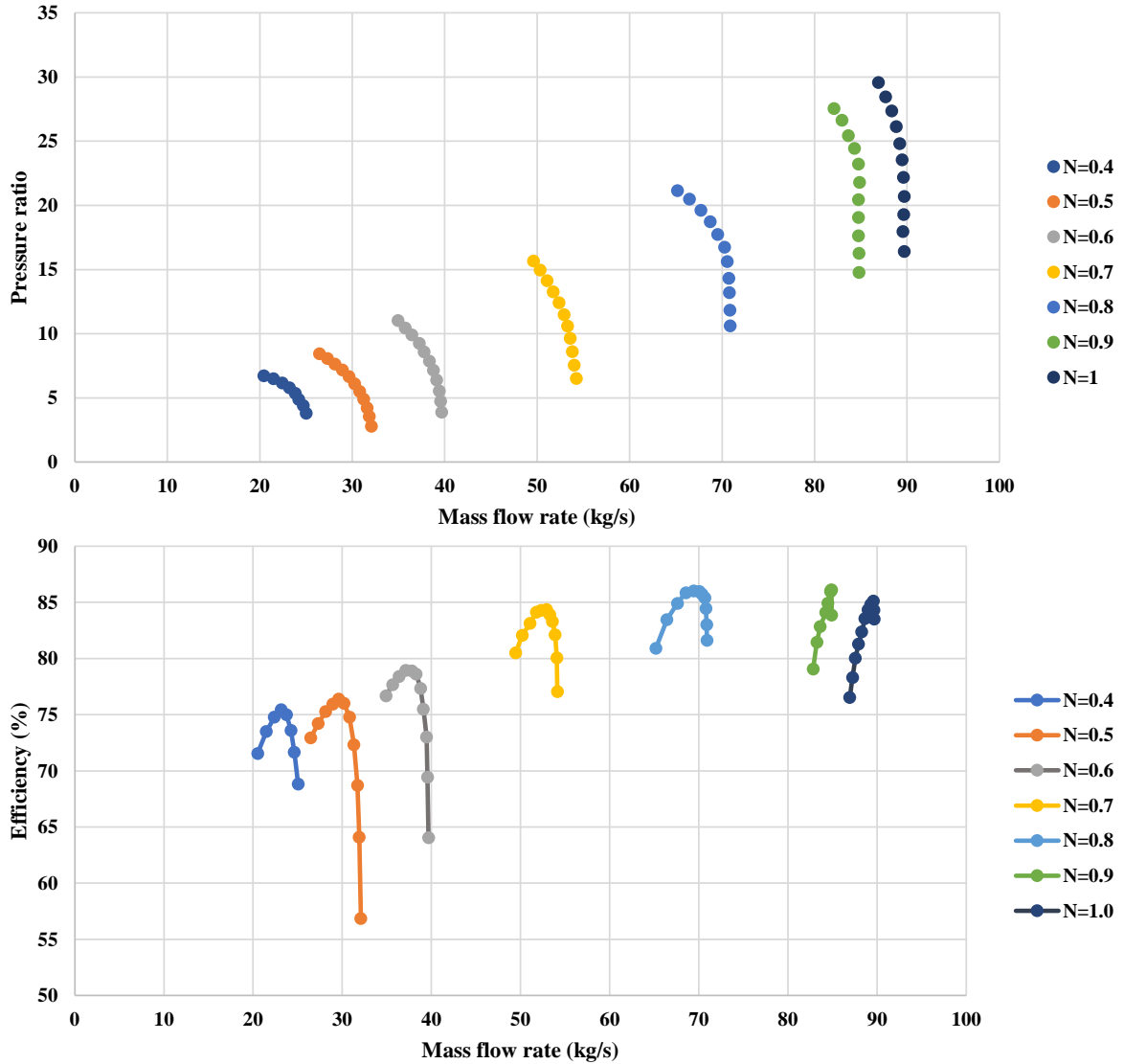
The pressure drop at the compressor inlet is a fixed parameter, and it is used to calculate the compressor inlet pressure accordingly with Equation (1).

$$p_1 = p_0(1 - \Delta p_{IN}) \quad (1)$$

The compressor behavior is described, in terms of its main parameters, by its characteristics maps, which presents the relationship among the air mass flow rate, isentropic

efficiency and pressure ratio. Figure 34 presents a nonnormalized compressor map for the LM2500+.

Figure 34 – LM2500+ compressor maps ( $N = \frac{N_1/\sqrt{T_1}}{N_{1DP}/\sqrt{T_{1DP}}}$ ).



Source: Adapted from Haglind and Elmegaard (2009).

Therefore, given the air mass flow rate, the compressor pressure ratio is calculated through the maps and, then, the compressor outlet pressure is given by,

$$p_2 = p_1 PR_C. \quad (2)$$

Once the compressor outlet pressure is calculated and the pressure ratio and efficiency come from the maps, the outlet temperature can also be determined,

$$T_2 = T_1 \left[ 1 + \frac{1}{\eta_c} \left( PR_C^{k_c - 1/k_c} - 1 \right) \right]. \quad (3)$$

As long as pressures and temperatures are known in the intake and exhaust, the compressor demand power is calculated by,

$$\dot{W}_C = \dot{m}_1 (h_2 - h_1). \quad (4)$$

Figure 33 introduces some components that are used in the model to accommodate premises and balances, such as the splitter and mixer. Air bleeds are taken from the compressor for surging control and turbines blade cooling, however, the exact position from where these bleeds are taken, i.e., after which stage, is unknown<sup>6</sup>. The splitter is thereupon used to comply with the mass balance as a result of these extractions, which are represented as fixed fractions in equations (5), (6), (7) and (8) map (HAGLIND, ELMEGAARD, 2009).

$$\dot{m}_{2A} = \dot{m}_2 y_{2A} \quad (5)$$

$$\dot{m}_{2PT} = \dot{m}_2 y_{2PT} \quad (6)$$

$$\dot{m}_{2CT} = \dot{m}_2 y_{2CT} \quad (7)$$

$$\dot{m}_{2P} = \dot{m}_2 - \dot{m}_{2CT} - \dot{m}_{2PT} - \dot{m}_{2A} \quad (8)$$

So far, no transient behavior was considered in the model because it is taken as premise that the air volume in the compressor is negligible. In order to represent the transient behavior

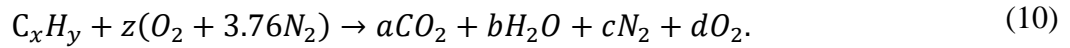
---

<sup>6</sup> This is commonly considered proprietary information.

of the gases, a plenum is used between the splitter and the combustion chamber, where the mass balance is represented by Equation (9).

$$\frac{dp_{2CC}}{dt} = p_{2CC} \frac{k_{PL1}}{M_{PL1}} (\dot{m}_{2CP} - \dot{m}_{2CC}) \quad (9)$$

In the combustion chamber, turbulent fuel-air mixing, ignition and burning take place, and the working fluid sees the addition of thermal energy. The model of this component can be defined into two parts. The first part refers to the combustion model, whereupon a generic fuel is considered and follows the reaction,



which allows the use of a generic hydrocarbon as fuel if its carbon-hydrogen ratio is known. The fuel to air ratio can be represented by Equation (11).

$$FAR = \frac{\dot{m}_F}{\dot{m}_{2CC}} \quad (11)$$

Considering the need to deal with a working fluid that is a mixture of gases, its thermodynamic properties are calculated from a weighted average of the properties of these components, considering the weights as the molar fraction of each gas, given in terms of the vector  $[fN_2, fO_2, fCO_2, fH_2O]$ .

Considering that the fuel mass flow rate is given by the actuation of the control system over the fuel valve and the air mass flow rate is known, it is possible to calculate the stoichiometric coefficients  $a$ ,  $b$ ,  $c$ , and  $d$  in each distinct operating point and, hence, the gas composition is also calculated as well as its thermodynamic properties.

The second part of the combustion chamber model refers to the energy balance over a single control volume represented by the Equation (12).

$$\frac{dT_{3CC}}{dt} = \frac{k_{CC}}{M_{CC}c_{p,CC}} (\dot{m}_{2CC}h_{2CC} - \dot{m}_F\eta_{CC}LHV - \dot{m}_{3C}h_{3C}). \quad (12)$$

A mixer is used to join all the main stream coming from the combustion chamber with the cooling stream coming from the compressor. The algorithm of this component considers the compositions of the streams to determine the composition of the gas after mixing. Accordingly, an energy balance is performed to have the thermodynamic state downstream calculated.

The turbines modeling (expanders, where the thermal energy is converted into shaft power) assumes that the flow is choked at the component nozzle, and, because of that, the relationship shown in Equation (13) is valid.

$$C_{CT} = \frac{\dot{m}_{3T}}{(p_{3T}^2 - p_{4P1}^2)} \sqrt{T_{3T}} \quad (13)$$

and, in this case, the expander efficiency can be taken as a constant value, even though this consideration can lead to higher discrepancies in lower loads. The most recommended practice is to use turbine maps, when available. The expander exhaust temperature can be calculated by Equation (14),

$$T_{4P1} = T_{3T} \left[ 1 - \eta_{CT} \left( 1 - ER_{CT}^{k_{CT}-1/k_{CT}} \right) \right]. \quad (14)$$

where,

$$ER_{CT} = \frac{p_{4P1}}{p_{3T}}. \quad (15)$$

The other components shown in Figure 33 but not mentioned so far can be modeled similarly to the equivalent components already presented (M2  $\approx$  M1; PL2  $\approx$  PL1; PT  $\approx$  CT; OUT  $\approx$  IN).

At this point, it is necessary to discuss the mechanical couplings in the LM2500+ model. This gas turbine is a two-shaft prime mover, where the gas generator consists of a compressor mechanically coupled to a turbine and, independently, the power turbine is coupled to an electric generator. The shaft speed can be calculated using Equation (16). The power turbine is coupled to an electric generator and, therefore, it is considered that the shaft speed is constant and equivalent into the electric frequency of 60 Hz, although it would follow a similar mathematical model if transitory electric phenomena are simulated.

$$\frac{dN_1}{dt} = \frac{N_{S1,DP}^2}{N_{S1}} (\dot{W}_{CT} - \dot{W}_C). \quad (16)$$

Finally, these equations can be used directly or with minor modifications for the development of the LM2500+ model and similar equipment. Nevertheless, some challenges need to be overcome independently of the machine type:

- Multiple parameters, such as pressure drops and efficiencies, need to be calibrated simultaneously.
- The gas turbine manufacturers restrict the access to compressor maps and even those available in literature need to be carefully treated.
- Operation or experimental data need to be carefully evaluated and treated, when available.
- The minimal amount of information about the control system can enrich the model and lead to the most accurate results.

#### 4.2.3 Control system

There are a multitude of scientific works discussing gas turbine control methodologies in the literature, but detailed design or model selection is out of the scope of the here presented modeling approach. However, the dynamic simulation of the LM2500+ demands an appropriate model that can reproduce the machine behavior during the load change, even though no detailed information on the control system of the equipment to be modeled is known. Then, given that the proportional-integral-derivative (PID) control is used in the majority of the industrial systems (LEVINE, 1999) (ASTROM, MURRAY, 2020), this method is adopted to simulate the power control in the gas turbine model presented here. The global arrangement of the

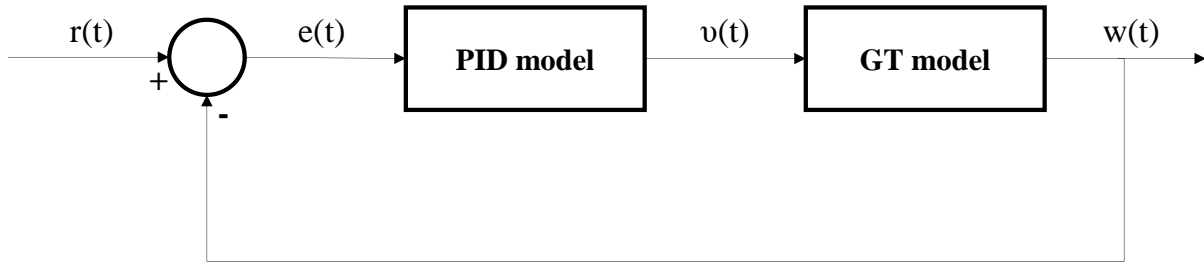
feedback control is shown in Figure 35. In this work, the control approaches will be given in the time domain. The GT model calculates the corrected load  $w(t)$  in each timestep, which is compared with the load setpoint defined by the user. The error is then calculated through the Equation (17),

$$e(t) = r(t) - w(t), \quad (17)$$

and the PID signal is given by,

$$v(t) = \kappa_p e(t) + \kappa_i \int_0^t e(t) dt + \kappa_d \frac{de(t)}{dt}. \quad (18)$$

Figure 35 – The control feedback defined for the gas turbine simulation. The output signal  $w(t)$  is the calculated load, which is compared with the setpoint  $r(t)$ .



Source: Author.

Here, the control signal  $v(t)$  represents the normalized fuel flow rate,  $\dot{m}_{F,norm} \in [0,1]$ , which is used as input for the gas turbine model. One of the major challenges of the use of the PID model is its parameter tuning to achieve system stability at an acceptable response time. Although some techniques can be employed for the tuning, such as the Ziegler-Nichols method (ASTROM, MURRAY, 2020), the approach taken in this work applies optimization methods for the proper determination of the parameters  $\kappa_p$ ,  $\kappa_i$  and  $\kappa_d$ , taken as design variables. The particle swarm method was used to provide these parameters, and the GT model was used as an objective function, returning a value accordingly with the following rules:

- A penalty value if convergence is not achieved.
- A penalty value if the system becomes unstable.
- The deviation between the time where the load setpoint was achieved by the model and that given as reference, taken from the literature (MEYER et al., 2014).



The detailed analysis on the optimization results and its consequence for the dynamic simulation will be given in Section 6.1.

#### 4.2.4 LM2500+: performance data selection and constructive information

As mentioned before, the LM2500 family has a long operational history, and the modeling of the most recent equipment requires careful selection of the constructive and performance parameters available in the literature. To guide the development of the model here presented, the information provided by Haglind and Elmegaard (2009) is used and the main performance data are shown in Table 5. Additionally, the compression bleeding configuration shown in Figure 33 is also based on this work.

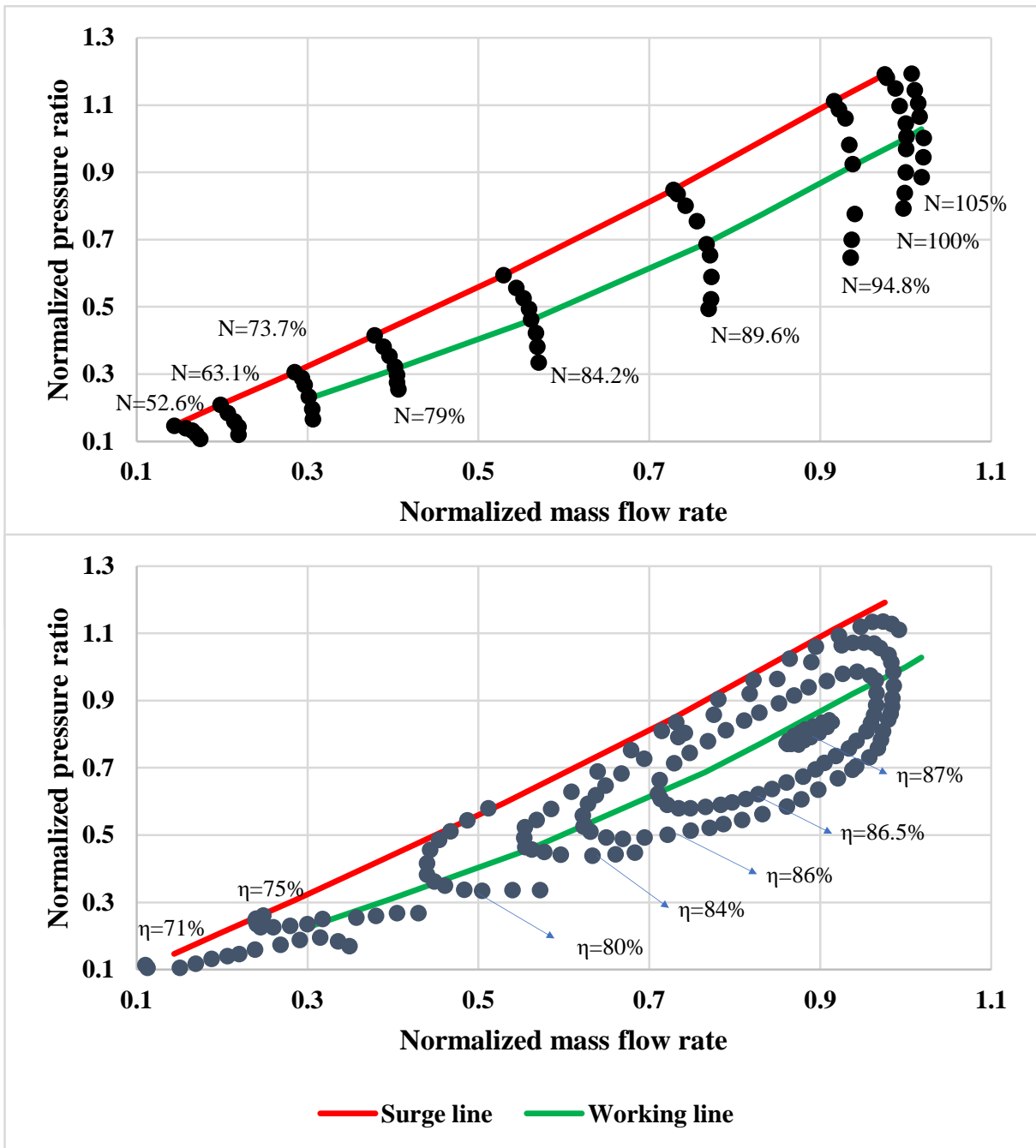
Table 5 – GE LM2500+ performance data at design point.

<b>Parameter</b>	<b>Value</b>
Inlet mass flow (kg/s)	88.4
Fuel flow (kg/s)	1.9
Compressor outlet temperature (°C)	495
Power turbine exhaust temperature (°C)	534
Compressor pressure ratio (-)	23.5
Electric power (MW)	23.5
Thermal efficiency (%)	37.7

Source: Haglind and Elmegaard (2009).

The selection of compressor maps is a key element for the successful gas turbine simulation. In this case, the map provided in the work of Klapproth, Miller and Parker (1979), shown in Figure 36, was used. Despite the fact that the map is of a quite old LM2500 model, it brings valuable information: the engine working line. This curve conceals the information on the path imposed by the inlet guided vanes on the compressor as the load varies and, since no detailed information on the control system is known, the working line allows the model to simulate off-design conditions accurately.

Figure 36 - Compressor characteristics used for the simulation LM 2500+.



Source: Adapted from Klapproth, Miller and Parker (1979).

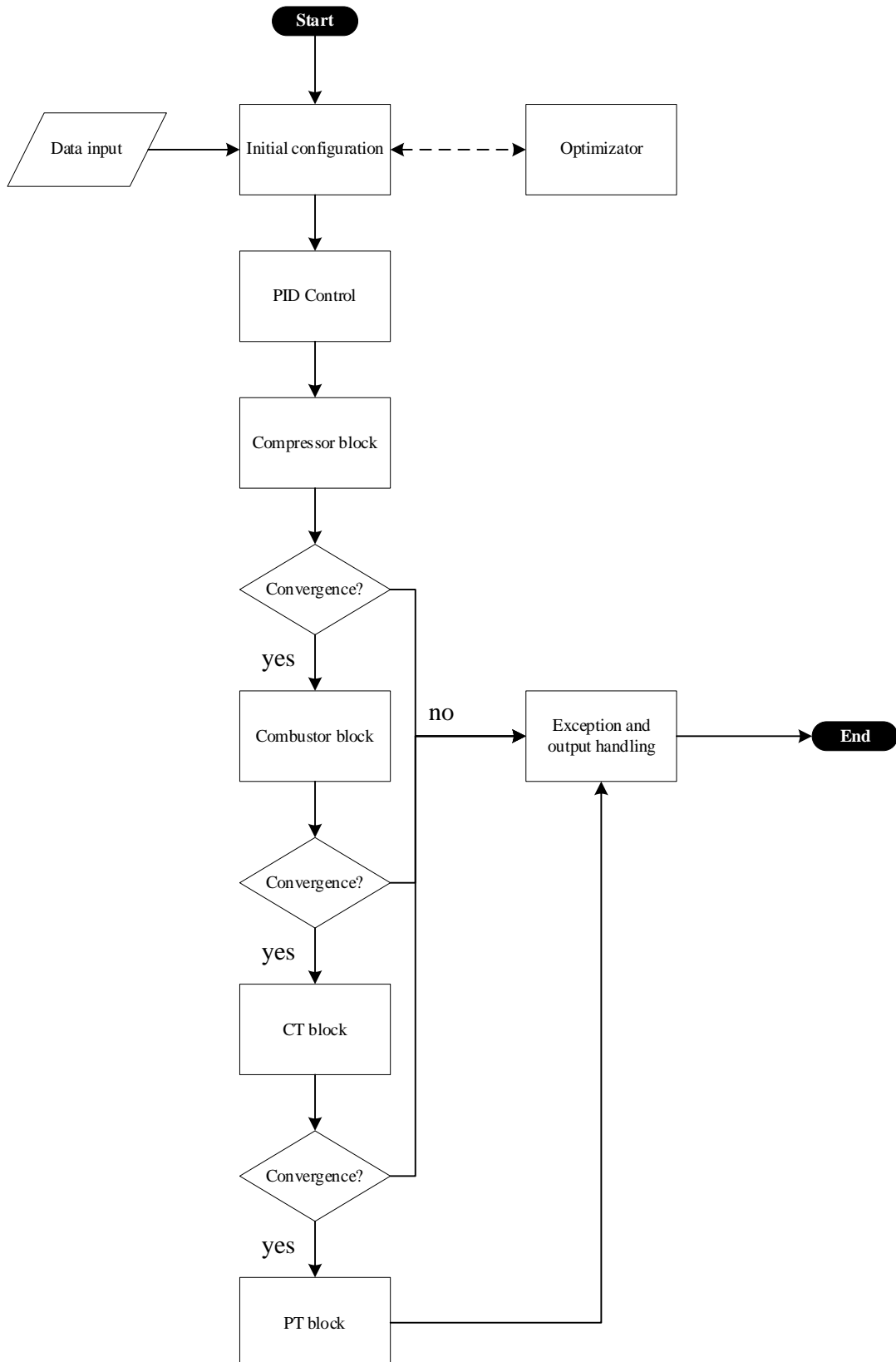
#### 4.2.5 The gas turbine computational model

Once established the main equations, the proper computational design needs to be made as a basis for the system development. Thereupon, the first step to build the computational model is to define its main requirements, as listed below:

- The system shall run steady-state and dynamic cases.
- Since there is a number of possibilities on the fuels to be used offshore, such as diesel and natural gas, the model shall allow some flexibility of choice.
- The model need to allow gas mixtures in order to represent the gas turbine working fluids and streams arrangements.
- An optimization suite needs to be included in the system to allow parameter fitting.

As shown in Figure 37, the system receives as input the ambient conditions (pressure and temperature), the initial state, the target load, and the time interval to simulate. Therefore, the model is initialized, and the control system defines the intake air mass flow rate and the fuel flow accordingly to the current load. Next, the compressor block calculates the behavior of this component. If there is an issue in convergence, the exception handler is called and terminates the execution. The process is similar to the other blocks and it continues until the last component is calculated.

Figure 37 - Computational model of the gas turbine - view on the workflow for each timestep.  
 In some cases, the block modules comprise the naming component and other minor components, e.g., Splitter 1 and the Plenum 1 are included in the Compressor Block; Plenum 2 and Mixer 2 are included in the CT block.



Source: Author.

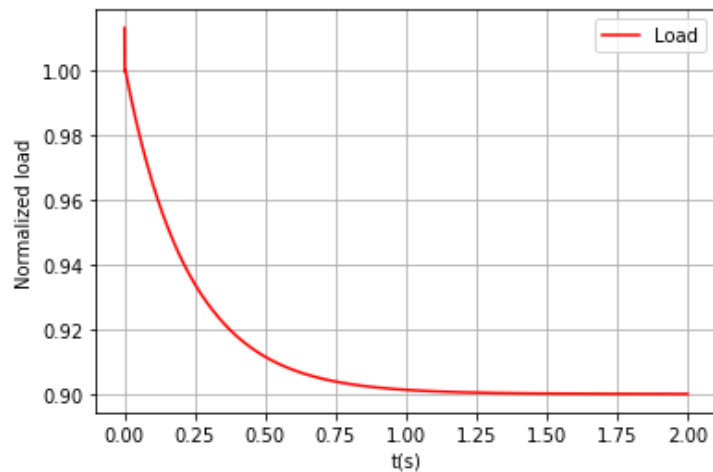
#### 4.2.6 Calibration methodology applied to simulate the FPSO gas turbine

Data from a real LM2500+ were used to calibrate the model. The design point was parametrized according to a single-objective optimization procedure, which was configured as presented below:

- (i) Definition of the design vector as:  $\bar{x} = [\eta_{CT}, \eta_{PT}, \eta_{ME}, \eta_M, \Delta p_{CC}, \Delta p_{CTPT}]$ , where  $\eta_{CT}$  and  $\eta_{PT}$  refers respectively to the isentropic efficiencies of the gas generator turbine and power turbine;  $\eta_{ME}$  is the efficiency that gathers the combined effect of mechanical and generator losses;  $\eta_M$  accounts for the mechanical losses in the gas generator; and  $\Delta p_{CC}$  and  $\Delta p_{CTPT}$  are, respectively, the pressure losses in the combustion chamber and between the gas generator and the power turbine.
- (ii) Definition of the model output as the objective function result. The following variables were selected to be compared with the reference:  $\dot{W}_E$ ,  $T_5$  and  $\dot{m}_F$ . In fact, this is a multi-objective problem transformed into a single objective one. The output taken as result is the sum of the differences between these values and those from the reference.
- (iii) The particle swarm optimization method was used with a swarm size of 1200 individuals,  $c_1 = c_2 = 0.5$  and  $\omega = 1.0$ .

The calibrated parameters for the design point are used in the model as fixed values for all load conditions. The values corresponding to the simulated design point conditions are presented henceforth as the 100% load condition. It is worth to mention that the gas turbine model here developed always perform transient calculations. Consequently, the steady state results presented in this subsection are the results of the calculation after the transient, once the load is stabilized, as Figure 38 shows.

Figure 38 - Load maneuver from 100% to 90% load. The steady-state results at 90% load are taken in  $t = 2$  s.



Source: Author.

### 4.3 Modeling Organic Rankine cycles

#### 4.3.1 Overview of techniques applied to modeling Rankine cycle-based plants.

Numerous approaches are available for the development of dynamic models for Rankine power plants. However, the modeling requires the scrutinization of several methodologies to verify its suitability to the system requirements, the equipment coupling arrangement, and the availability of operational and technical data. In the case here in discussion, the development of such nonlinear models aims to describe the ORC system-level behavior. Therefore, the ORC model developed in this work, rather than that developed for the gas turbine, does not have the objective of simulating a specific subsystem in a micro-component level. In the case here presented, the model is an auxiliary system for the ORC design and control system tuning and therefore need to be implemented to be suitable to these applications.

The system-level approaches presented in this section follow the general guidelines provided in the works dedicated to steam power plants and ORC (ORDYS et al., 1994) (COLONNA, PUTTEN, 2007) (PUTTEN, COLONNA, 2007) (CASELLA et al., 2013), mostly driven to the development of hi-fidelity power plant simulators.

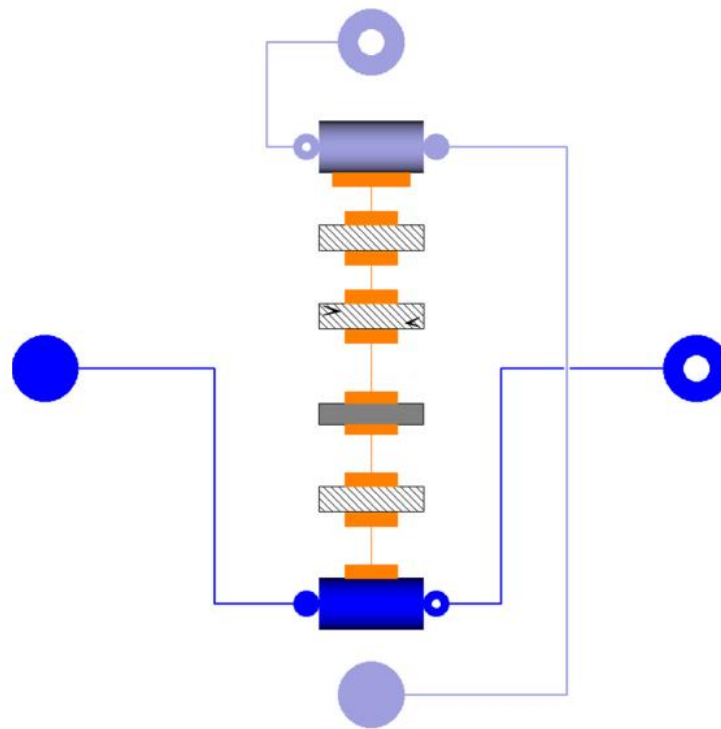
As discussed in the case of the gas turbine modeling, presented in Section 4.2.1, the construction of the model based on the components is a path to provide modularity to the system. This equipment-level approach is the same developed for ThermoPower in Modelica (CASELLA, LEVA, 2003), which has been used in several works related to ORC modeling, as seen in Chapter 2.

Regarding the mathematical model, for each component/equipment to be applied to compound the ORC system, the conservation equations are applied, in conjunction with its constitutive equations. In a general view, the following good practices can be applied for the ORC equipment and other components:

- For turbines, as presented for the expander in the gas turbine case, the inlet nozzle can also be considered choked.
- The condenser pressure is typically a design parameter. Therefore, the condenser can be considered a fixed pressure sink.
- Pump models can be described by their characteristic curves, if available. If these curves are not available, the model can be simplified using a generic head (polynomial) curve.
- The global convective heat transfer coefficient is selected according to the type of the heat exchanger. The type typically selected for ORC applications is the shell and tube.
- Storage and resistive models can be added to equipment-specific components. The storage models that are most commonly applied are the plenum to accommodate the fluid dynamics when in gas phase, and the solid (wall) heat accumulation module.
- Fluid properties are calculated from libraries as much as possible.

Even with dedicated constitutive equations for each equipment, depending on its complexity, the model can be composed of the combination of several components. For example, the evaporator shown in Figure 39, is modeled by the combination of a heat exchanger module, plenums, and solid storage components. Figure 40 presents an even more complex composition, developed by using a modular and causal approach.

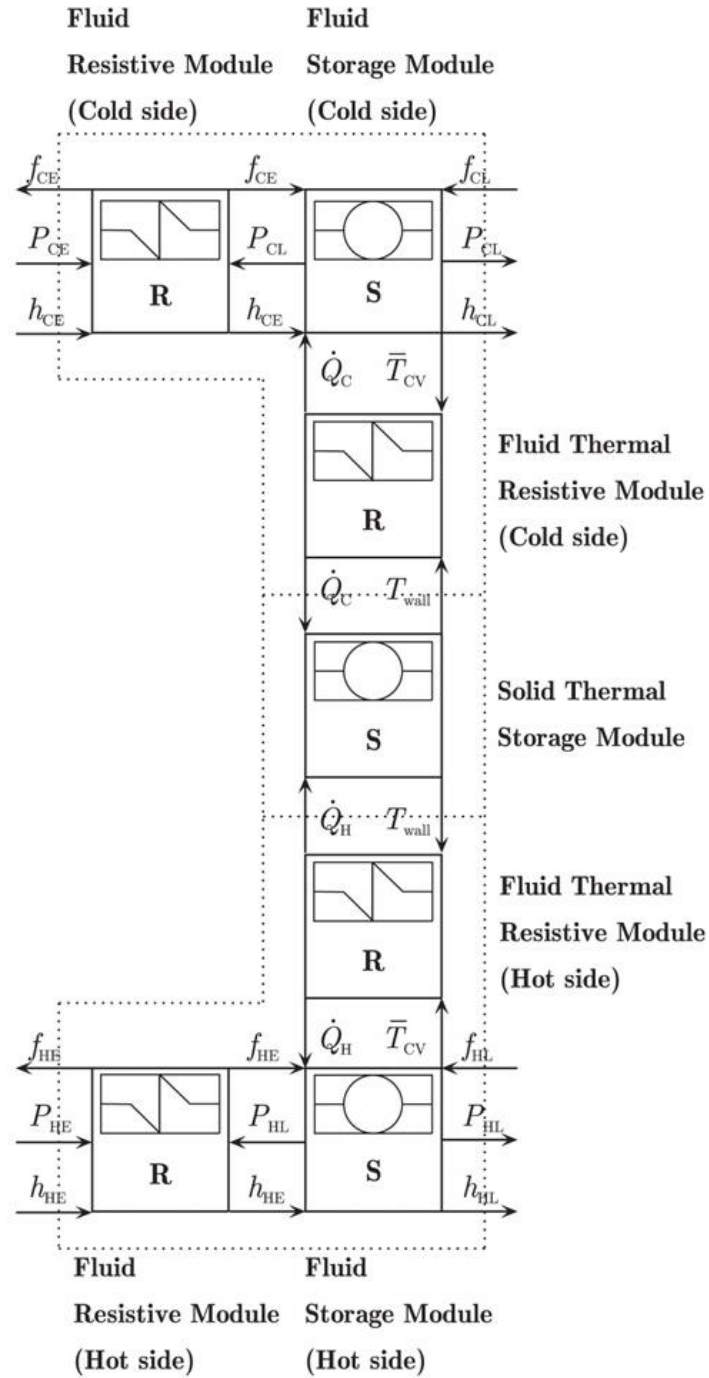
Figure 39 – Multi-component model of the ORC evaporator.



Source: CASELLA et al. (2013).

Figure 40 - Model of the heat exchanger in a modular and causal approach. This technique improves the reusability and reconfiguration, but the mathematical model imposes an extra simplification to allow simultaneous solution of the DAE system.





Source: Colonna and Putten (2007).

The lumped dynamic model that arises from the application of these techniques leads to a differential and algebraic system of equations, as represented by Equation (19).

$$\bar{\Phi}(\bar{x}, \dot{\bar{x}}, t) = 0 \quad (19)$$

The solution of this system is non-trivial and requires extensive numerical effort. Therefore, adopting a modular approach, it is possible to break down the intricate system into

independent sub-problems, reducing the complexity of the overall mathematical problem. The modular approach implies that the system described in Equation (20), smaller subsystems can be composed by the functions  $\Phi_i$  and solved independently.

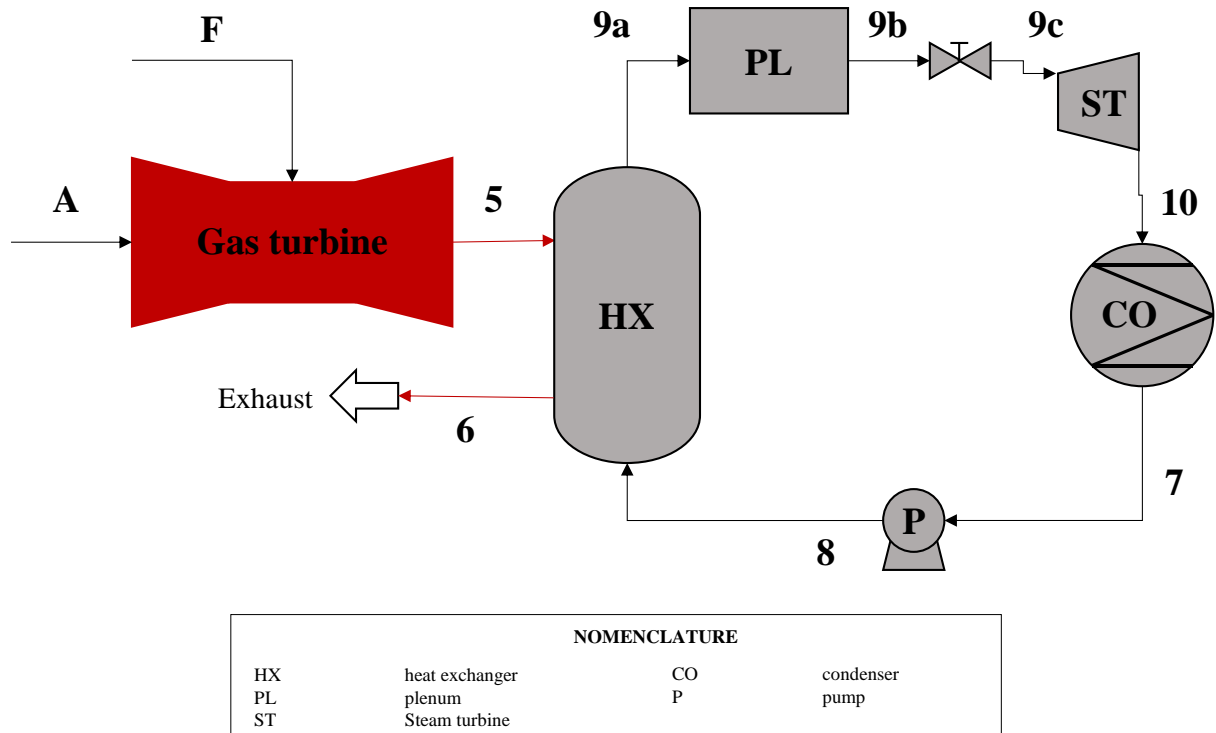
$$\left\{ \begin{array}{l} \Phi_1(\bar{x}, \dot{\bar{x}}, t) = 0 \\ \Phi_2(\bar{x}, \dot{\bar{x}}, t) = 0 \\ \vdots \\ \Phi_{n-1}(\bar{x}, \dot{\bar{x}}, t) = 0 \\ \Phi_n(\bar{x}, \dot{\bar{x}}, t) = 0 \end{array} \right. \quad (20)$$

#### 4.3.2 The ORC model

Model-based design is an approach that allows the evaluation of the equipment configuration and the test of the plant under several operational scenarios. Specifically, for the work presented in this thesis, the ORC model is of the utmost importance, since the generated designs will be applied to two complex systems in oil platforms: the gas turbine and the compressor.

Moreover, the ORC model plays an important role in the design process, since it operates as the objective function for the optimization system, as will be discussed in Section 5.1. This model was developed as a modular composition of components of the ORC cycle according to the arrangement defined for each heat source. Figure 41 presents the arrangement for the heat recovery from the GE LM2500+.

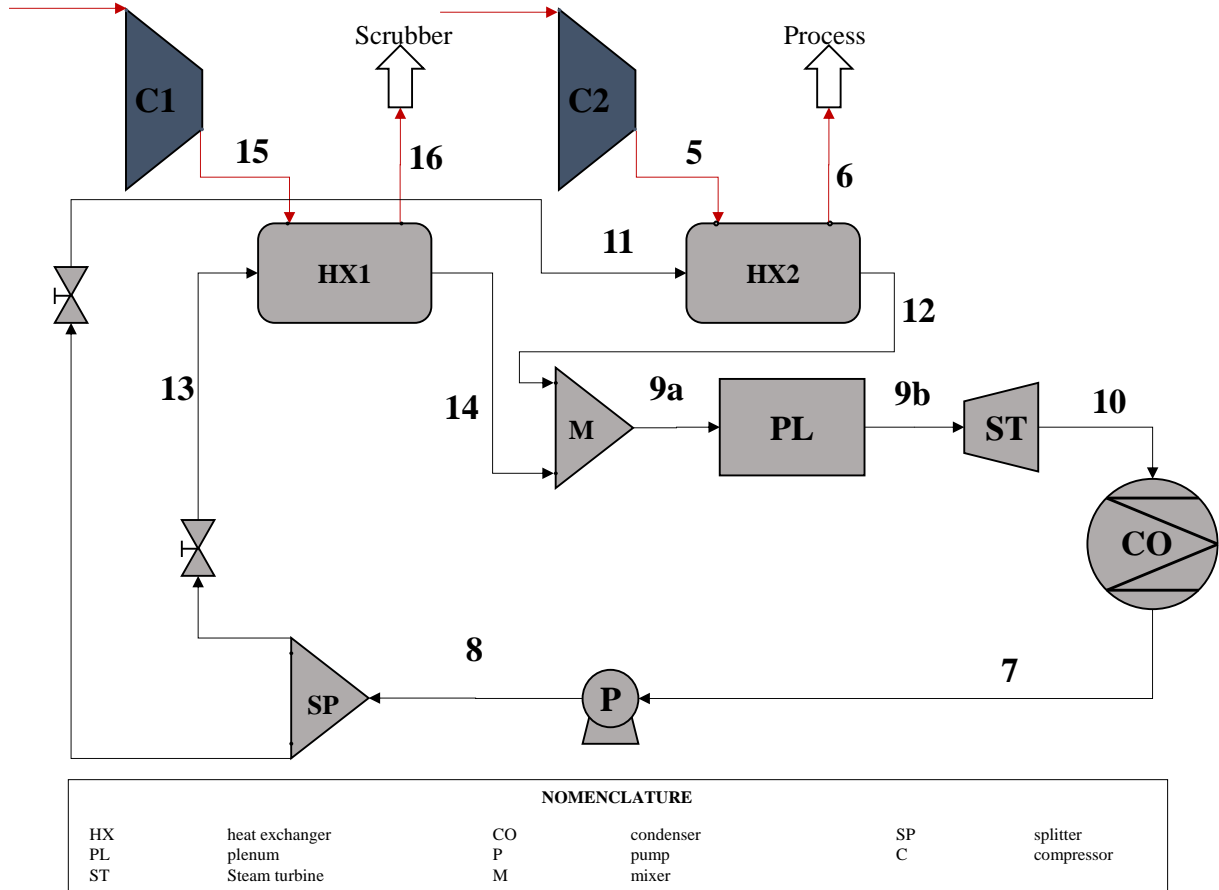
Figure 41 - ORC equipment arrangement for gas turbine waste heat recovery.



Source – Author.

Since the computational model for each component/equipment is modular, its mathematical model is the same applied for the gas turbine and compressor scenarios. The only difference is in the arrangement. The arrangement defined for the heat recovery and temperature control on the compressor train is presented in Figure 42.

Figure 42 - ORC arrangement proposed for the heat recovery and temperature control of the compression train.



Source – Author.

The mathematical model for each equipment was based on works presented in the literature regarding plant simulation (ORDYS et al., 1994) (COLONNA, PUTTEN, 2007) (QUOILIN et al., 2011) (CASELLA et al., 2013) (PIEROBON et al., 2014) and can be described as follows: the conservation equations are applied for each equipment, as defined in Equations (21) and (22).

$$\frac{d\rho V}{dt} = \sum \dot{m}_i - \sum \dot{m}_o \quad (21)$$

$$\frac{d\rho V u}{dt} = \dot{Q} - \dot{W} + \sum \dot{m}_i h_i - \sum \dot{m}_o h_o \quad (22)$$

Specifically for the heat exchanger, in this case an evaporator, the heat transfer rate is given by,

$$\dot{Q}_{HX} = A_{HX} U_{global} \Delta T_{LM}, \quad (23)$$

where the value of  $A_{HX}$  is calculated according to the shell and tube design method presented by Kakaç, Liu and Pramuanjaroenkij (2002). The heat transfer coefficient is given by (COLONNA, PUTTEN, 2007):

$$U_{global} = \beta \dot{m}_5^\alpha, \quad (24)$$

and

$$\Delta T_{LM} = \frac{((T_{Hi} - T_{Co}) - (T_{Ho} - T_{Ci}))}{\ln \left( \frac{T_{Hi} - T_{Co}}{T_{Ho} - T_{Ci}} \right)}. \quad (25)$$

In addition, the thermal inertia due to the metal parts is taken into account for the dynamic calculation. The heat balance for this case is given by,

$$\dot{Q}_w = \dot{Q}_H - \dot{Q}_C, \quad (26)$$

where,

$$\dot{Q}_w = M_w Q_w \frac{dh_{Co}}{dt}, \quad (27)$$

$$\dot{Q}_C = \dot{m}_C (h_{Co} - h_{Ci}), \quad (28)$$

and,

$$\dot{Q}_H = \dot{m}_C (h_{Hi} - h_{Ho}). \quad (29)$$

The pressure drop on both the hot and cold sides of the heat exchanger is considered as a percentage of the upstream pressure. It is also important to mention that a pinch point approach is used to avoid thermodynamically absurd fluid propositions in the heat exchanger.

A plenum model is considered upstream of the steam turbine to accommodate the steam dynamics, where the mass conservation equation given in Equation (21) is applied. The steam turbine model is based on a choked-nozzle model, where the mass flow rate at the inlet is given by,

$$\dot{m} = \rho_i a_i A_{ST}. \quad (30)$$

The power of the steam turbine is calculated by the application of Equation (22). However, the electric power is calculated by considering the losses in the shaft and generator.

For the condenser, the heat transfer coefficient is calculated using Equation (31) (PUTTEN, COLONNA, 2007) and its heat transfer rate is given using Equation (32).

$$U_{CO} = k_C T_7^\beta \quad (31)$$

$$\dot{Q}_{CO} = A_{CO} U_{CO} (T_7 - T_{shell}) \quad (32)$$

For the pump, a simple fixed efficiency model is adopted.

The model, therefore, in view of the nature of the equations presented before, can be characterized as dynamic, given its dependence on time, and lumped, because of its temporal derivatives. Considering these characteristics and taking into account that the system of equations needs to be solved in parallel to the optimization process, the computation processing time is an important concern. With the aim of developing a lightweight numeric solution, a solution that considers:

- Finite-difference method for the approximation of the differential equations.
- An explicit method for solving the initial value problem.
- A sequential approach to solving the equation system.

It is worth pointing out that control systems play an important role in the solution, as will be further explored in Section 4.4.

### 4.3.3 Fluid models

As discussed in section 4.2.1, the thermodynamic properties of the fluid play an important role in the thermal system modeling. Most conspicuously, for the design and optimization of the ORC, the calculation of the fluid thermodynamic properties is critical, since the fluid selection is an element of the design vector. Therefore, the modeling and calculation of such properties need to be carefully addressed.

For the ORC, two types of fluids are considered for both applications: the hot side fluid and the organic working fluid.

At the heat source side, for the case of the gas turbine waste heat recovery, the discussion was made in section 4.2.1. For the compressor application, the model follows a similar approach. The fluid properties are calculated by using each of the substances that compose the natural gas. Since the reference that provide the dataset (LIEDMAN, MAANSSON, 2013) do not present details on the natural gas composition, the composition given in other work on North Sea oil platforms was used as reference (NGUYEN et al., 2012). Then, the hot side fluid is a composition of the gases shown in Table 6.

Table 6 – Natural gas composition used for the calculation of the properties of the compressor working fluid.

<b>Gas</b>	<b>Composition (%)</b>
N <sub>2</sub>	4.4
CO <sub>2</sub>	1.5
CH <sub>4</sub>	73.7
C <sub>2</sub> H <sub>6</sub>	6.1
C <sub>3</sub> H <sub>8</sub>	6.7
C <sub>4</sub> H <sub>10</sub>	7.6

Source: Adapted from Nguyen et al. (2012).

For the cold side, the analysis is straightforward since it is a pure substance and its calculation is directly provided by CoolProp. Fluid selection during the optimization is performed over a selected database, shown in Table 7. The number (ID) in the first column provides the reference during optimization. This ID is provided in the design vector so that the fluid selection is made similarly to a discrete optimization problem.

Table 7 – Organic fluids database used for the ORC optimization.

<b>ID</b>	<b>Fluid</b>
0	Acetone
1	Isohexane
2	Cyclopentane
3	Cyclohexane
4	n-Hexane
5	n-Heptane
6	R11
7	R123
8	R113
9	Benzene
10	R245ca
11	nPentane
12	Ethanol
13	R141b
14	Toluene

Source: Author.

This fluid dataset was defined from the typical fluids mentioned in literature and from an analysis of the fluid critical temperature against the heat source temperature.

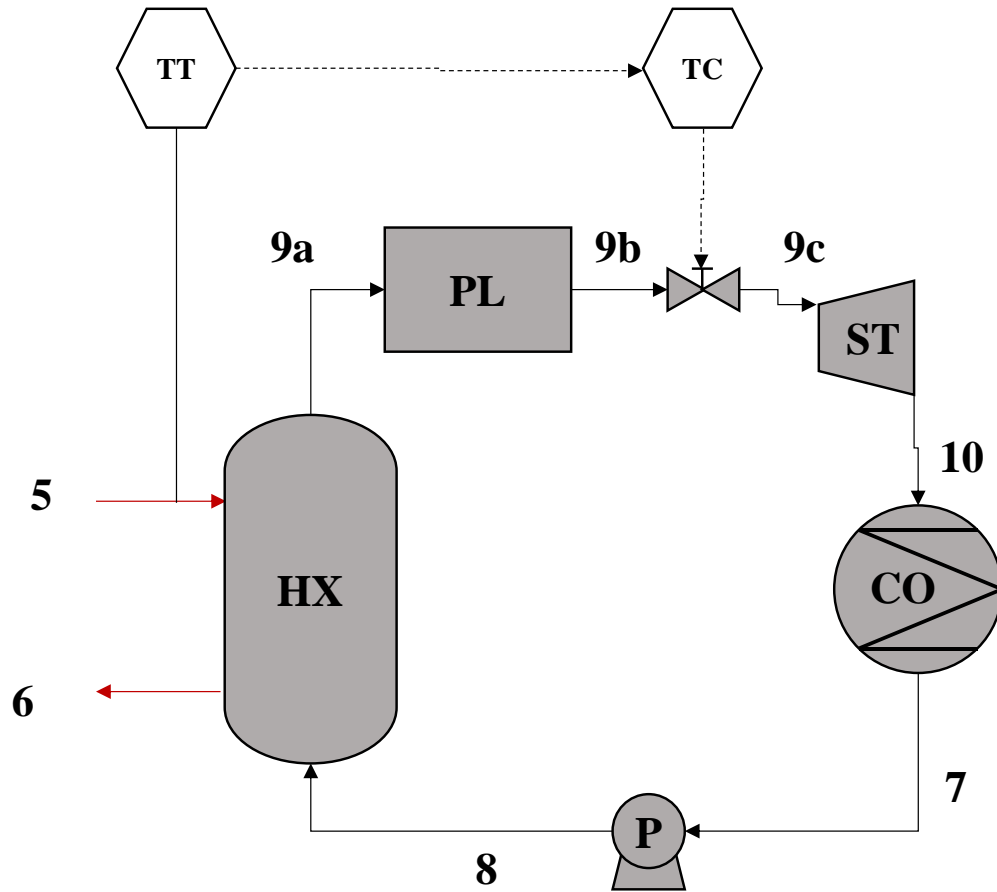
#### *4.4 The ORC control model*

##### 4.4.1 Control method for the ORC used for waste heat recovery in the gas turbine exhaust

For the control of the ORC used for the waste heat recovery of the gas turbine, a simple proportional approach was selected. Therefore, the valve upstream of the steam turbine is controlled according to the exhaust temperature of the gas turbine, as presented in the diagram shown in Figure 43.



Figure 43 - Mass flow control at the steam turbine inlet, defined as a function of the gas turbine exhaust temperature.



Source: Author.

In this case, the controlled variable ( $\dot{m}_{9c} = v_p$ ) is calculated by,

$$v_p = \kappa_p e(t), \quad (33)$$

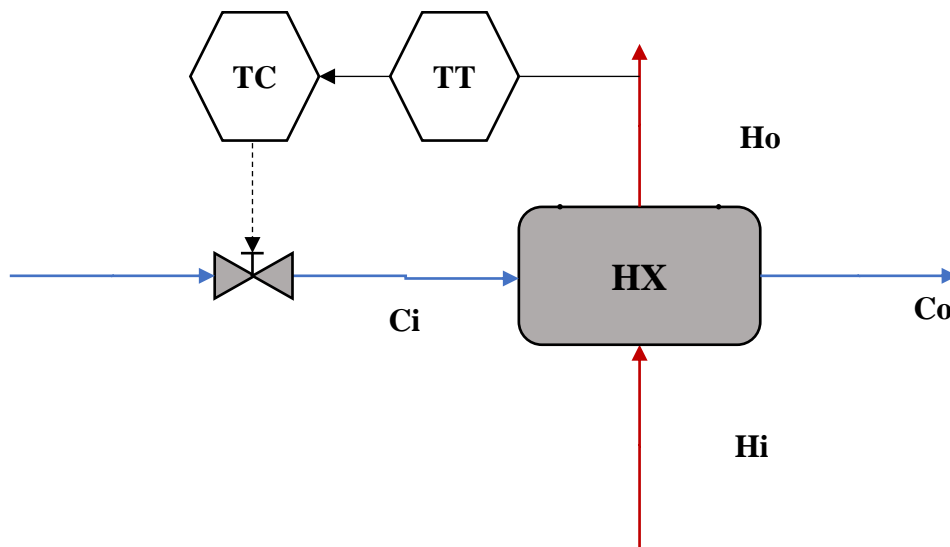
where

$$e(t) = T_{5,sp}(t) - T_5(t). \quad (34)$$

#### 4.4.2 Temperature control at the compressor discharge

The control model developed here consists in regulating the temperature of the hot stream, compressed natural gas - by controlling the flow of the organic fluid, as presented in Figure 44.

Figure 44 - Process and instrumentation diagram for the heat exchanger - hot stream temperature control.



Source: Author.

Considering that the control model needs to be robust enough to be used as a generic solution coupled to an optimization algorithm, the natural choice for this application is the PID controller (LEVINE, 1999). The control model representation in the time domain is given by Equation (35),

$$v(t) = \kappa_p e(t) + \kappa_i \int_0^t e(t) dt + \kappa_d \frac{de(t)}{dt}, \quad (35)$$

where  $v = \dot{m}_{Co}$  and  $e(t)$  is the error,

$$e(t) = T_{Hi,sp}(t) - T_{Hi}(t). \quad (36)$$

The parameters  $\kappa_p$ ,  $\kappa_i$  and  $\kappa_d$  are typically rewritten as,

$$\begin{cases} \kappa_p = K \\ \kappa_i = K/T_i \\ \kappa_d = KT_d \end{cases} \quad (37)$$

The controller tuning depends directly on the proper adjustment of these parameters. However, when considering several designs, specific tunings need to be made for each generated design. Since the computational effort to calibrate the controller in several design cases by applying the same approach used for the gas turbine, i.e., optimization applied to find each of these parameters, a resource that can be applied in such cases is the Ziegler-Nichols tuning method. In this approach, the parameters of Equation (37) can be rewritten as follows:

$$\begin{cases} K = 1.2/a \\ T_i = 2L \\ T_d = L/2 \end{cases} \quad (38)$$

where  $a$  and  $L$  are constants defined for each design and controller. The Ziegler-Nichols can provide robust control and its tuning process can easily be coupled to an algorithmic tuning process, though some underdamped responses with a reasonable level of overshoot can be expected.

#### 4.5 Optimization methods

The mathematical models presented in the previous sections provide an accurate guide for the forecast of the thermal system behavior. The equations that make up these models can have parameters that are intrinsic elements of the design of the equipment or the plant. Therefore, the responsible for the design, by applying these models, can either get the parameters from standards, rules of thumb, and best practices or establish a structured method to define them.

Optimization is a powerful resource for defining the design parameters, most conspicuously, when considering that the elements usually considered to have a major impact on design success, such as cost, temperatures, pressures, performance, power output, and power

consumption can be calculated through the mathematical model and therefore can compose the objective function outputs (JALURIA, 2019). In addition, natural constraints related to design variables can be easily accommodated in the optimization process. The focus of this thesis is on the multi-objective optimization of the ORC design, meaning that two of the results of the solution of Equation (20) will be considered for the design evaluation. The details on the approach adopted for the multi-objective optimization are presented in Chapter 5. For the sake of introducing the subject, this section presents an overview of the optimization techniques, mostly within a single-objective perspective but that fits to the overall principles discussed in this work.

First, it is important to define the single optimization problem. Equation (39) shows the three parts of optimization characterization, the minimization<sup>7</sup> of a function, subjected to constraint inequalities and equalities.

$$\left\{ \begin{array}{l} \text{minimize } f(\bar{x}) \\ \text{subjected to } \bar{g}(\bar{x}) \leq 0 \\ \text{and } \bar{h}(\bar{x}) = 0 \\ \bar{x} \in \mathbb{R}^n \end{array} \right. \quad (39)$$

The numerical solution of this problem depends broadly on the knowledge of the objective function, its behavior, constraints and particularities of the thermal system. The classes of solution methods can be summarized in two types: the calculus-based (deterministic) and the search-based (heuristic) (JALURIA, 2019) (COLAÇO, DULIKRAVICH, 2009).

The deterministic methods are based on the gradient of the objective function and its generic form is given by Equation (40).

$$\bar{x}_{k+1} = \bar{x}_k + \alpha_k \bar{d}_k \quad (40)$$

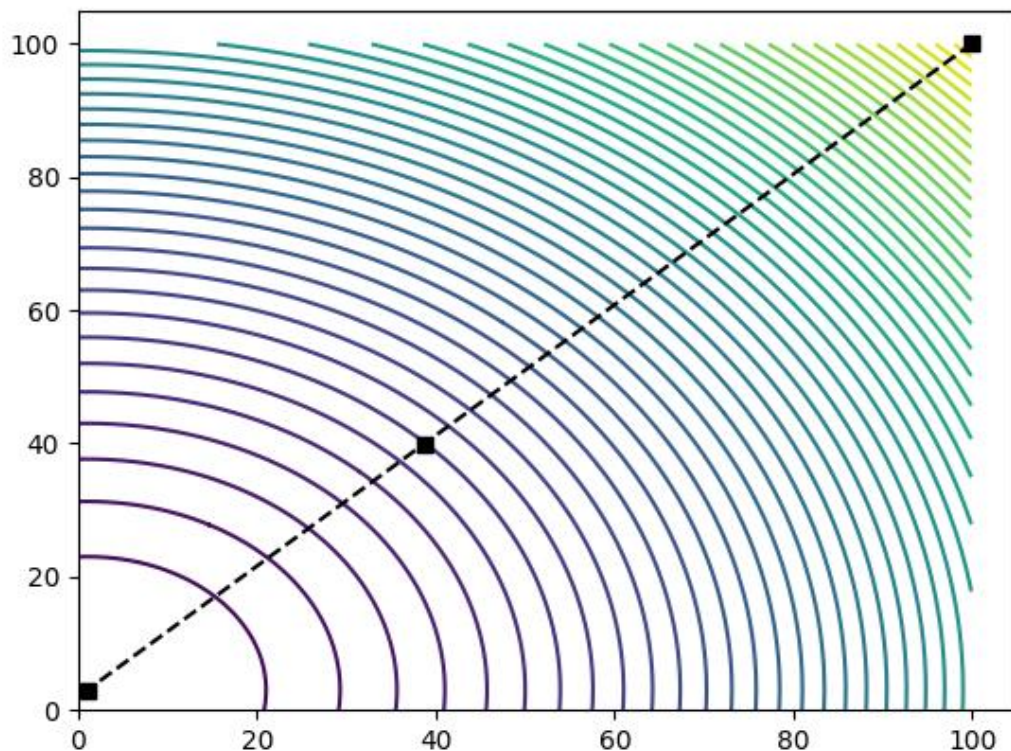
In this approach, the design vector is updated in each iteration by its value in the previous iteration  $k$  added to the product of a learning rate parameter (step size)  $\alpha$  by the deterministic search step,  $\bar{d}$ . This optimization methods class rely on distinct ways to calculate the vector  $\bar{d}$ , which, in its simplest representation is the gradient of the function  $f(\bar{x})$ . The

---

<sup>7</sup> In this text, for the sake of clarity, only the minimization is mentioned. Maximization problems can be converted into minimization ones with minor algebraic manipulation.

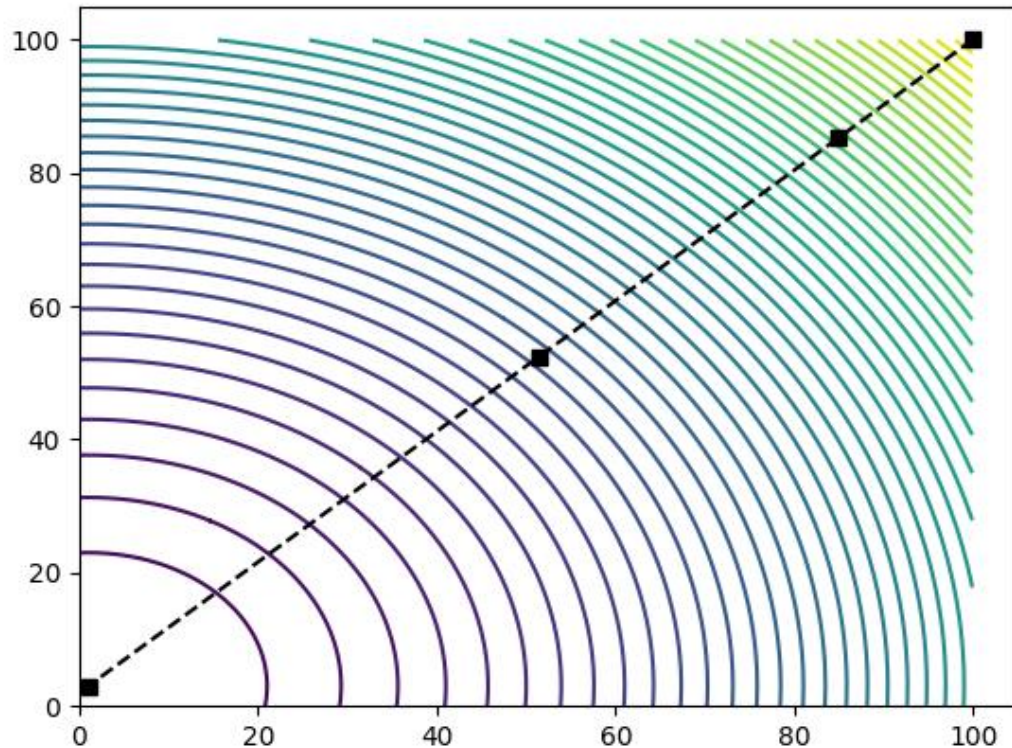
different representation of this vector observed throughout the deterministic methods have a remarkable impact on the convergence speed. In the Newton-Raphson method, for instance, this vector is calculated through the Hessian matrix and in the steepest descent method, this vector is given by the negative value of the gradient of the objective function. The high computational cost of building the gradient or the inverse Hessian matrix (when feasible) need to be considered when developing the optimization strategy. However, when these calculations are feasible, the solution can be found with very few calculations. In the examples given below, it is used the simple function  $f(\bar{x}) = (x(1) - 1)^2 + (x(2) - 3)^2$  as the reference, as presented in the contour lines. Figure 45 and Figure 46 present the results of the of the minimization of this function using the conjugate gradient (HESTENES, STIEFEL, 1952) and the BFGS (as implemented in NOCEDAL and WRIGHT, 2006) methods, respectively. The solution is given through the Python Scipy Optimize library.

Figure 45 – Conjugate gradient convergence tracking.



Source: Author.

Figure 46 – BFGS convergence tracking.

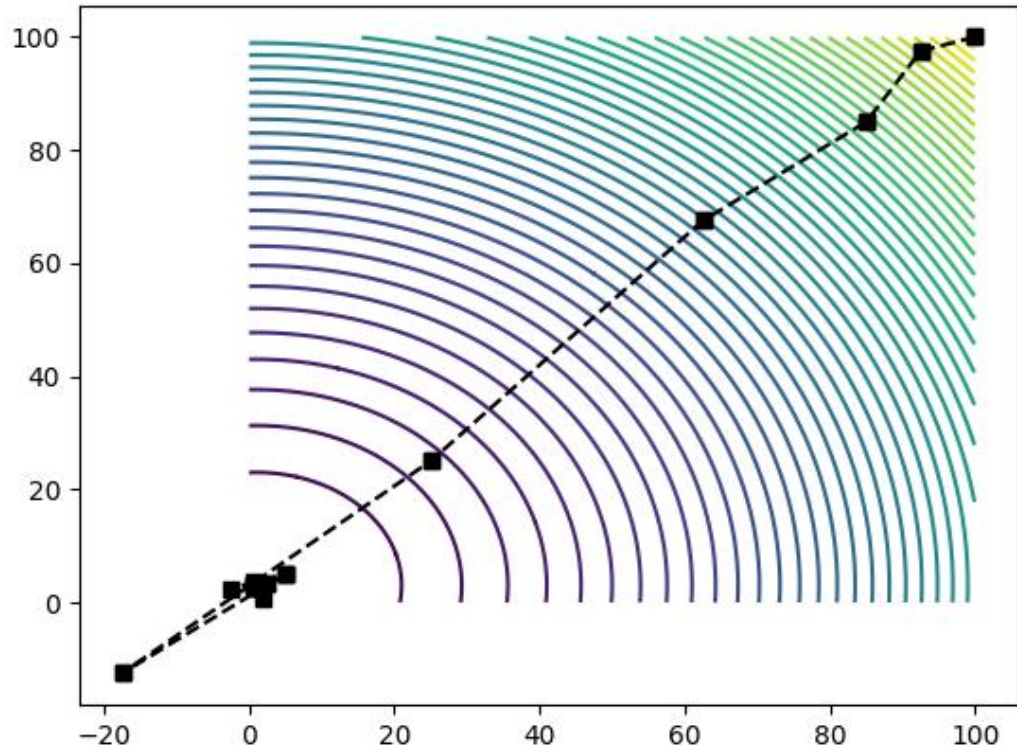


Source: Author.

Specifically for thermal system optimization models, mainly those that represent real-life equipment, the objective function topology is not necessarily smooth, continuous, or convex. Thus, in most cases the use of deterministic methods is not feasible. Another of the main cons of using these classes of methods is the dependence of a ‘good’ initial guess, which, in some cases, is impossible to determine.

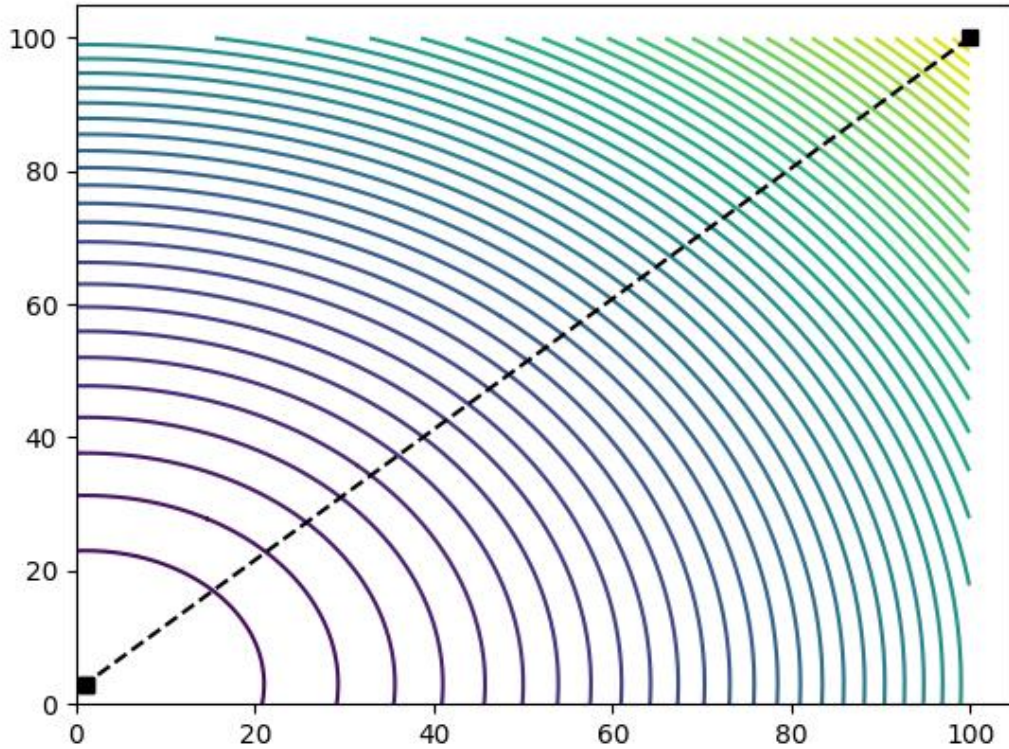
It is relevant to mention the methods that do not rely on the calculation of derivatives. There is a broad variation of these methods, such as the Nelder-Mead simplex, whose result for the reference function is given in Figure 47. Another relevant technique to be mentioned is the Powell method, whose result is given in Figure 48.

Figure 47 – Nelder-Mead simplex convergence tracking.



Source: Author.

Figure 48 – Powell's method convergence tracking.



Source: Author.

Regarding heuristic methods, there is a broad variety of available methods, which usually mimic a behavior found in nature to determine the minimum of the objective function. Some of notorious examples of these methods are: simulated annealing, differential evolution, and genetic algorithms. This class of methods usually does not require a significant amount of mathematical manipulation of the objective function. In this work, for the sake of exemplification, the particle swarm method (EBERHART, KENNEDY, 1995) will be discussed.

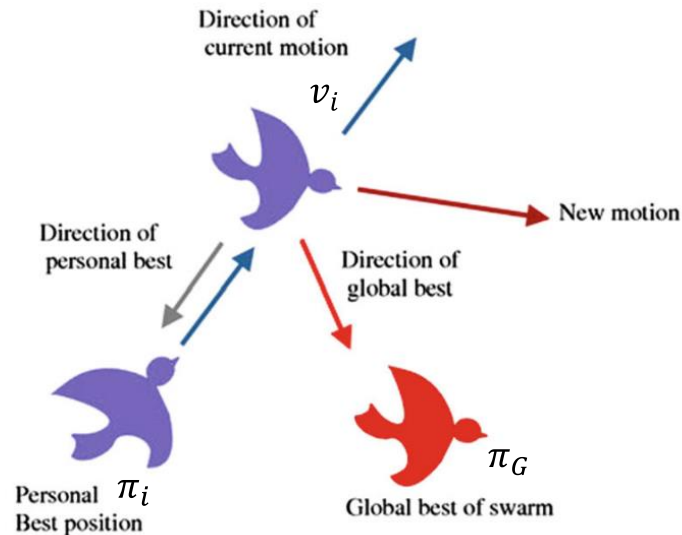
The particle swarm method was developed from the observation of groups of birds looking for nesting places, where the best places are found through the knowledge sharing among the individuals. The mathematical representation of the best point found in a specific iteration is given by Equation (41).

$$v_i(t + 1) = \omega v_i(t) + c_1 r_1 (\pi_i(t) - x_i(t)) + c_2 r_2 (\pi_G - x_i(t)) \quad (41)$$



As represented in Figure 49, the search vector for each individual is given by adding the vector of the best direction found by the group in the previous iteration and the best position found by the individual.

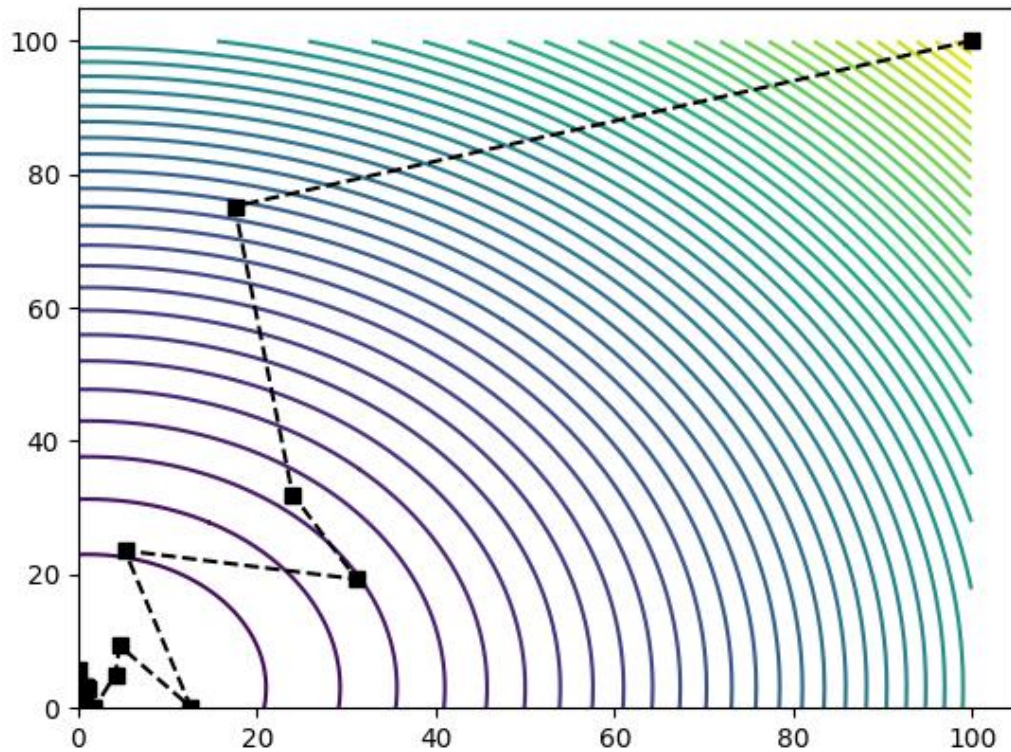
Figure 49 – Search representation in terms of vector composition per iteration.



Source: Adapted from Esmín, Coelho and Matwin (2015).

At the beginning of the searching process, the individuals are randomly spread over the design space and, after some iterations, local minima are eventually found, but they are continuously discarded as better options are found. This method has a slow convergence rate when in the vicinity of the global minimum, as shown in Figure 50 presents. However, considering the intricacies of thermal system optimization, its lightweight calculations and independence from complex algebraic manipulation of the objective function are well suited for the design process.

Figure 50 – The particle swarm convergence tracking for the reference function. Here it is presented the best element found ( $\pi_G$ ) in each iteration. The search was conducted by using the Python pyswarm library.

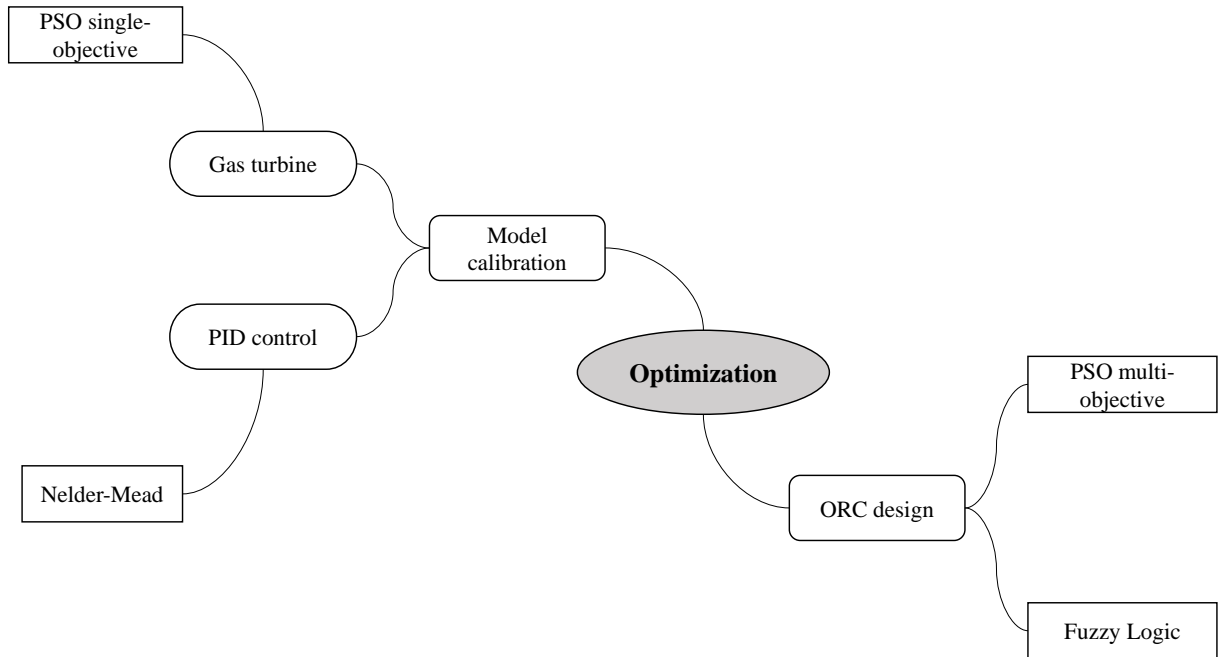


Source: Author.

#### 4.6 Optimization applications throughout the thesis

The optimization is a powerful resource for the modeling, simulation, and design of thermal systems. Therefore, it was extensively employed throughout this thesis. Figure 51 shows a map of these applications. The core of the application is the ORC design, where PSO and Fuzzy Logic are employed. For the calibration of the simulation models, PSO is also applied for the single-objective optimization, and the Nelder-Mead simplex method is used to calibrate the PID control model, since it is a quick, lightweight and gradient-free optimization method.

Figure 51 – Map of the optimization applications in this thesis.



Source: Author.

## 5. THE ORC DESIGN SYSTEM

### 5.1 *The design process*

The design of an ORC plant, similar to other thermal systems, is a complex multicriteria problem that requires a structured and systematic definition and exploration of design possibilities. To get along with this scenario and in a generalist view, the design of such thermal systems is based on the designer know-how and experience, whose steps include, but are not limited to: the system architecture selection; equipment model definition; basic parameters configuration; choice of base-case scenarios, and the proper optimization methods selection. Additionally, as the multi-objective optimization runs iteratively with the system simulation, the designer needs to take actions and interfere accordingly with the preliminary results. It can be noticed that this design process, although it can be performed by using the state-of-the-art in modeling, simulation and optimization tools; it lacks automation and relies on human actions for decision making, which can lead to mistakes, and it can demand a massive amount of time.

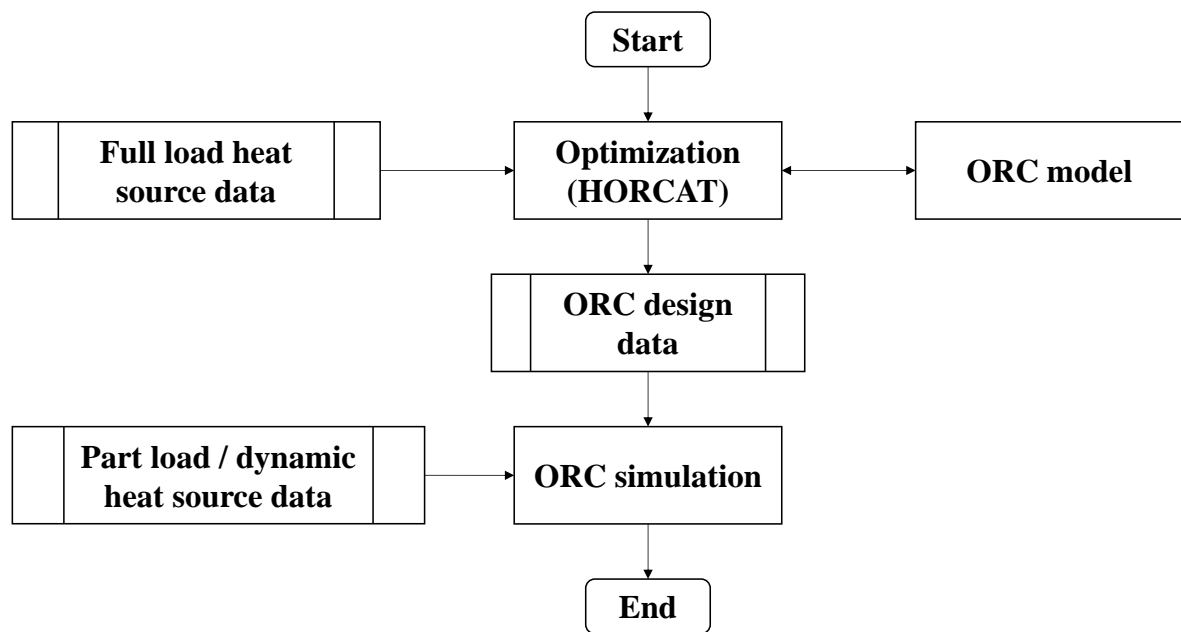
Taking into account these aspects, the ORC design process presented in this work is implemented as a multi-component computational system, as Figure 52 shows. Therefore, before detailing the methodology applied to each of these components, it is important at this point to present an overview of the system. The optimization process starts with the definition of the heat source data to which the ORC will be designed. In this case, two methods can be applied: the reading of datasets containing equipment or plant data and the use of computational models to generate the data. To evaluate the applicability of ORC in two main thermal systems in an oil platform, two different heat sources are evaluated: the first is a GE LM2500+ gas turbine, whose model follows the configuration of real-life equipment used for power generation on an FPSO, as described in section 4.2 . The second is the data from a compressor train operating in an oil platform. In this step, only full load data from the heat source are used, which means that the generated designs are optimized for this condition. After defining the data from the heat source, the optimization process is started. An PSO-based algorithm, HORCAT<sup>8</sup>, was specifically developed for ORC design and optimization. Therefore, before optimization is performed, constraints and limits for the design vector are established. Then, the particle swarm parameters are defined: number of iterations, population size, acceleration coefficients, and

---

<sup>8</sup> HORCAT - Hunting ORCs with Asa-de-Telha: asa-de-telha is the name in Portuguese for the Harris's hawk, a very common hawk in Brazil, which has the unusual characteristic of hunting in cooperative packs. This approach is not linked to the Harris Hawk Optimization algorithm (HEIDARI et al., 2019).

initial values for the inertia weight. In addition, the initial population (initial guess) is provided. Details on the optimization process are given in Section 5.2. The ORC parameters, generated through the optimization process, are used to evaluate the off-design performance, including dynamic conditions. In this step, control models can be applied to cope with dynamic conditions.

Figure 52 - General process of design, optimization, and evaluating the ORC design.



Source: Author.

Some remarks can be made on the overall optimization process:

- To enhance computational efficiency, the ORC simulation is performed using a parametrized model based on the data generated for each design.
- Analyzing the trade-offs among the identified designs is not the objective of this work. Instead, the main goal is to assess the performance of these designs under conditions other than full load.
- The system was fully implemented in Python and the thermal properties are calculated using the CoolProp library (BELL et al., 2014) since it has been applied in the simulation of thermal systems and ORC and, besides, it has a high-level interface in Python and can be called as a native library.

The simulation model for the discovered designs constitutes a complex subsystem, which will be comprehensively discussed in the following sections.

### 5.2 The optimization algorithm: HORCAT

Due to space limitations for the installation of equipment on offshore platforms, the ORC equipment volume footprint is a challenge for its implementation in real-world plants (PEREIRA, YANAGIHARA, 2022). In addition, it is intended that, once implemented, the Rankine cycle can generate relevant power output. Therefore, for design purposes, these two requirements need to be taken into consideration, but an agreement for both conditions is, most of the time, impossible to be managed without a proper algorithmic process. In this sense, the optimal ORC design developed in this work considers as objectives the minimization of the equipment volume and the maximization of the electric power output, consequently defining a multi-objective optimization problem.

This class of problems can be described analytically as follows. The minimization of  $n$  objectives given by the objective function  $\bar{f}(\bar{x})$  is formulated as:

$$\begin{cases} \text{minimize } \bar{f}(\bar{x}) = [f_1(\bar{x}), f_2(\bar{x}), \dots, f_n(\bar{x})] \\ \text{subjected to } \bar{g}(\bar{x}) \leq 0 \\ \text{and } \bar{h}(\bar{x}) = 0, \end{cases} \quad (42)$$

where the design vector is

$$\bar{x} = [x_1, x_2, \dots, x_m], \quad (43)$$

and  $\bar{x} \in D$ , where  $D$  is the search space.

For this class of problems, there is no unique solution, and, hence, a set of feasible solutions can be organized as a Pareto front. Considering the characteristics of the optimization algorithm presented here, it is important to present some concepts on Pareto optimal conditions. Decision vectors are design vectors taken in a given interaction during minimization in an optimization process. Therefore, a decision vector  $\bar{u}$  Pareto-dominates a decision vector  $\bar{v}$  when,

$$\left\{ \begin{array}{l} \forall i \in \{1, 2, \dots, n\}, f_i(\bar{u}) \leq f_i(\bar{v}) \\ \text{and } \exists j \in \{1, 2, \dots, n\} \mid f_j(\bar{u}) < f_j(\bar{v}). \end{array} \right. \quad (44)$$

A Pareto optimal solution is a decision vector  $\bar{x}^*$  which is not dominated by any  $\bar{x} \in D$ . Therefore, a Pareto optimal front is defined as the matrix composed of all found objective vectors  $\bar{f}(\bar{x}^*)$ .

Once these preliminary concepts are established, it is possible to shed light on the ORC design process. In this specific case, two objective functions are calculated: the global equipment volume and the electric power output of the steam turbine; hence,

$$\bar{f}(\bar{x}) = [\mathcal{V}(\bar{x}), W_{ST}(\bar{x})], \quad (45)$$

where the design vector can be written as

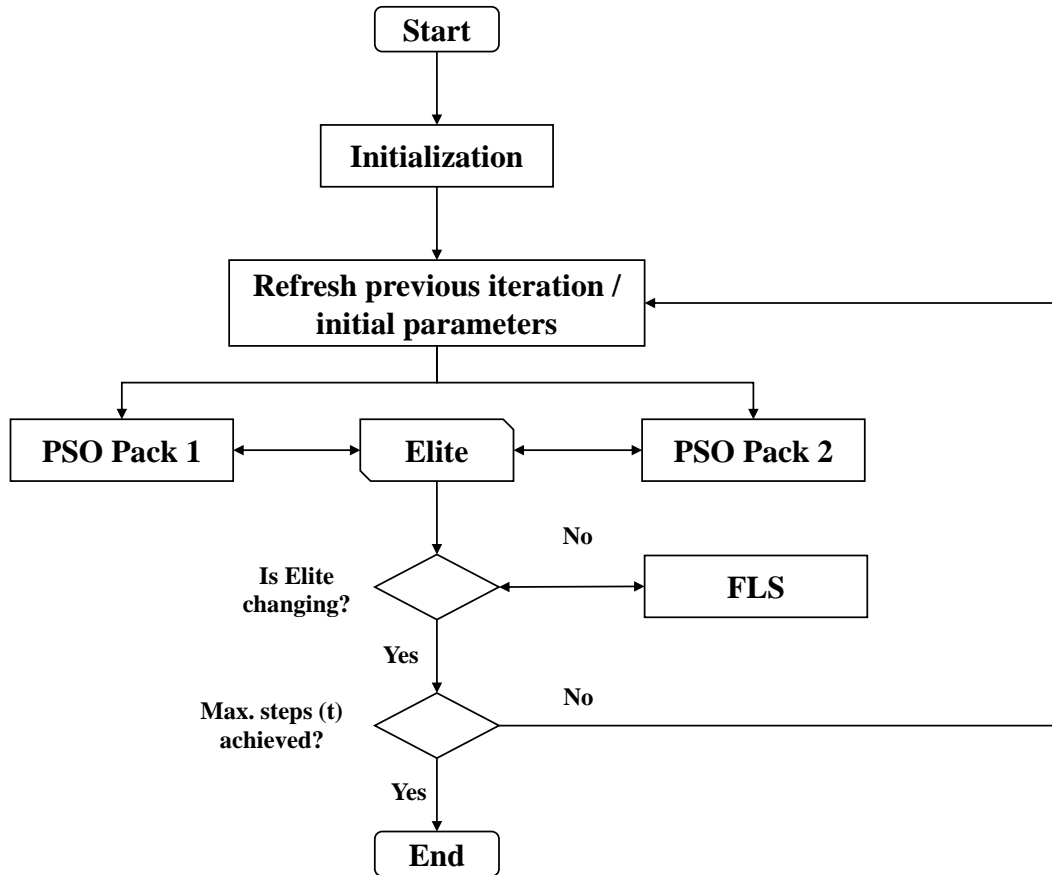
$$\bar{x} = [\text{fluid}, A_{ST}, p_{10}, \mathcal{L}_{HX}, A_{CO}], \quad (46)$$

i.e., the design variables considered in the problem are: the fluid, here represented by an integer, the area of the steam turbine inlet nozzle  $A_{ST}$ , the condenser pressure  $p_{10}$ , the heat exchanger characteristic length  $\mathcal{L}_{HX}$  and the heat exchange area of the condenser,  $A_{CO}$ .

In this case, once the ORC model can be seen as the objective function, the optimization method to be applied to such a complex model demands an algorithm that can deal with highly non-linear conditions from which it is impossible to calculate or to approximate its Jacobian or Hessian matrices and whose domain cannot be properly defined. This is a situation where heuristic optimization methods are typically employed (PEREIRA, YANAGIHARA, 2022). Most specifically, due to its lightweight calculations and suitability to complex systems (ESMIN, COELHO, MATWIN, 2015), the particle swarm method is used as the core of HORCAT. Figure 53 presents an overview of the components of HORCAT and its functional behavior. The structure of the algorithm is mainly based on the works of Liu et al. (2017) and Kouka et al., (2020), especially considering the cooperation between the populations (packs).

Most specifically, there is a pack dedicated to each of the objectives and each of these packs is initialized by testing each individual against its dedicated objective function  $f_i$ . Only the individuals that provided valid results are considered for the pack. At this moment, the ‘Elite’ is also initialized, which is the Pareto front, composed of the best results found in both packs.

Figure 53 - Optimization process implemented in HORCAT.



Source: Author.

Once the packs are initiated, the search loop is started. During this process, the packs share information about their best individual so that both packs know the best global individual. Elite ( $\bar{E}$ ) is therefore composed, defined as a matrix containing the best results,

$$\bar{E} = \begin{bmatrix} \mathcal{V}_{1,1} & W_{ST1,2} \\ \mathcal{V}_{2,1} & W_{ST2,2} \\ \vdots & \vdots \\ \mathcal{V}_{m,1} & W_{STm,2} \end{bmatrix}, \quad (47)$$



each result ( $\bar{f}_k$ ) from an evaluated design (an element of the pack,  $\bar{x}_k$ ) is compared with each element of Elite. If  $\bar{x}_k$  Pareto dominates a given  $\bar{x}_\ell$  where  $f_\ell \in \bar{E}$ , this specific element is replaced by  $f_k$ , i.e., given

$$\bar{f}(\bar{x}_k) = [\mathcal{V}(\bar{x}_k), \dot{W}_{ST}(\bar{x}_k)], \quad (48)$$

if  $\mathcal{V}(\bar{x}_k) \leq \bar{E}(\ell, 1)$  and  $\dot{W}_{ST}(\bar{x}_k) > \bar{E}(\ell, 2)$ , then  $\bar{E}(\ell, 1) = \mathcal{V}(\bar{x}_k)$  and  $\bar{E}(\ell, 2) = \dot{W}_{ST}(\bar{x}_k)$ .

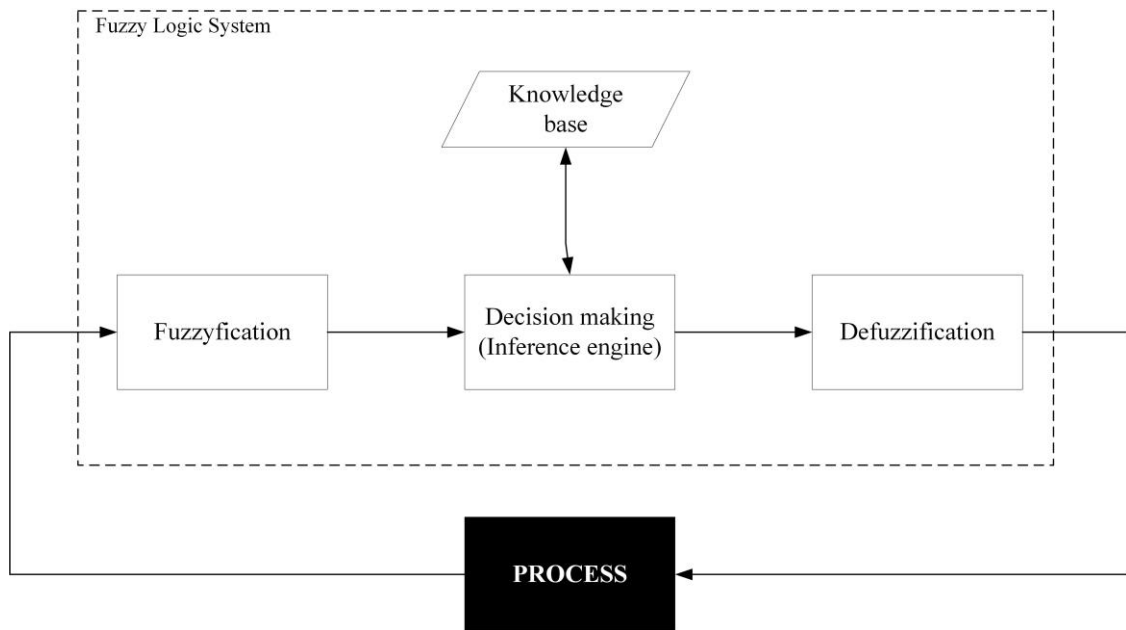
During the search iterations, the Elite behavior is monitored to avoid stagnation in the course of the survey. Hence, a Fuzzy Logic System (FLS) is coupled to the optimization loop. The FLS plays, therefore, the role of the user, monitoring the potential stagnation and taking decision to change the search parameters, if necessary. The aim is to dynamically change the PSO parameters shown in Equation (41). These features will be properly discussed in Section 5.3. If no change in the Elite is observed after a certain number of iterations, even with the action of the FLS, the entire population is replaced.

### 5.3 Decision-making during the optimization process

In order to have an automated process for decision making, computer systems have been studied to take the designers place and provide accuracy and speed up the design (MOSAVI, 2013). Therefore, Fuzzy Logic has been considered in this class of problems (YU et al., 2020). Fuzzy Logic has been applied since the 70's as a tool to mimic the human decision-making process to deal with information that is interpreted qualitatively, inexactly, or uncertainly (LEE, 1990) (ZADEH, 2008). It has been used to develop robust control systems, robotic programming, signal processing, and intelligent decision-making applications. The Fuzzy Logic System (FLS) is the basic element for real-world applications. This construct performs a nonlinear mapping of the inputs that come from the process into a scalar output, as shown in Figure 54. The FLS amasses four procedures: the fuzzification is the mapping of the inputs – variables coming from the process – into the associated membership functions for each defined Fuzzy set. The decision-making procedure is performed by evaluating rules that are directly related to the expertise required to analyze the process. In this step, the fuzzy sets defined for

the inputs are associated with those defined for the outputs. Finally, the defuzzification procedure performs the conversion of the membership function defined in the decision-making procedure into the output value.

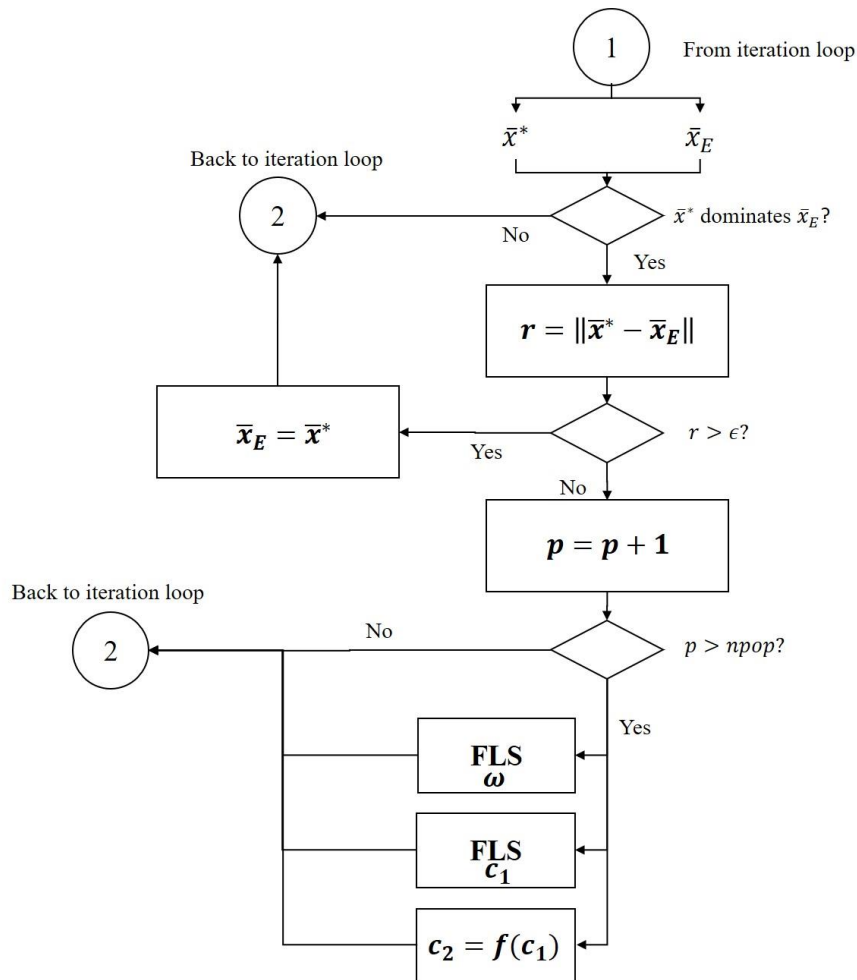
Figure 54 - Generic representation of a Fuzzy System.



Source: Author.

Taking into account the architecture of HORCAT, the FLS is applied during the design process for change tracking and management. Figure 55 presents a flowchart of the evaluation made during the iteration process. A given vector  $\bar{x}^*$  is compared with a vector  $\bar{x}_E$ , where  $f(\bar{x}_E)$  is part of the Elite array. If  $\bar{x}^*$  dominates  $\bar{x}_E$ , the Euclidean distance of these two vectors is calculated. The objective is to check whether these design vectors are similar. If the distance is greater than the reference value  $\varepsilon$ ,  $\bar{x}^*$  replaces  $\bar{x}_E$ . Otherwise, the solutions are considered too similar and a counter  $p$  measuring the number of trials to change Elite is updated. If this counter achieves a threshold, which is equal to the population size, an FLS changes the value of  $\omega$  and other FLS changes the value of  $c_1$ .  $c_2$  is updated according to the same variation applied to  $c_1$ . The Python library `skfuzzy` is used to run the FLS.

Figure 55 - Decision-making process during HORCAT search.



Source: Author.

## 5.4 Demonstrating performance in real-world applications

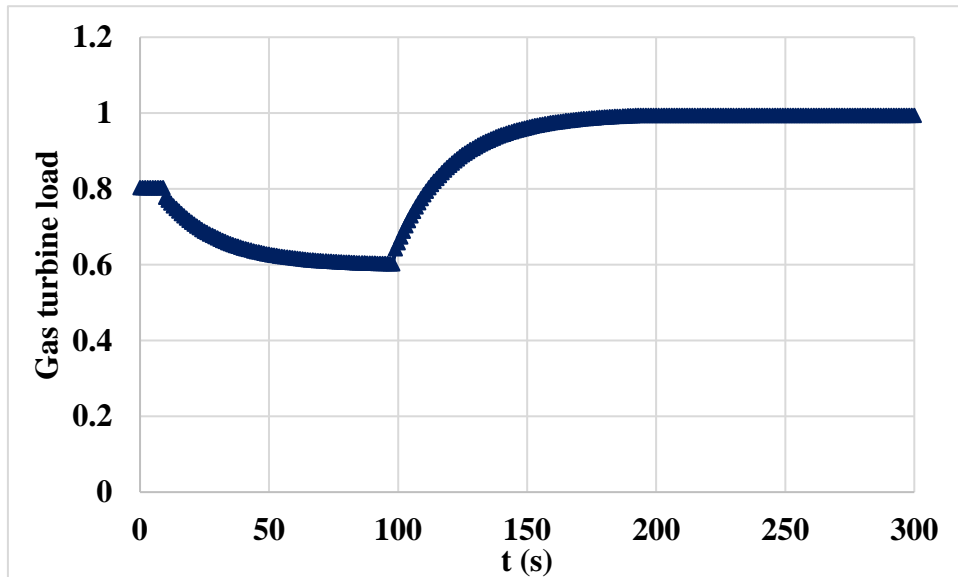
### 5.4.1 Gas turbine loads and transient maneuver

Data used for ORC design and analysis of the recovery of ORC applied for the waste heat of a gas turbine was provided by a computational model that simulates the steady-state and dynamic behavior of a GE LM2500+, configured for application in an FPSO operating in Santos Basin, Brazil. The ORC design is performed under full load conditions. Then, partial loads and dynamic conditions are used to evaluate the design under typical situations seen in an oil platform power plant.

Given the prevailing context, the initial set of generated data comprises the steady-state data, entailing the following cases of the gas turbine operation: 100, 75 and 50% load, considering ISO conditions. The data associated with the dynamic conditions reflect the load

change shown in Figure 56, where a load rejection (80 to 60%) is followed by a load increase of up to 100%.

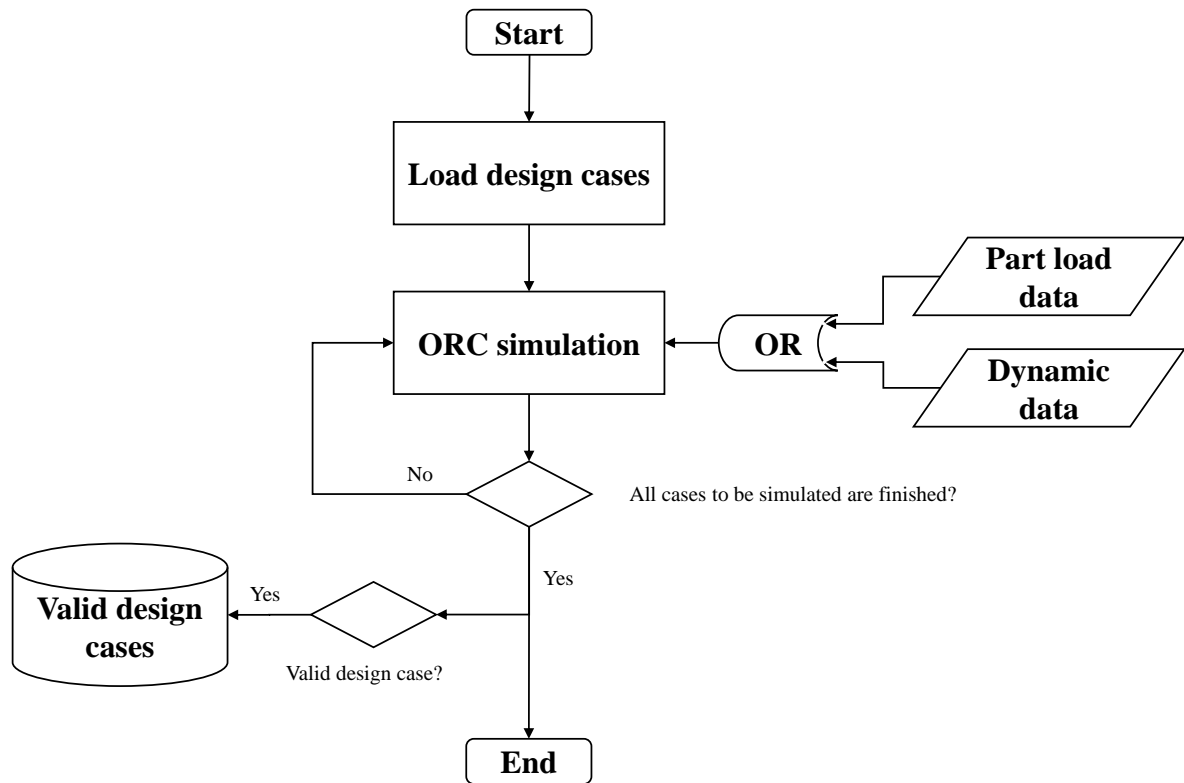
Figure 56 - Dynamic load maneuver used to evaluate the ORC designs.



Source: Author.

Taking into account the flexibility provided by an available model to simulate the operational conditions of the gas turbine, the ORC design cases are evaluated according to the flow chart presented in Figure 57. Initially, the ORC designs generated by HORCAT are loaded and its simulation is started. The simulation is carried out according to the data to be tested, at steady-state and transient conditions. Once the simulation is finished, if the design case has successfully withstood the simulated conditions, it is stored as a valid design.

Figure 57 – Process implemented for the evaluation of ORC designs generated for the waste heat recovery from the gas turbine exhaust.



Source: Author.

#### 5.4.2 The compressor dataset

The compressor train used as reference for this work is described in the work of Liedman and Maansson (2013). The two-stage compressor, then operated on a platform located in the Norwegian Sea, was used for natural gas compression. Its design point parameters are given in Table 8.

Table 8 – Compressor train design point parameters.

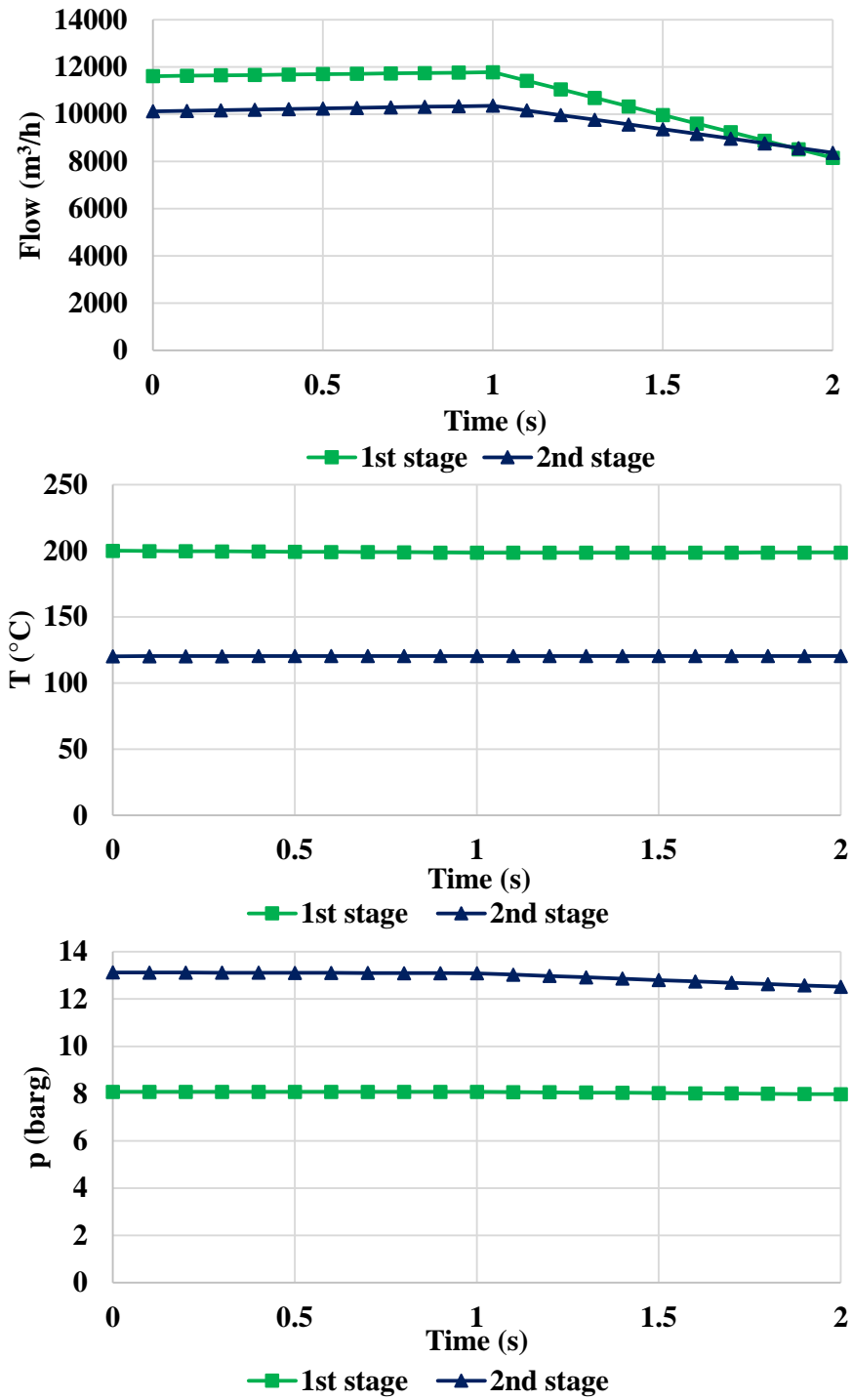
<b>COMPRESSOR DATA</b>		
<b>Parameter</b>	<b>1st stage</b>	<b>2nd stage</b>
Molecular weight (g/mole)	27.9	27.05
Flow (Sm <sup>3</sup> /h)	15850	14453
Inlet pressure (barg)	0.75	5.61
Outlet pressure (barg)	7.74	13.41
Inlet temperature (°C)	40.2	50.5
Outlet temperature (°C)	163.4	115.6

Source: Liedman and Maansson (2013).

Taking into account the PID control adopted for this case, its tuning strategy associated with the characteristics of the available data demanded a more specific simulation approach. Given the data limitation, the controller calibration and validation according to the ORC design were defined as follows:

- Calibration of the Ziegler-Nichols parameters for each design, considering a dataset containing a smooth transient, presented in Figure 58.
- Verification and validation of the controller parameters for each generated design, also considering a smooth transient. It is worth mentioning that this dataset, presented in Figure 59, was originally part of the same time series used for the calibration dataset.
- Simulation of an intense transient and analysis of the controller behavior under transient conditions. The dataset used as input for this simulation is shown in Figure 60.

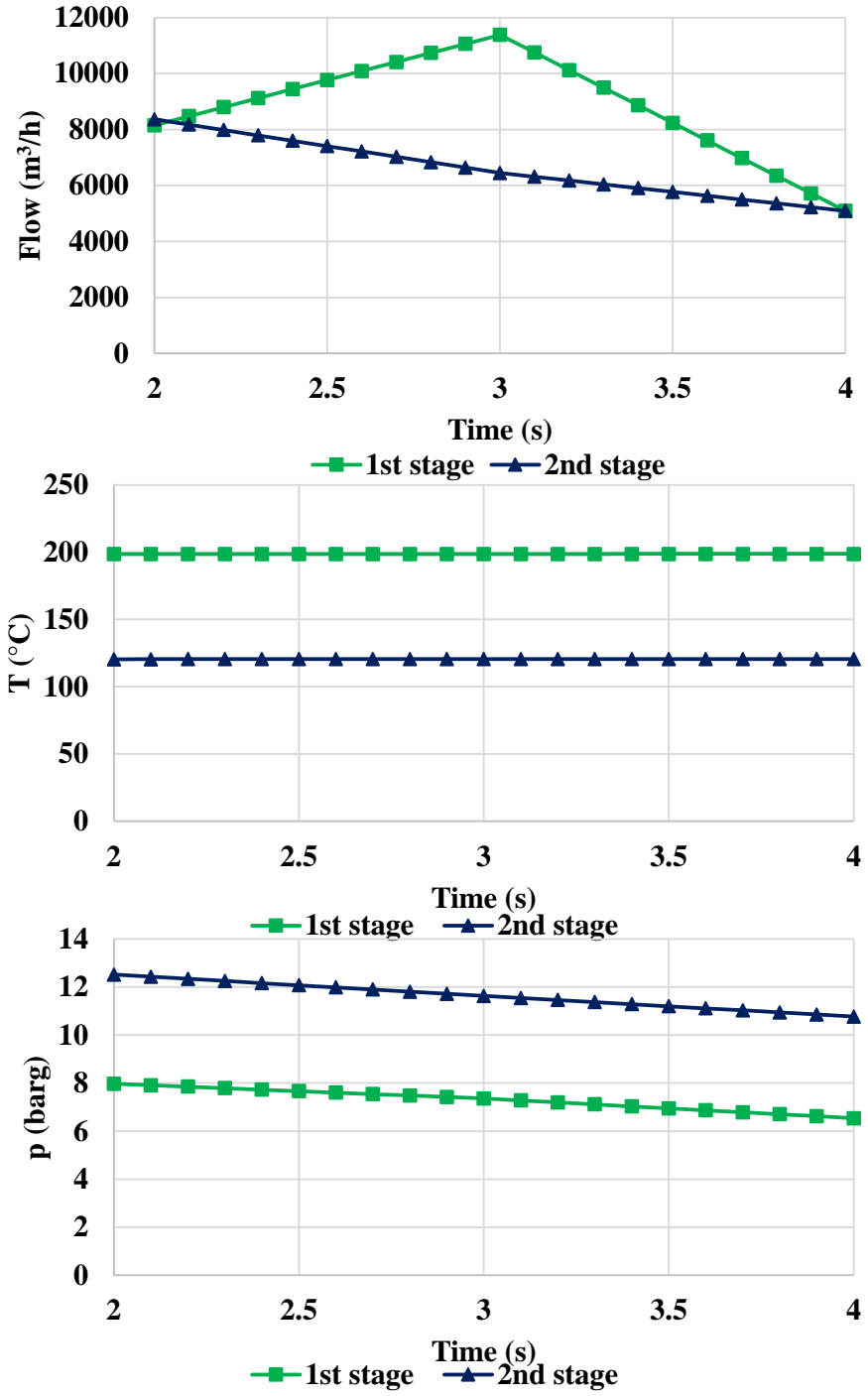
Figure 58 – Compressor data used for the calibration of the PID parameters.



Source: Author.

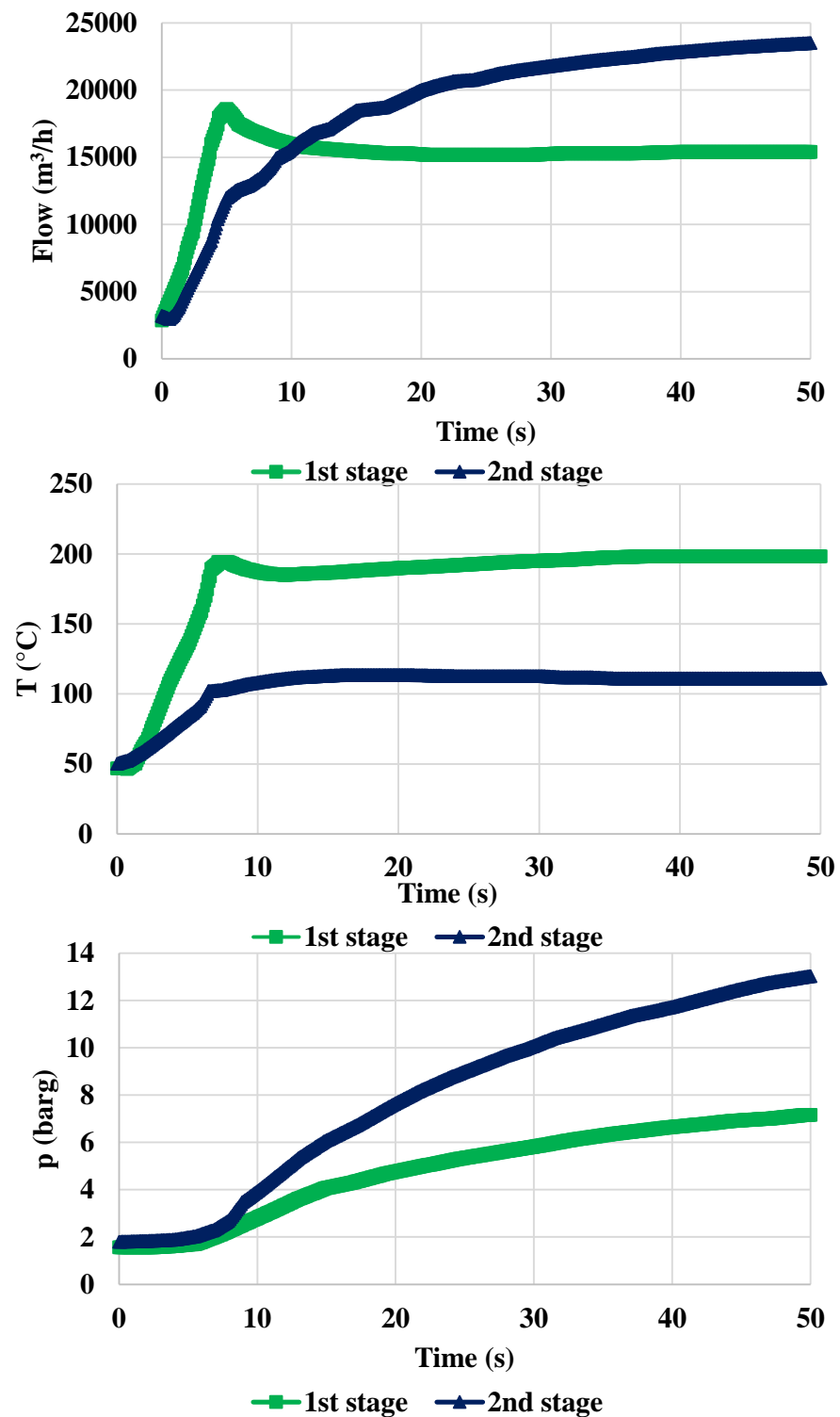
Figure 59 – Compressor data used for the validation of the PID parameters.





Source: Author.

Figure 60 – Compressor dataset used for the simulation of the ORC for temperature control.



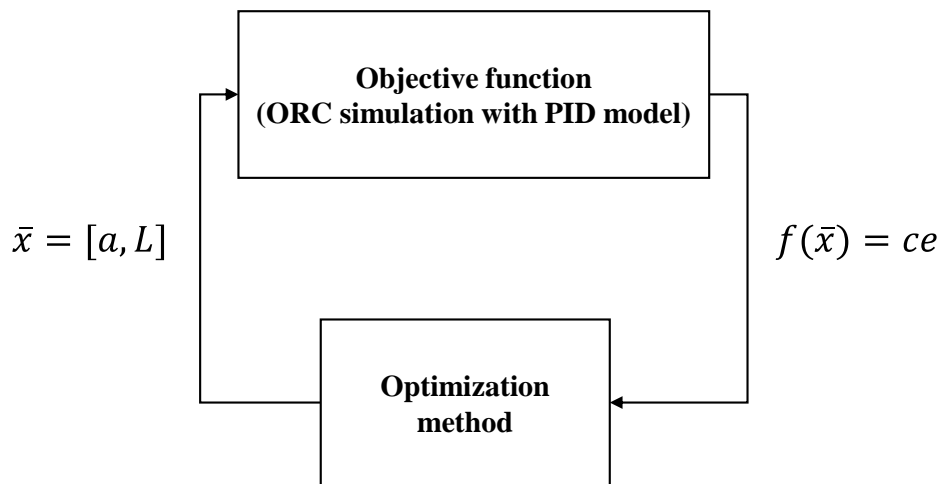
Source: Author.

Considering these aspects on the data availability and, additionally, the need of the controller parameter tuning, an initial value problem was modeled, in association with a single-

objective optimization to define the Ziegler-Nichols parameters for each design. The optimization problem is defined as depicted in the flowchart shown in Figure 61. The inputs (guesses) to calculate the Ziegler-Nichols parameters are provided by the selected optimization method. Then, the ORC model provides an output of cumulative error, which is calculated by,

$$ce = \sum_{t=0} e(t). \quad (49)$$

Figure 61 – Optimization process applied to the calibration of PID parameters.



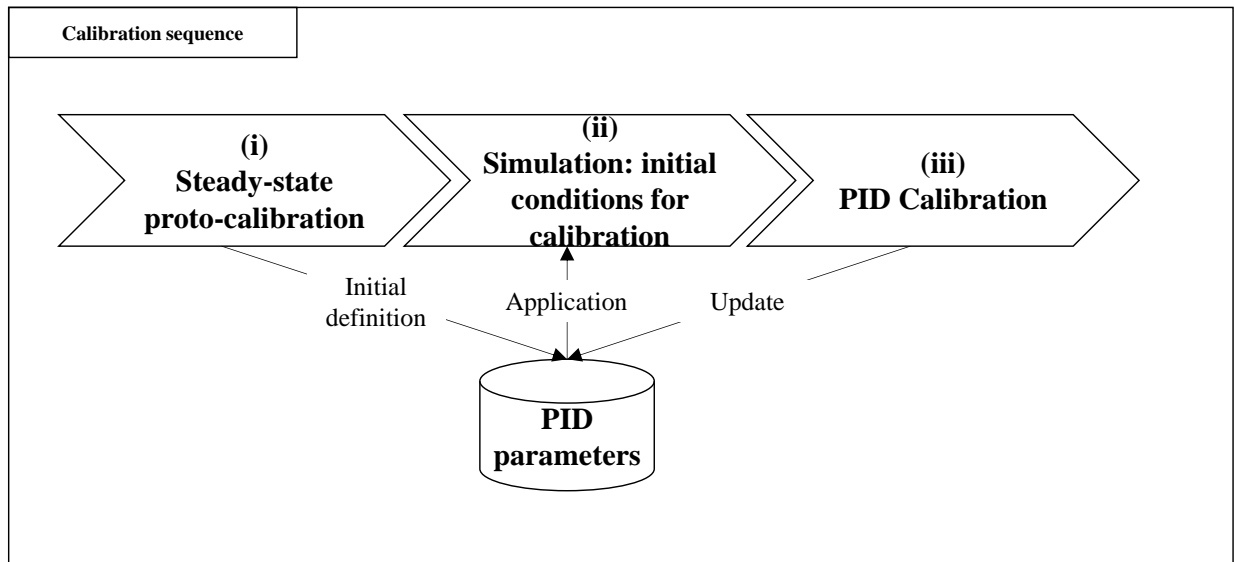
Source: Author.

Given that this problem is characterized as a simple single objective optimization, the Nelder-Mead method was employed as implemented in the SciPy-Optimize library.

Then, the simulation algorithm was developed into two key subsystems. For the first subsystem, shown in Figure 62, the main calculation steps are the following:

- (iv) Steady-state protocalibration to generate preliminary PID parameters and allow calculation of initial conditions.
- (v) Simulation to generate the initial conditions for calibration.
- (vi) PID calibration: optimization to determine the Ziegler-Nichols parameters  $L$  and  $a$ . The objective function returns the cumulative error (the difference between the setpoint and the heat exchanger heat side discharge temperature).

Figure 62 – First subsystem of the calibration algorithm, where the Ziegler-Nichols parameters are optimized for each ORC design.

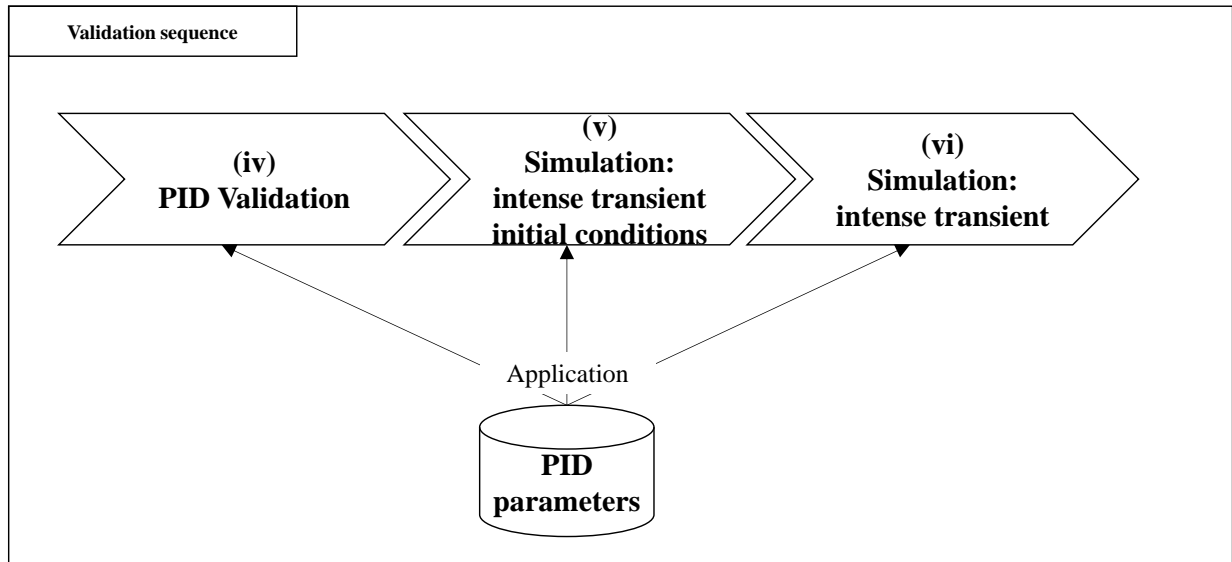


Source: Author.

The second subsystem, presented in Figure 63, is used to perform the verification and validation of the PID controller and the simulation of ORC performance under intense transient conditions. The calculation sequence is described below.

- (vii) PID validation of the optimized parameters, using the smooth transient dataset.
- (viii) Simulation to generate the initial conditions for the intense transient.
- (ix) Simulation of intense transient conditions.

Figure 63 – Second subsystem, where the validation and intense transient simulation are performed for each ORC design.



Source: Author.

This simulation algorithm was used to run the 6 steps for the generated design cases. Each of these designs was evaluated in terms of suitability for transient conditions when provided with an optimized PID controller.

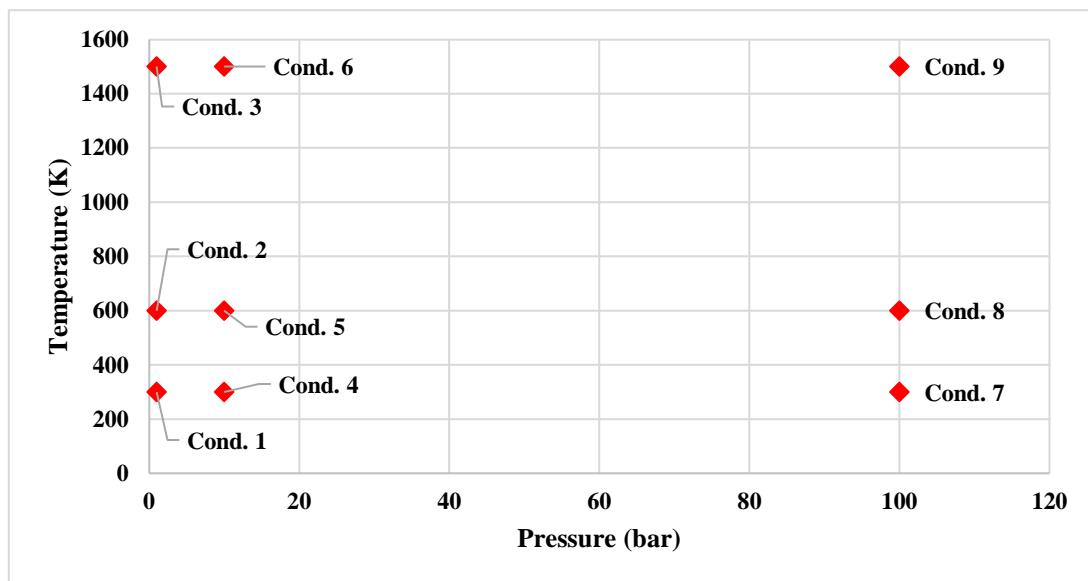
## 6. RESULTS

### 6.1 Gas turbine model – calibration, verification and validation

#### 6.1.1 Thermodynamic properties – verification of the weighted calculation

In order to cope with the change in fluid composition due to the combustion and the stream mixtures, the working fluid was considered as a gas mixture of four components:  $[N_2, O_2, CO_2, H_2O]$ . Then, to verify the thermodynamic properties calculation, the data from Lemmon et al. (2000) for the dry air at the conditions indicated in Figure 64 was used.

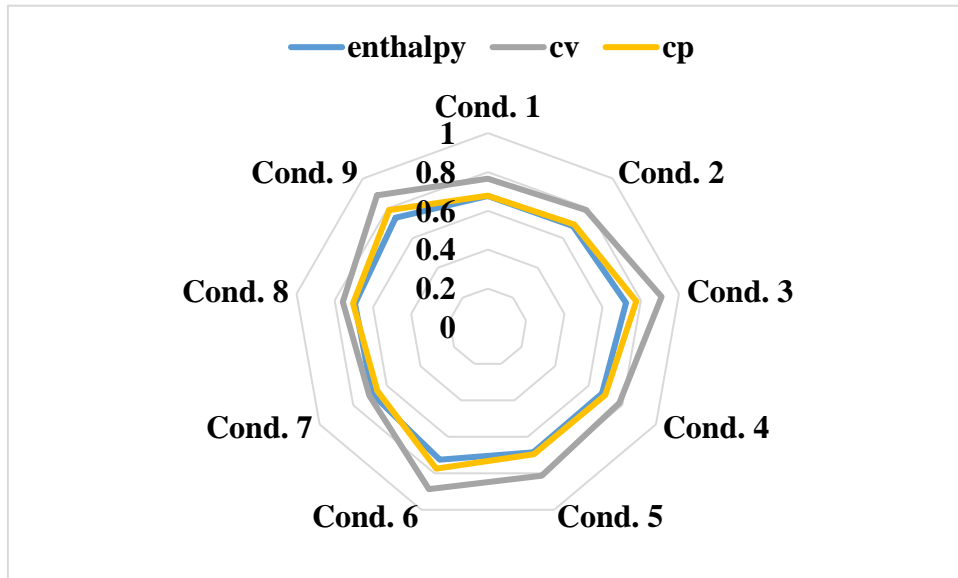
Figure 64 – Selected dry air conditions for the verification of the thermodynamic properties methodology.



Source: Adapted from Lemmon et al. (2000).

The enthalpy and specific heats were calculated for these points using the methodology implemented in the gas turbine simulator and compared to those given in the reference. The deviations between the calculated and reference values can be seen in Figure 65. It can be noted that the deviations are below 1% for all cases.

Figure 65 – Verification of the thermodynamic properties calculation – deviation between the calculated values and the reference.

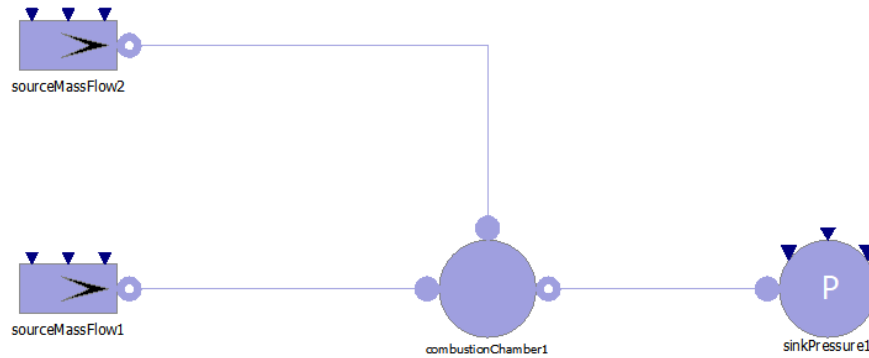


Source: Author.

### 6.1.2 Combustion chamber

Considering that the combustor model is a critical component for the overall gas turbine simulation results, a specific reference model for the combustion chamber was built using Modelica and the Thermopower library. The results of this model are compared with those generated by the model presented in this work, implemented for the simulation of the GE LM 2500+. The diagram of the model at the Open Modelica interface is shown in Figure 66.

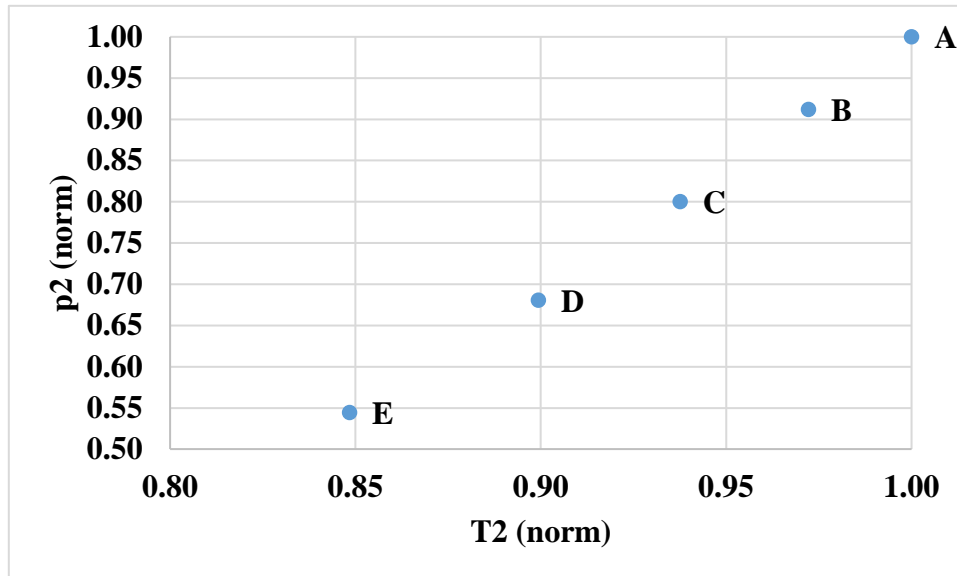
Figure 66 - Modelica model, which employs the Thermopower library. This model is used as a reference for the verification of the combustor model implemented for the simulation of the GE LM2500+.



Source: Author.

For the verification, it was used pure  $\text{CH}_4$  as fuel and air conditions were taken from data measured at the compressor exhaust in a real LM2500+ gas turbine. Figure 67 presents the normalized values of the air pressure and temperature used in the simulation.

Figure 67 - Normalized air pressure and temperature selected for the verification.



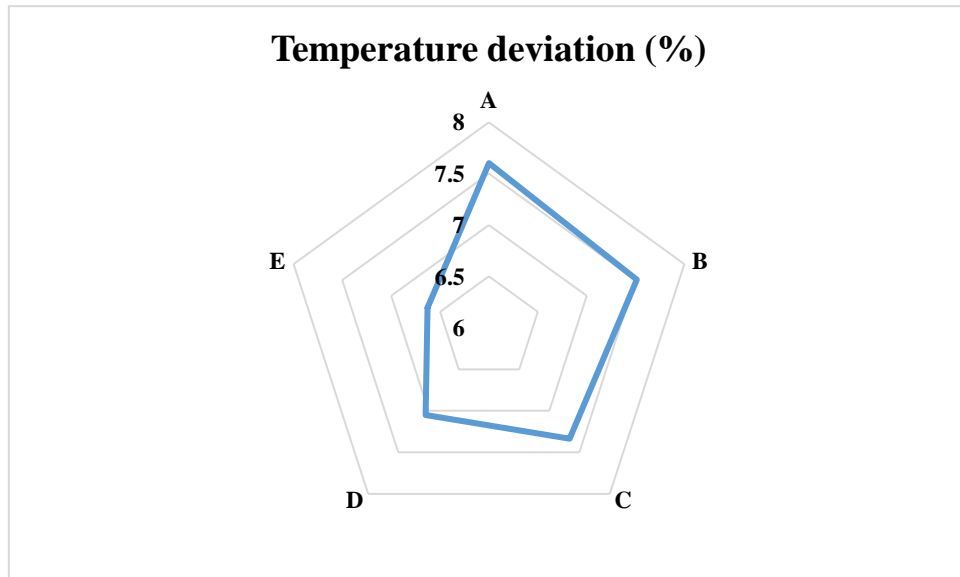
Source: Author.

The goal of this analysis is to compare the calculated values of the gas temperature leaving the combustion chamber. The results, presented in Figure 68, show an agreement



between the values calculated by the Modelica/Thermopower model and the model developed in this work.

Figure 68 - Comparison between the combustor exhaust temperature calculated through a Modelica/Thermopower model and the model presented in Section 4.2.5.



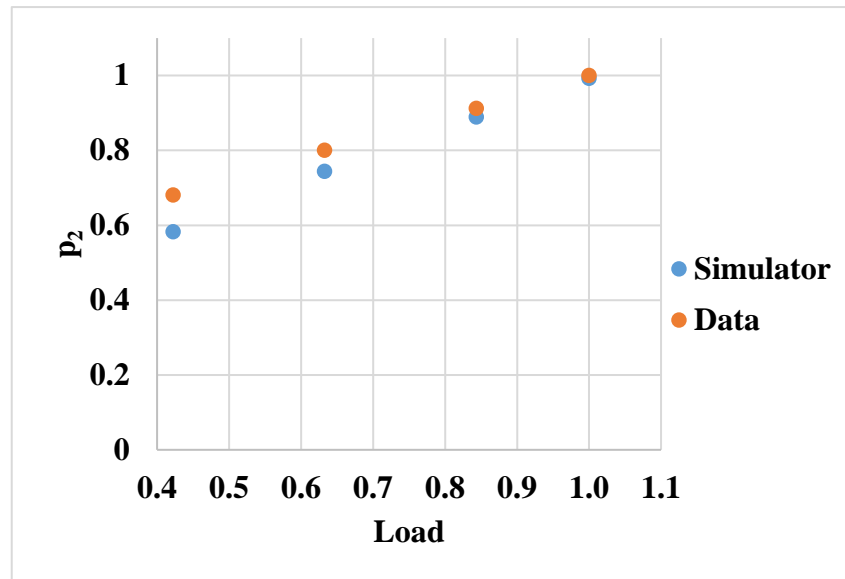
Source: Author.

### 6.1.3 Calibration at the design point and steady-state simulation

The results are presented as a comparison between the normalized simulated values and the measured data at different loads<sup>9</sup>: 1.0, 0.84, 0.63 and 0.42. Additionally, the results are presented in normalized values to preserve OEM critical data. Regarding the fluid condition at the compressor outlet, the calculated pressure results are presented in Figure 69 and Figure 70 shows the results for the temperature. These results show good agreement between the measured and simulated data, and, most specifically, it shows that the selected compressor map is suitable to predict the machine behavior.

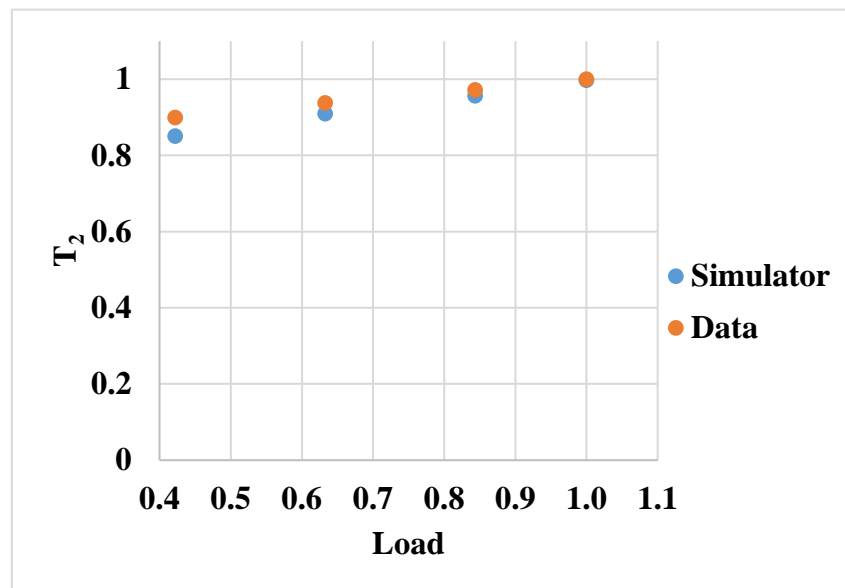
Figure 69 - Results for the compressor outlet pressure at the selected loads.

<sup>9</sup> Where  $Load = \dot{W}_{E,corrected} / \dot{W}_{E,DP}$ .



Source: Author.

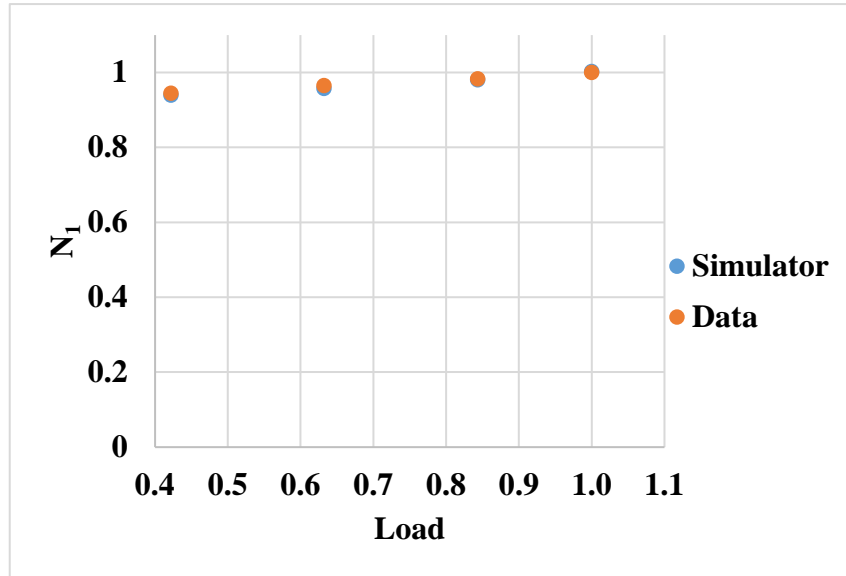
Figure 70 - Results for the compressor outlet temperature at the selected loads.



Source: Author.

The mechanical model of the gas generator shaft is coupled to the global aerothermodynamic model through the power demanded/generated by the compressor/turbine. This fact imposes that the results of the shaft model are a good indicator on the gas generator model accuracy, once it accumulates effects and cumulate error in its output. As Figure 71 shows, the result is fitted to the measured data in all the operated ranges evaluated.

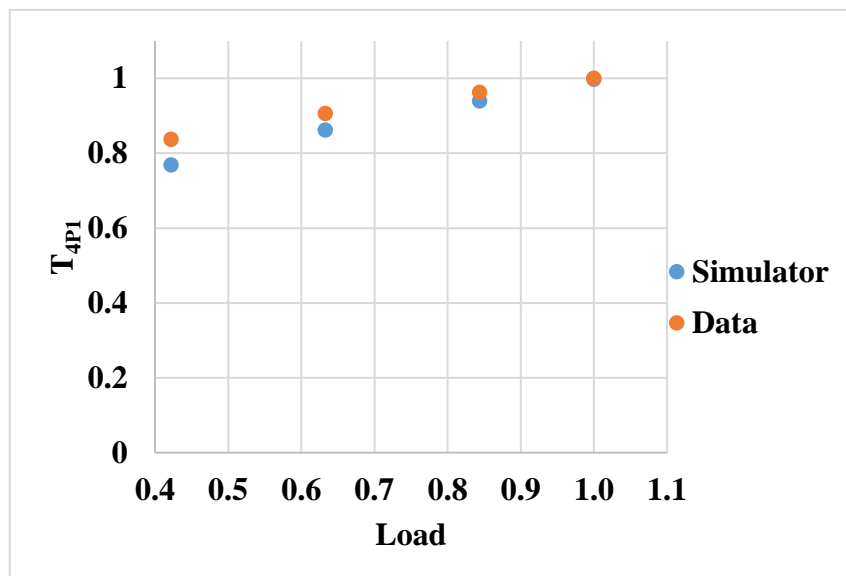
Figure 71 - Results for the gas generator shaft speed at the selected loads.



Source: Author.

The results on the temperature of the gas generator are one of the accuracy of the indicators of the combustion model. Indeed, the measurement taken in this position is a resource for evaluating the combustion performance, and it is a parameter for the combustor fault diagnostics. Figure 72 indicates that the model is able to correctly simulate the variable over the selected operational envelope.

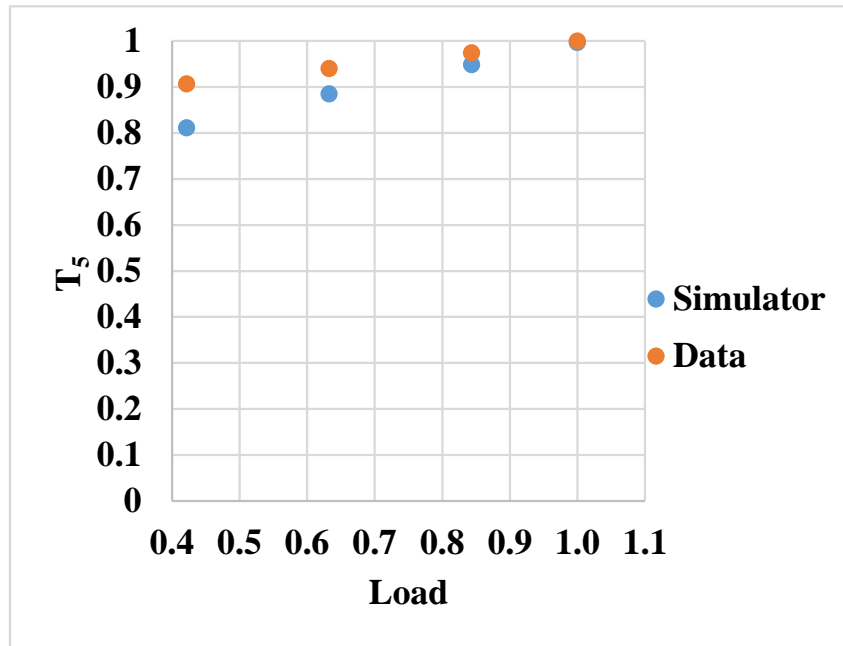
Figure 72 - Results for the gas generator outlet temperature at the selected loads.



Source: Author.

In addition to the electric power output, the gas turbine exhaust temperature is a fundamental parameter to evaluate the waste heat recovery potential and, as shown in Figure 73, the simulation results reproduce the actual machine behavior.

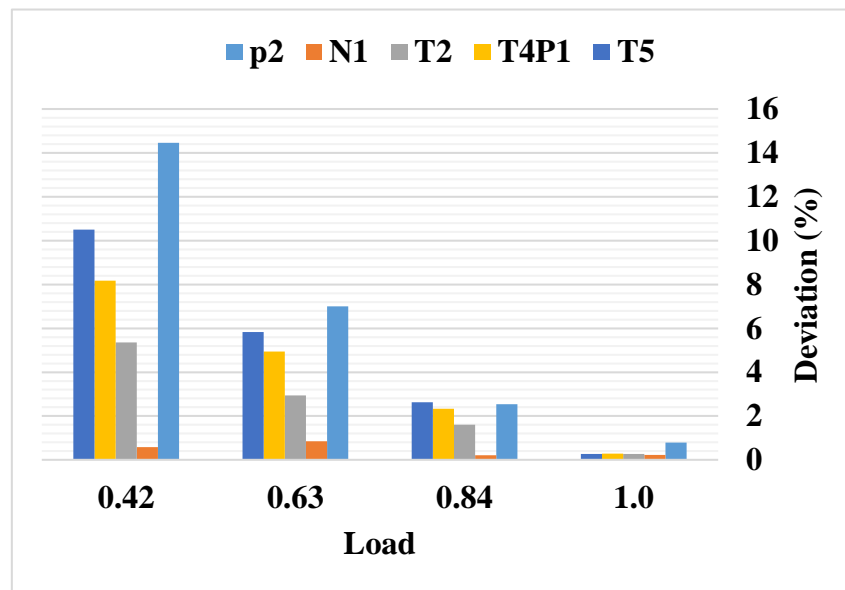
Figure 73 - Results for the gas generator outlet temperature at the selected loads.



Source: Author.

Finally, Figure 74 gives an overview of the accuracy of the results by presenting the deviation between the calculated and measured variables. The deviation remains below 10% in most cases. It can be seen that the deviation increases with decreasing load and a peak in the discrepancy is particularly noted for the exhaust temperature. This fact is explained by three factors: (i) The compressor map data is not fully suitable for and  $\dot{m}_{1,corr} < 0.5$ . (ii) For lower loads, there are other operational considerations that could not be considered here, such as air extractions and IGV positioning for anti-surge configuration. And (iii) the use of fixed efficiencies for the expanders leads to the discrepancy in the results for lower loads.

Figure 74 – Deviation between the simulated and reference values.



Source: Author.

#### 6.1.4 Control calibration and dynamic simulation

First, to properly simulate the gas turbine under dynamic conditions, a proper control model need also to be calibrated, as stated in Section 4.2.3. Table 9 presents the results of the optimization performed to fit the PID parameters for the gas turbine.

Table 9 – Parameters obtained for the gas turbine PID controller.

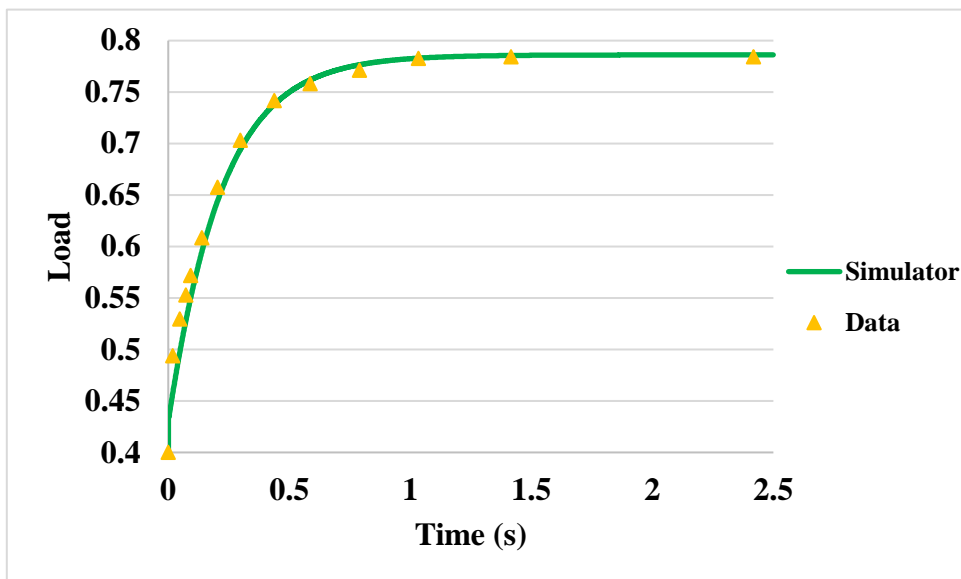
Coefficient	Value
$\kappa_p$	$6.9 \cdot 10^{-2}$
$\kappa_i$	4.0
$\kappa_d$	$-8.0 \cdot 10^{-5}$

Source: Author.

The resulting low value for  $\kappa_d$  shows a tendency of the control mode to behave as a proportional-integral model, as employed for modeling by Camporeale, Fortunato and Mastrovito (2006) and as defined for the control components of a real LM2500 machine and presented by Howell and Hartshorn (1995).

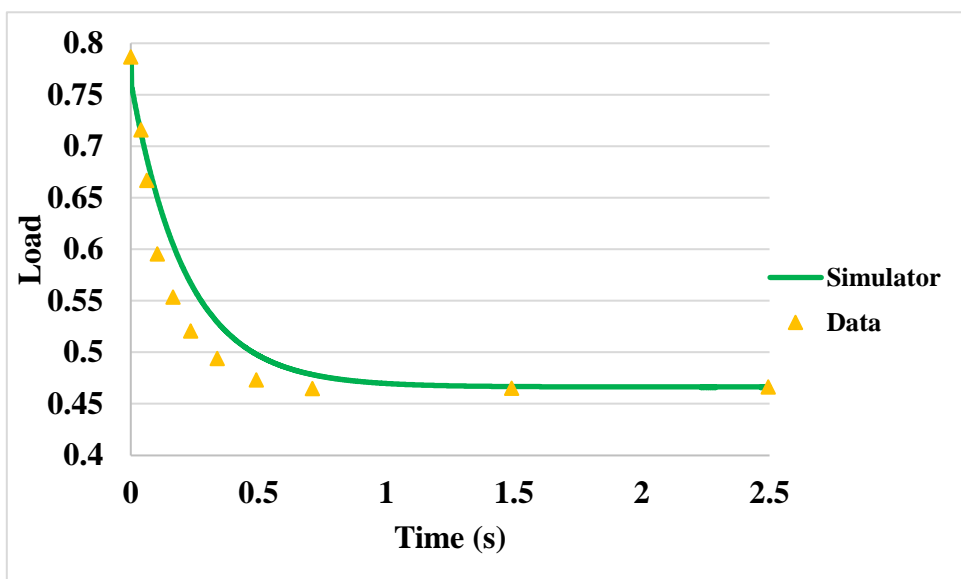
Once the PID controller was calibrated, the dynamic simulation could be performed. Since no data on dynamic conditions is available for the real gas turbine, the model was validated against the data provided by Meyer et al. (2014). Two sets of data were used in this validation, one for a load increase and the other for a load decrease. The results for each of them are shown in Figure 75 and Figure 76, respectively.

Figure 75 - Dynamic response to a load increase, from load = 0.4 to 0.79.



Source: Author.

Figure 76 - Dynamic response to a load decrease, from load = 0.79 to 0.47.

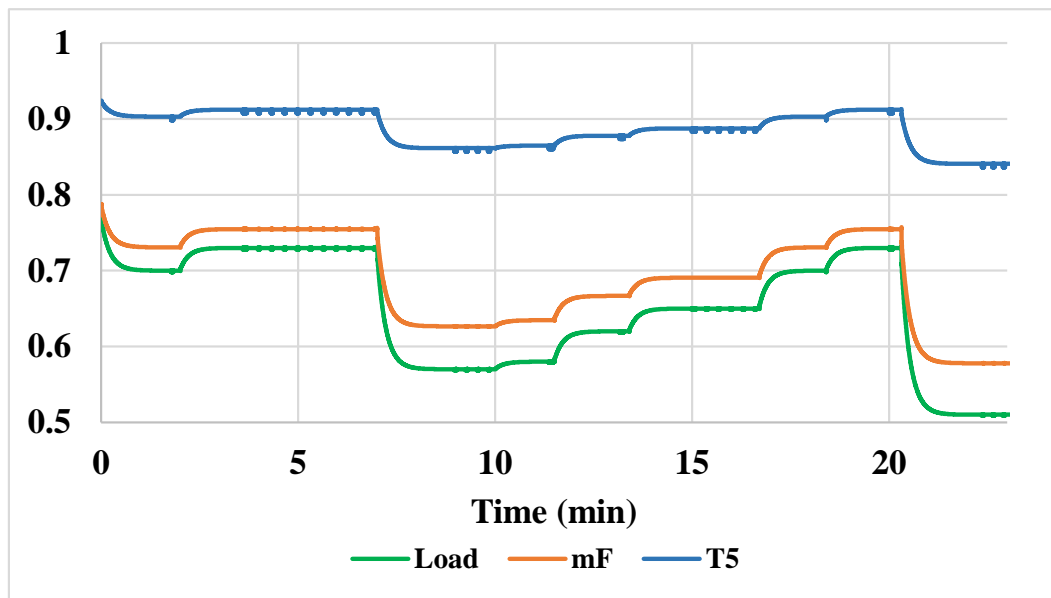


Source: Author.

The results show that the simulation predicts machine behavior very closely. Even for the load decrease where a small delay is observed when compared to the reference, it can be taken as negligible, as the time maximum delay is 0.35 s.

The computational model was also used to simulate the typical operational load demand observed in the FPSO, such as sudden load decreases which are observed after an equipment trip, for instance. In the same way, load increases are observed when electric powered equipment is started or another turbine is shut down. The developed simulator is applied to evaluate this typical behavior. The overall results for the dynamic simulation are given in Figure 77, which shows the variation of the normalized values of the load, exhaust temperature, and fuel mass flow rate with time. The results confirm the robustness of the model throughout all the simulated range.

Figure 77 – Results of the dynamic simulation of the critical performance parameters under typical operational demand. The results are normalized for all parameters.



Source: Author.

## 6.2 HORCAT verification

The implementation of HORCAT represents a novel approach in terms of methodology and application. Before the algorithm is used for thermal optimization and design problems, it was necessary to perform its verification and check its robustness and suitability to handle complex objective functions. To achieve this, objective functions from the literature, commonly

employed to assess multi-objective optimization algorithms, were used. These functions facilitated the evaluation of the effectiveness of HORCAT in dealing with highly nonlinear conditions and non-continuous domains. Specifically, three test functions were selected for application, as Table 10 shows. The test functions are listed in order of complexity, and the comparison was made against data presented in recent works for state-of-the-art optimization algorithms.

Table 10 – Test cases and references used for the verification of HORCAT.

CASE	FUNCTION NAME	ORIGINAL PUBLICATION	REFERENCE DATA	FUNCTION DESCRIPTION
(A)	Binh & Korn	Binh and Korn (1996)	Maghawry et al. (2021)	$\begin{cases} f_1(\bar{x}) = 4x_1^2 + 4x_2^2 \\ f_2(\bar{x}) = (x_1 - 5)^2 + (x_2 - 5)^2 \end{cases}$
(B)	ZDT $\tau_1$	Zitzler, Deb and Thiele, (2000)	Pereira et al. (. 2022)	$\begin{cases} f_1(\bar{x}) = x_1 \\ f_2(\bar{x}) = g(\bar{x})h(f_1(\bar{x}), g(\bar{x})) \end{cases}$ $g = 1 + \frac{9}{n-1} \sum_{i=2}^n x_i$ $h(f_1, g) = 1 - \sqrt{\frac{f_1}{g}}$ $0 \leq x_i \leq 1$ $0 \leq i \leq 30$
(C)	ZDT $\tau_3$	Zitzler, Deb and Thiele, (2000)	Pereira et al. (. 2022)	$\begin{cases} f_1(\bar{x}) = x_1 \\ f_2(\bar{x}) = g(\bar{x})h(f_1(\bar{x}), g(\bar{x})) \end{cases}$ $g = 1 + \frac{9}{n-1} \sum_{i=2}^n x_i$ $h(f_1, g) = 1 - \sqrt{\frac{f_1}{g}} - \frac{f_1}{g} \sin(10\pi f_1)$ $0 \leq x_i \leq 1$ $0 \leq i \leq 30$

Source: Author.

In addition, the effect of the FLS was evaluated in all cases, and the results are presented with the FLS enabled and disabled for each case. It is important to mention that HORCAT discards similar designs, leading to sparse Pareto fronts, but with actual and unique solutions.

For validation, the initial parameters of Equation (41), used for the PSO algorithms for both packs, are given in Table 11. These parameters are changed during the iterations according



to the decision-making made by the FLS. The general configuration for the optimization is presented in Table 12.

Table 11 – Initial parameters of the PSO defined for each of the packs of HORCAT.

$\omega$	$c_1$	$c_2$
1.2	0.5	0.5

Source: Author.

Table 12 – General configuration of the algorithm for the optimization defined for each test function.

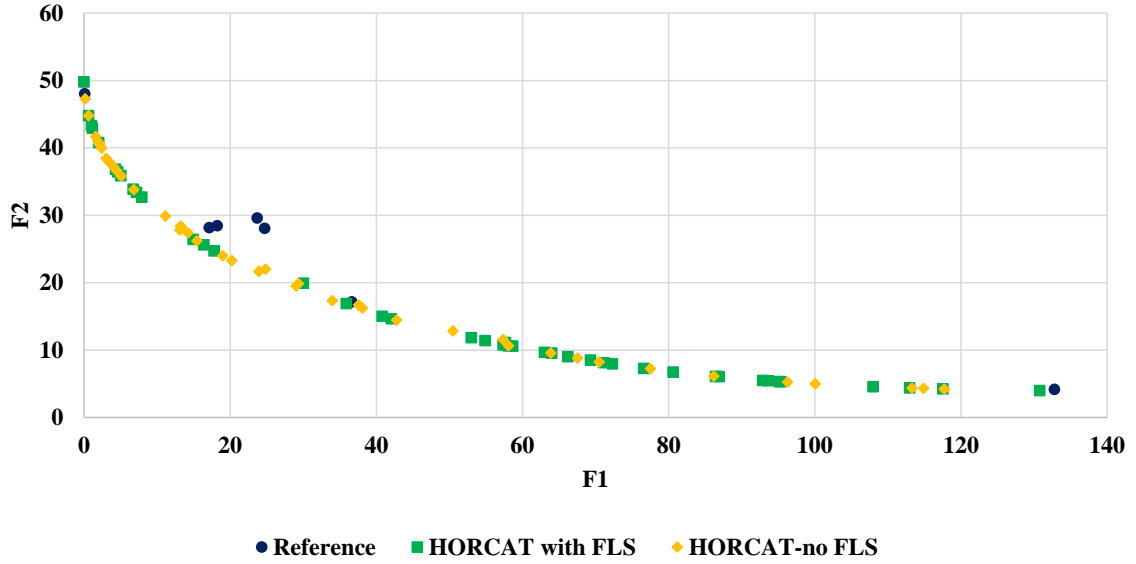
<b>CASE</b>	<b>GLOBAL ITERATIONS</b>	<b>PACK ITERATIONS</b>	<b>DESIGN VECTOR DIMENSION</b>	<b>POPULATION SIZE</b>	<b>OBJECTIVE FUNCTION CALLS</b>
(A)	3	3	2	42	3024
(B)	3	9	30	630	136080
(C)	3	9	30	630	136080

Source: Author.

The results obtained for the validation are given in Figure 78, Figure 79, and Figure 80. For all cases, the HORCAT optimized results were similar (or even better) than the references given in literature. The effect of the FLS during optimization can also be observed. For the case (A), with a simple and well-behaved test function, the effect is barely noted. For cases (B) and (C), with more complex test functions and more cases to be evaluated, it can be noted the presence of solutions with are not exactly over the Pareto front. This can be explained by the fact that the Elite dimension is fixed for a given evaluation. For the same number of iterations, when the FLS is enabled, the potential solutions are sufficiently stressed. When the FLS is disabled, more iterations would be needed to achieve the same Pareto front pattern.

Figure 78 – Pareto fronts for the minimization of functions F1 and F2 (Binh & Korn).

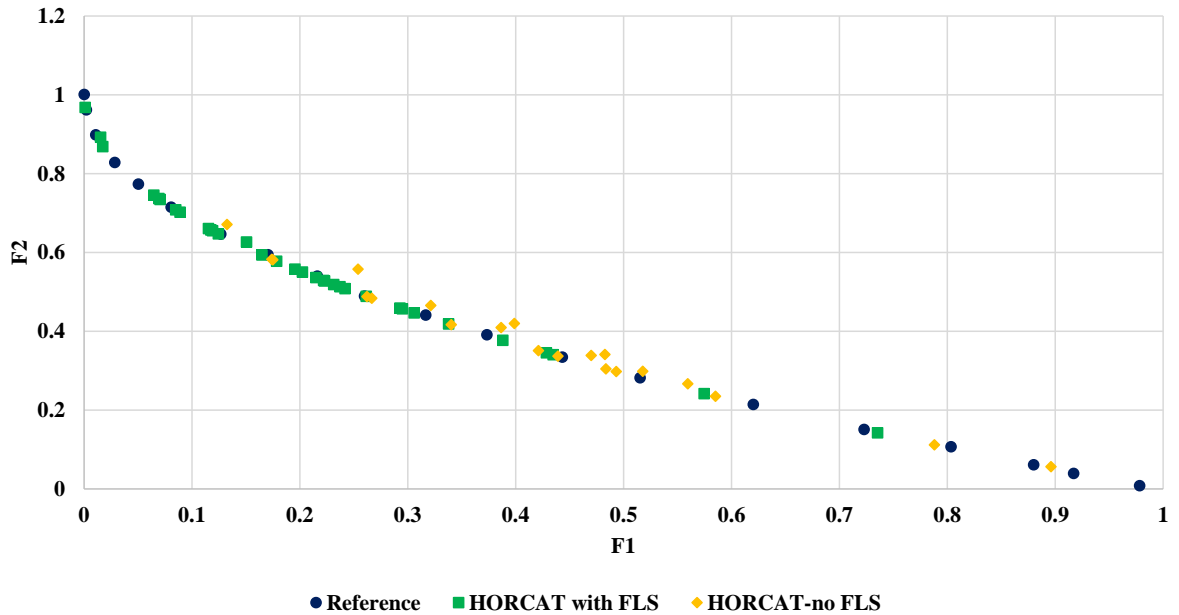
(A) Binh & Korn function



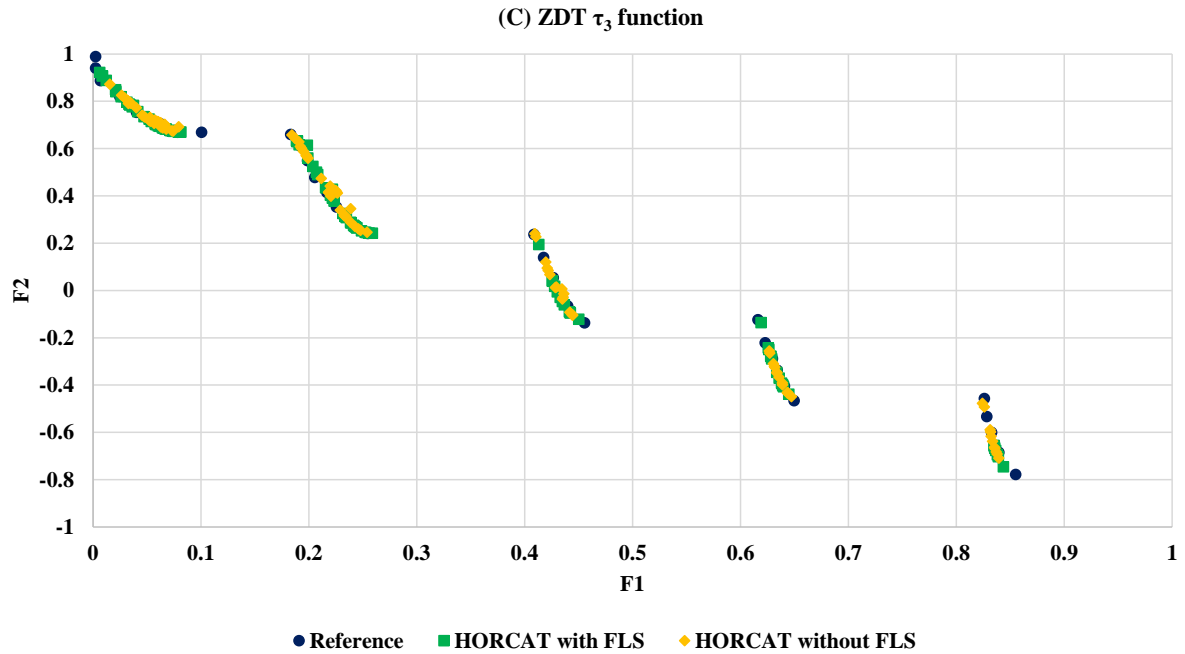
Source: Author.

Figure 79 – Pareto fronts for the minimization of functions F1 and F2 (ZDT  $\tau_1$ ).

(B) ZDT  $\tau_1$  function



Source: Author.

Figure 80 – Pareto fronts for the minimization of functions F1 and F2 (ZDT  $\tau_3$ ).

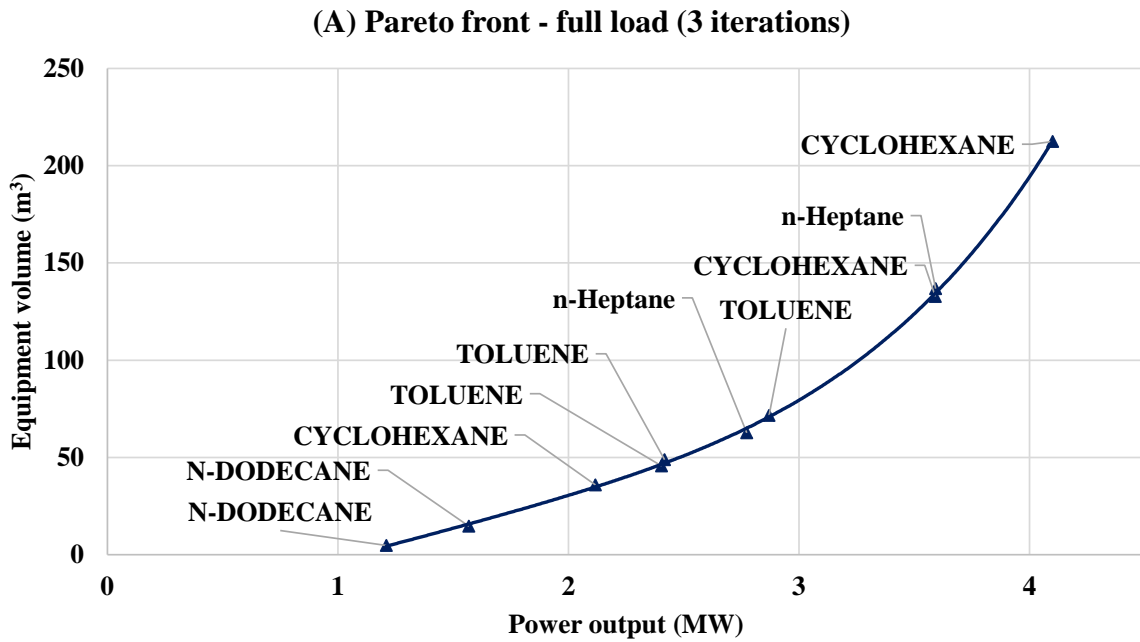
Source: Author.

### 6.3 ORC design applied for gas turbine waste heat recovery

#### 6.3.1 Gas turbine in steady state

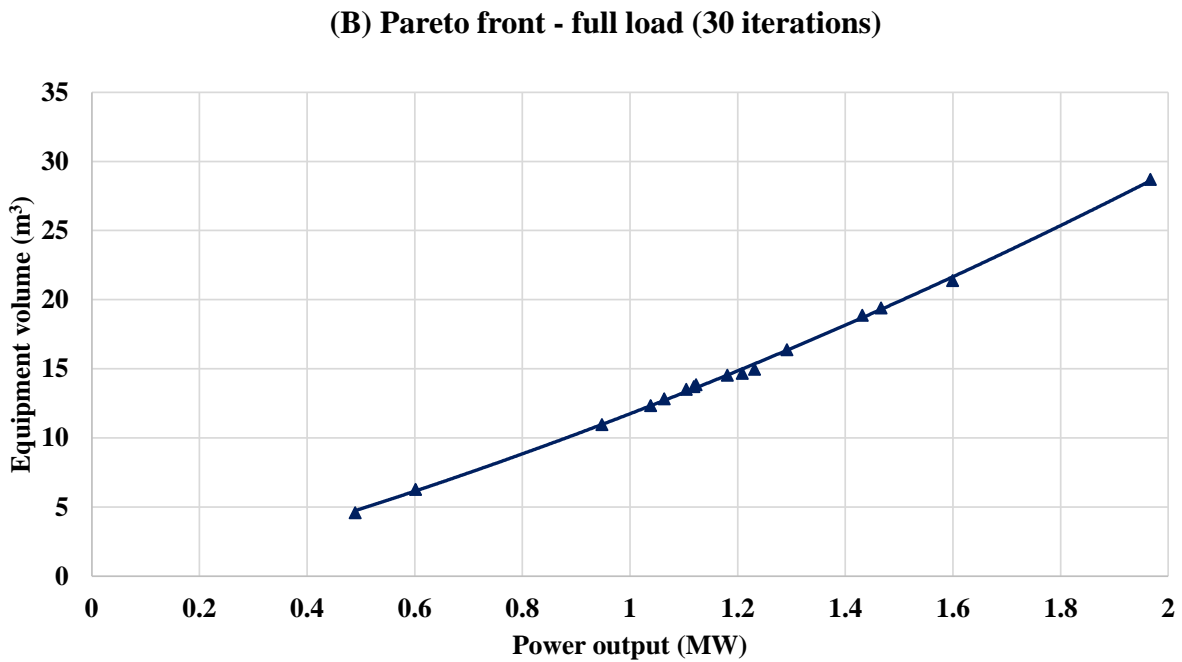
To generate ORC designs considering the gas turbine full load condition, the HORCAT setup considered two packs of 100 individuals. Initially, still aiming to evaluate the performance of HORCAT, two scenarios were considered: (A) running the optimization with 3 iterations and (B) with 30 iterations. The results for both scenarios are presented in Figure 81 and Figure 82.

Figure 81 – Optimization results for the ORC design considering only the gas turbine at full load: scenario (A): after 3 iterations performed by HORCAT.



Source: Author.

Figure 82 – Optimization results for the ORC design considering only the gas turbine at full load: scenario (B): after 30 iterations performed by HORCAT.

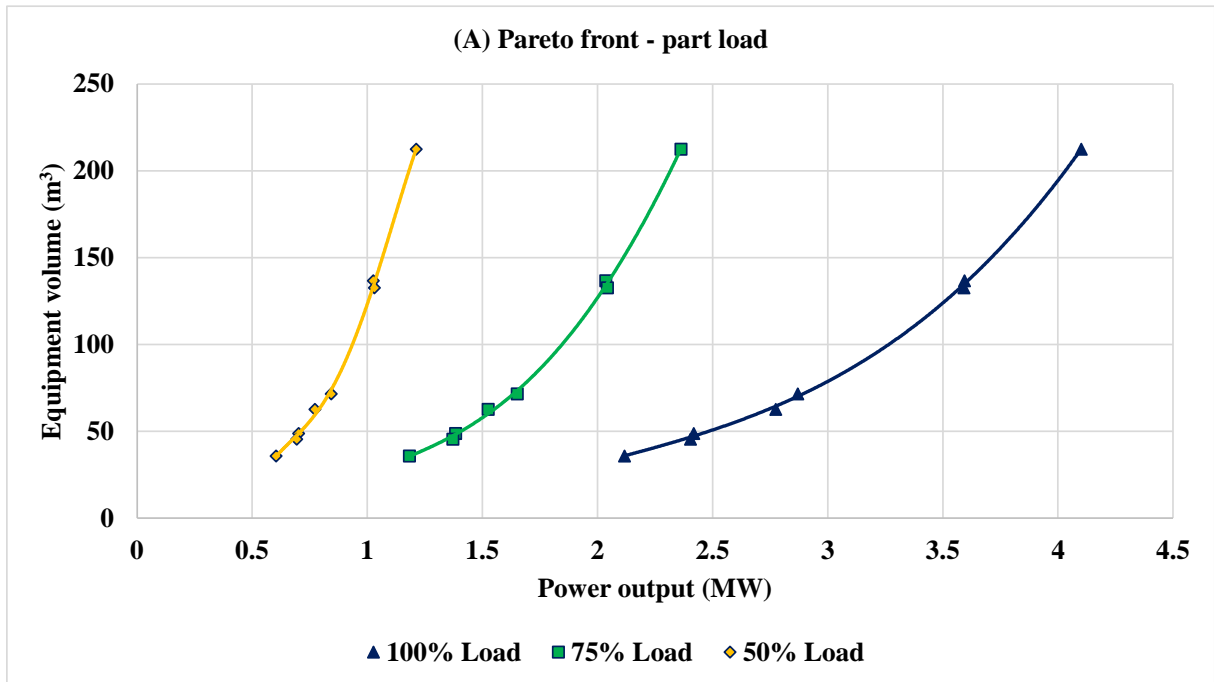


Source: Author.

In scenario (A), 10 valid designs were generated and, of a total of 18 organic fluids available for selection, only 4 resulted in the valid ORC designs. However, in this suboptimal condition, a wide ORC electrical power range (1.2 - 4.1 MW) can be seen with large and unfeasible equipment volumes. There is a sensitive change in these conditions in scenario (B), where the effects of Pareto domination can be seen after several iterations and a higher power/volume ratio is obtained. In scenario (A), only toluene results as a valid design working fluid. In scenario (B), 16 valid designs were generated, with an ORC electric power range from 489 kW to 1.97 MW, which can lead to an increase of more than 8% in the power output when considering the gas turbine and the ORC combined. Furthermore, the Rankine cycle thermal efficiency of these valid designs is in the range 27-29%. The effect of Pareto dominance is evident when comparing scenarios (A) and (B). First, the lower number of valid designs in scenario (A) is a consequence of insufficient iterations, so that the HORCAT packs were still unable to find a broader number of solutions that makes sense in terms of thermodynamic validity. As the number of iterations increases, more solutions are found in scenario (B). These solutions Pareto-dominate those found in scenario (A) and, additionally, there is a clear and expected migration of the Pareto front to the bottom (lower equipment volume) and to the right (lower power output).

To test the ORC designs generated in scenarios (A) and (B) in load conditions typically found in FPSOs, the proposed solutions were simulated under part load conditions (50 and 75%) of the gas turbine. Figure 83 presents the Pareto fronts for scenario (A). Under part load conditions, the valid designs dropped from 10 to 8 cases, since ORCs operating with n-dodecane were not able to operate at lower temperatures and remain thermodynamically feasible, given the geometry of the components that were designed for the full load condition.

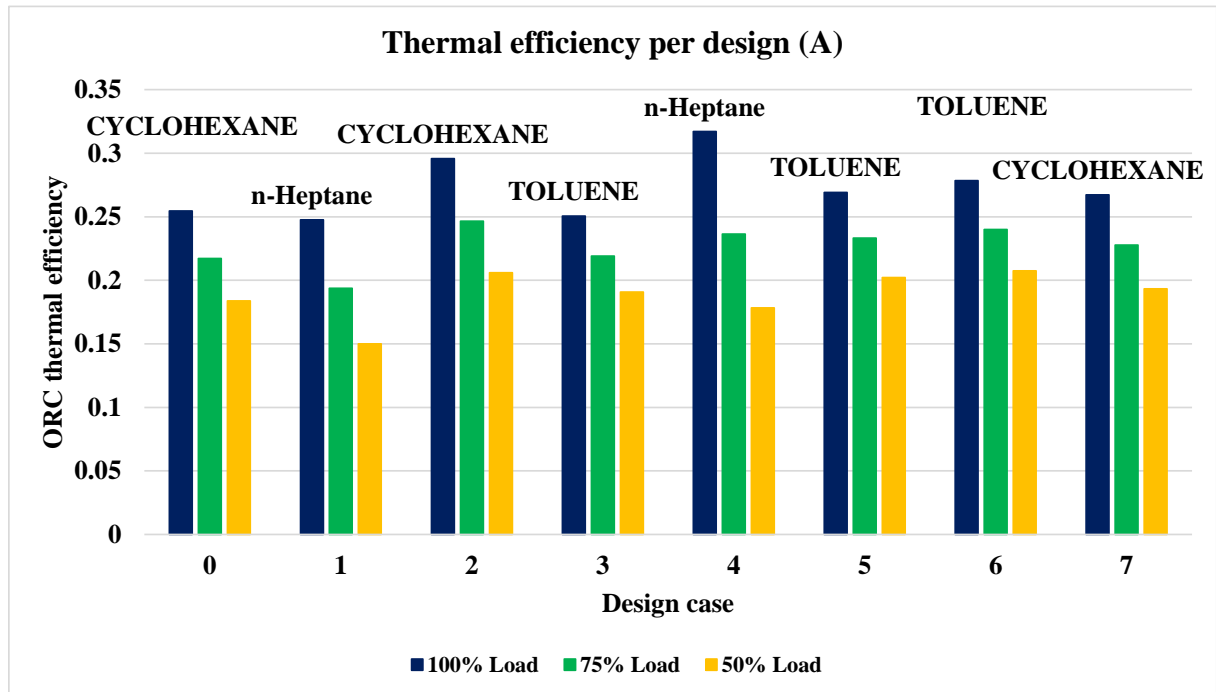
Figure 83 – Pareto fronts for the scenario (A) proposed designs under the gas turbine loads of 50%, 75% and 100%.



Source: Author.

Regarding thermal efficiency, as seen in Figure 84, there is a significant drop under part loads for all fluids, with toluene having the lowest variation. It is important to highlight the case 5 as an example where the full load condition do not forecast a good solution at partial loads. Although it presents the higher efficiency at full load, it also has the second worst performance at 50% load.

Figure 84 – Thermal efficiencies for each valid design under part load conditions - scenario (A).

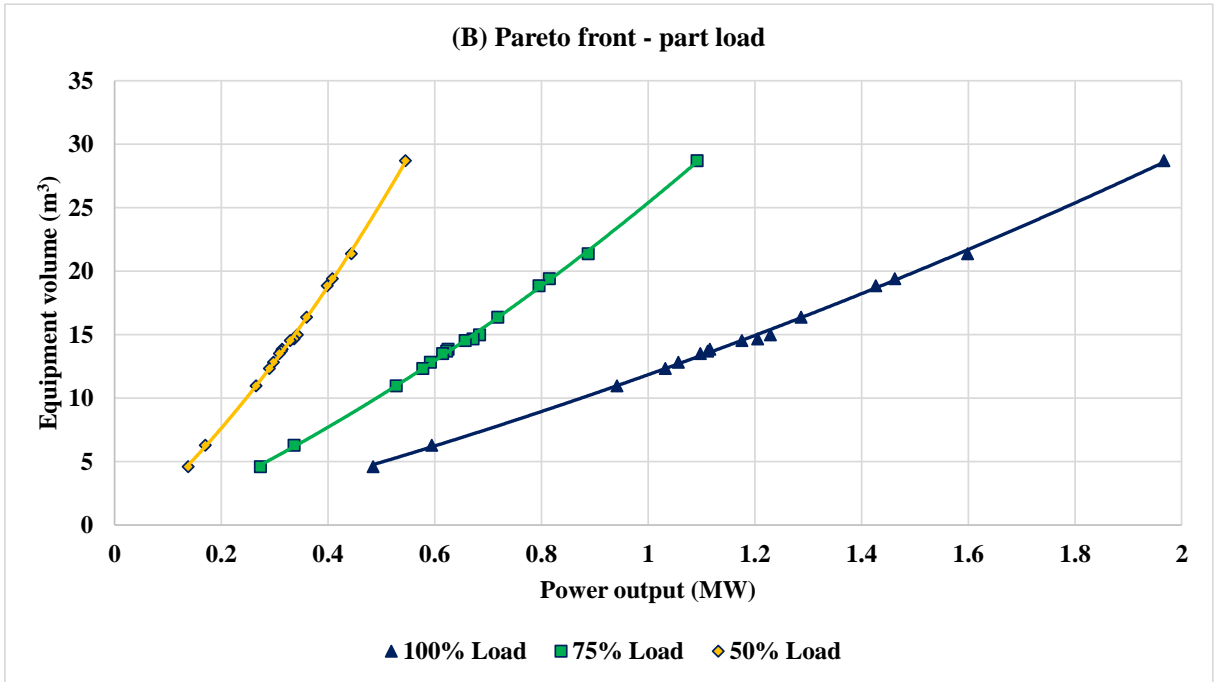


Source: Author.

The comparative analysis considering part loads applied for scenario (B) returned more stable conditions compared to scenario (A). The number of solutions found after 30 iterations at full load did not drop under part load conditions, which can be explained by two factors: the highly optimized solutions and the suitability of toluene under such conditions. Figure 85 shows the Pareto fronts for each condition.



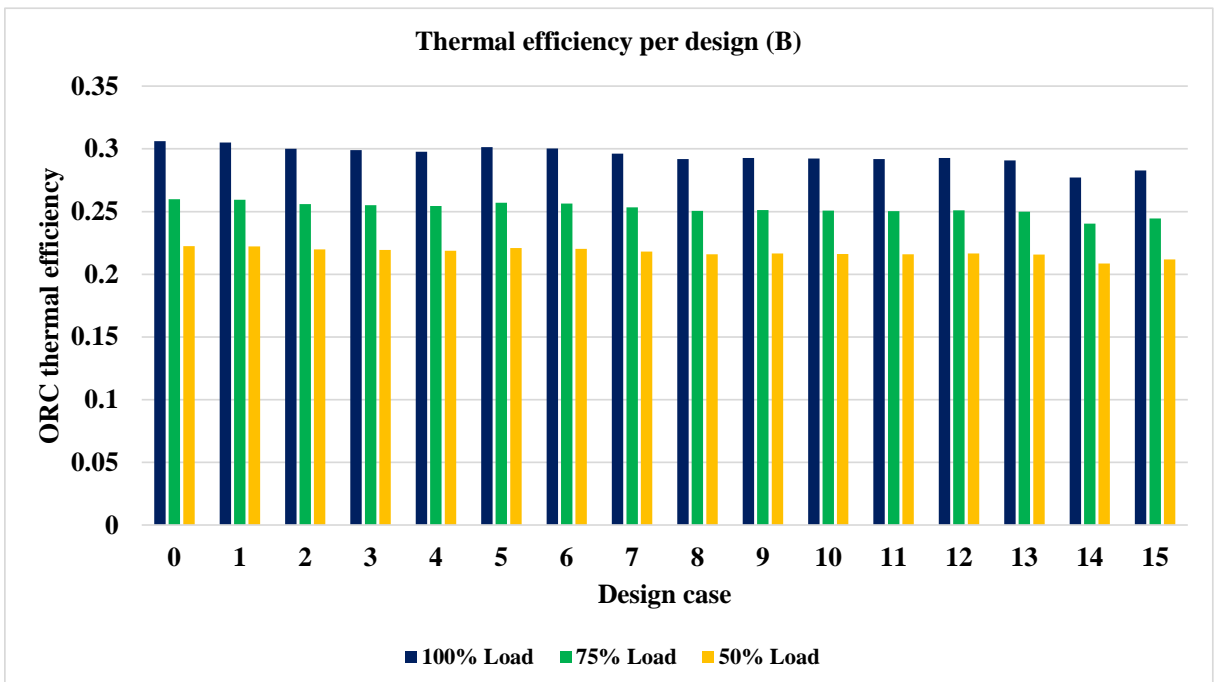
Figure 85 – Pareto fronts for the scenario (B) proposed designs under the gas turbine loads of 50%, 75% and 100%.



Source: Author.

Moreover, as seen in Figure 86, the thermal efficiencies found for all cases remain high even under partial loads.

Figure 86 – Thermal efficiencies for each valid design at part load conditions - scenario (B).



Source: Author.

As a matter of reference, the thermodynamic parameters for the design that returned the highest power output for Scenario B are given in Table 13.

Table 13 – Main thermodynamic parameters of the ORC design with the biggest power output – Scenario B.

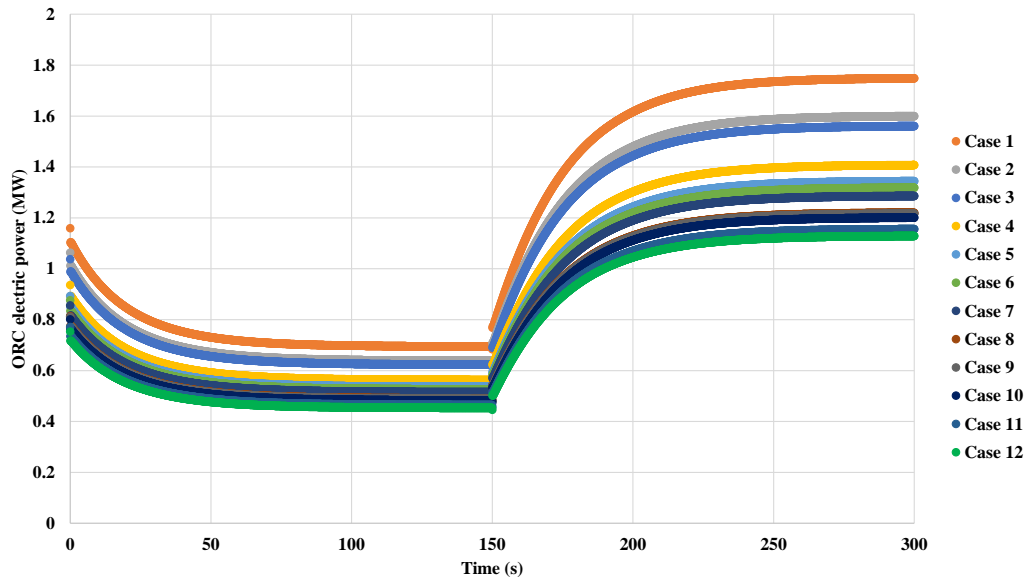
<b>Parameter</b>	<b>Value</b>
Case	1
Fluid	Toluene
$T_9$ (°C)	274.2
$p_9$ (bar)	12.3
$\dot{W}$ (kW)	1967
$\dot{m}$ (kg/s)	11.2
$p_{10}$ (bar)	0.9
$T_{10}$ (°C)	380.5

Source: Author.

### 6.3.2 Gas turbine dynamics

The designs provided for scenario (B), as described in section 6.3.1 were used for the evaluation of the ORC transient response. The dynamic behavior of the ORC designs for heat recovery was evaluated considering the dynamic gas turbine maneuver shown in Figure 56. The response of the ORC plants to the dynamic input given by the exhaust temperature is presented in Figure 87.

Figure 87 – Transient response of the dynamic maneuver of the ORC, given the gas turbine.



Source: Author.

These results reveal a notable reduction in the number of valid designs from 16 to 12 when considering the dynamic conditions. This decrease is primarily attributed to factors such as thermal inertia, moisture at the steam turbine inlet under lower loads, and the thermodynamic state outside the computational library domain. Such situations require an evaluation beyond steady-state conditions.

It is crucial to emphasize that, despite the apparent proximity of designs along the Pareto front, indicating potential similarity, the diverse responses to dynamic input underscore the variability among the parameters of the ORC designs. Furthermore, certain aspects of the adopted control strategy warrant discussion. As seen in section 4.2.3, the gas turbine power output is regulated by a robust PID controller, and the ORC control strategy is designed not to interfere with the upstream system. The proportional control adopted here effectively regulated the working fluid, allowing the bottoming plant to adapt itself to the response of the gas turbine response. Additionally, it is pertinent to note, particularly from a numerical point of view, that the rapid dynamic response of the gas turbine requires a smaller increment for finite differences. Without proper adjustment, the thermodynamic response of the bottoming cycle could render some designs unfeasible, despite the increased computational effort in this scenario.

## 6.4 ORC design applied for the compressor train temperature control

### 6.4.1 Compressor at steady-state – ORC designs

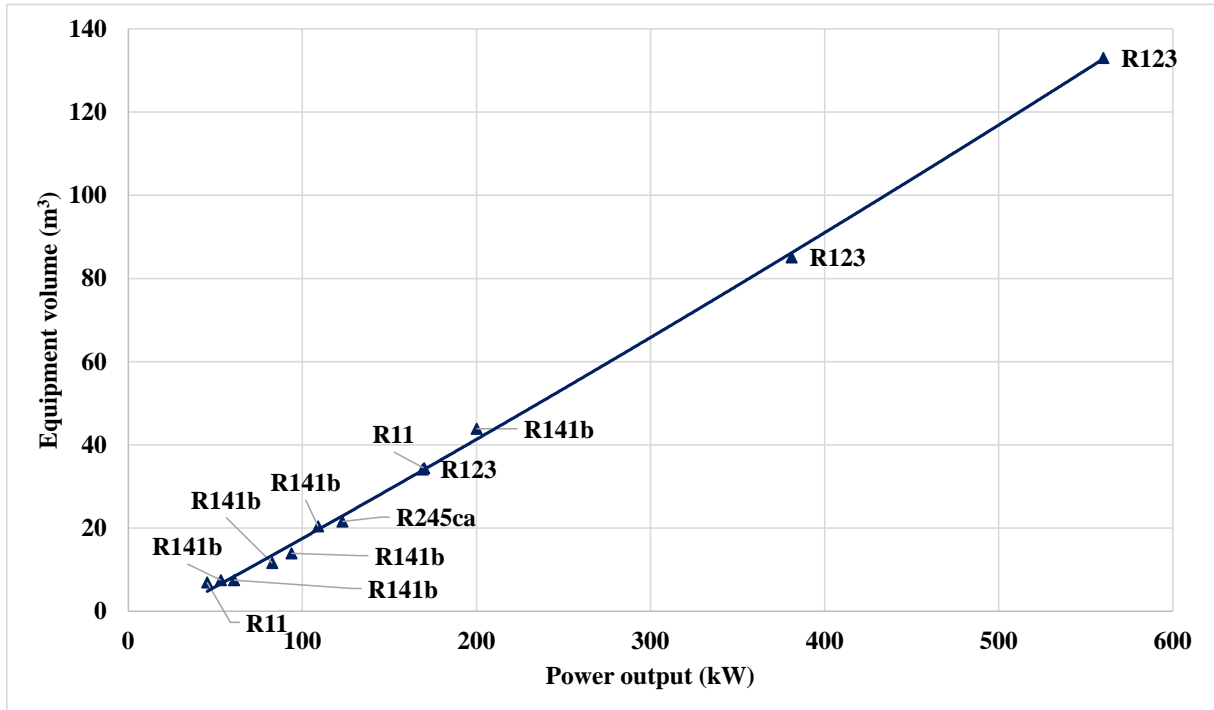
The same analysis applied to generate the designs for the gas turbine at steady state was applied for the compressor. HORCAT was used in the search for optimal designs considering the compressor data for calibration, presented in Section 5.4.2. Consequently, 12 valid designs were generated, featuring 4 different working fluids. The Pareto front, resulting from optimizing the ORC for maximum power output and minimum volume, is shown in Figure 88. Despite the challenge of relatively low temperatures (116 °C - 163 °C) for heat recovery, HORCAT successfully produced ORC designs with significant power output, reaching up to 560 kW. The thermodynamic parameters of the design that generates the highest power output is presented for reference in Table 14.

Table 14 – Main thermodynamic parameters of the ORC design with the biggest power output – Compressor.

<b>Parameter</b>	<b>Value</b>
Case	11
Fluid	R123
$T_{9b}$ (°C)	91.9
$p_{9b}$ (bar)	4.5
$\dot{W}$ (kW)	560
$\dot{m}$ (kg/s)	14.7
$p_{10}$ (bar)	0.9
$T_{10}$ (°C)	62.2

Source: Author.

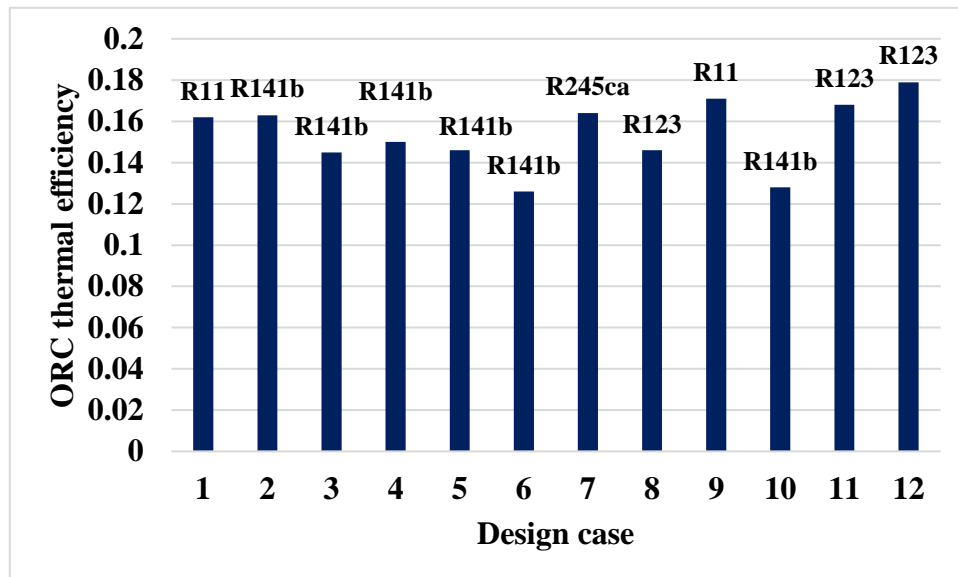
Figure 88 – Optimization results for the ORC design for the heat recovery at the compressor discharge.



Source: Author.

When comparing the designs generated for the gas turbine and for the compressor, a notable disparity arises in the variety of working fluids used. The temperature of the gas turbine exhaust gases imposes significant constraints on the organic fluids that can withstand such conditions. However, it is essential to note that, due to HORCAT's tendency to discard similar designs, the number of diverse solutions for the compressor case is smaller. The thermal efficiency of the generated designs can be seen in Figure 89. The efficiencies for this case are similar to those seen in real-life for low-temperature applications.

Figure 89 – ORC thermal efficiency for the design cases generated for the compressor waste heat recovery.



Source: Author.

#### 6.4.2 Compressor dynamics

Considering the characteristics of the available data with respect to the detailed compressor and the step-by-step validation process presented in Section 5.4.2, the PID calibration process plays an important role in the overall analysis. Therefore, it is relevant to evaluate the calibration results before discussing the dynamic simulation. According to the ORC generated designs and following the process presented in Figure 61, Table 15 presents the PID parameters calibrated through the optimization process using the Ziegler-Nichols tuning. Each design undergoes a singular calibration tailored to its dynamic response during tuning.

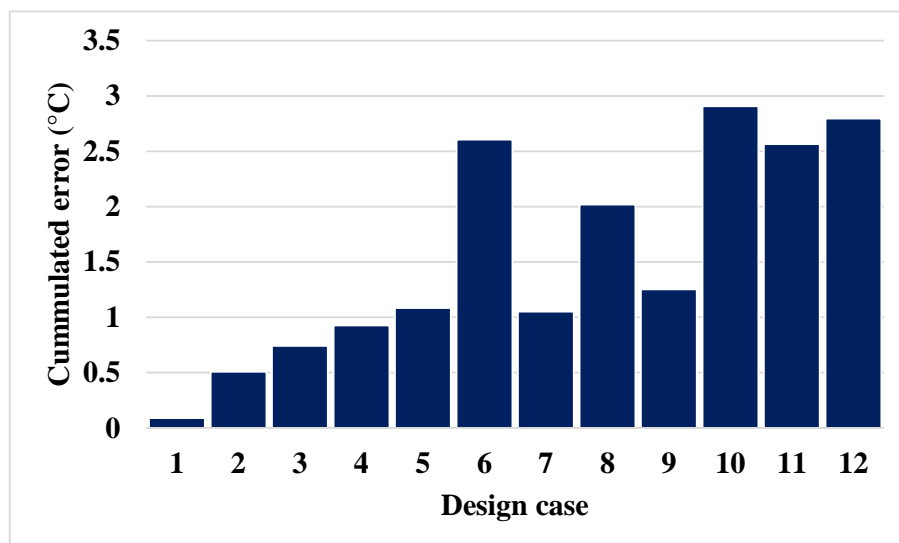
Table 15 – Results obtained for the PID parameters after the calibration.

Case	$\kappa_p$	$\kappa_i$	$\kappa_d$
1	2.04E-02	7.79E-02	1.34E-03
2	4.00E-02	2.32E-01	1.72E-03
3	1.94E-02	4.48E-02	2.09E-03
4	1.70E-02	2.03E-02	3.55E-03
5	2.72E-02	5.28E-02	3.50E-03
6	1.55E-02	4.65E-02	1.28E-03
7	1.70E-02	2.03E-02	3.55E-03
8	1.27E-02	2.59E-02	1.56E-03
9	3.01E-02	4.57E-02	4.95E-03
10	1.47E-02	3.86E-02	1.41E-03
11	1.47E-02	4.44E-02	1.23E-03
12	1.41E-02	3.86E-02	1.29E-03

Source: Author.

The outputs (the objective function results) of the PID tuning are presented in Figure 90. In particular, the maximum cumulative error for the temperature at the compressor discharges remains below 3 °C. Taking into consideration that during transitory phases there is a natural divergence between the setpoint and the calculated value, these cumulative errors are observed to be quite minimal.

Figure 90 – The outputs of the objective function defined for the PID calibration. The function gives the cumulated error of the difference between the setpoint and simulated discharge temperatures.



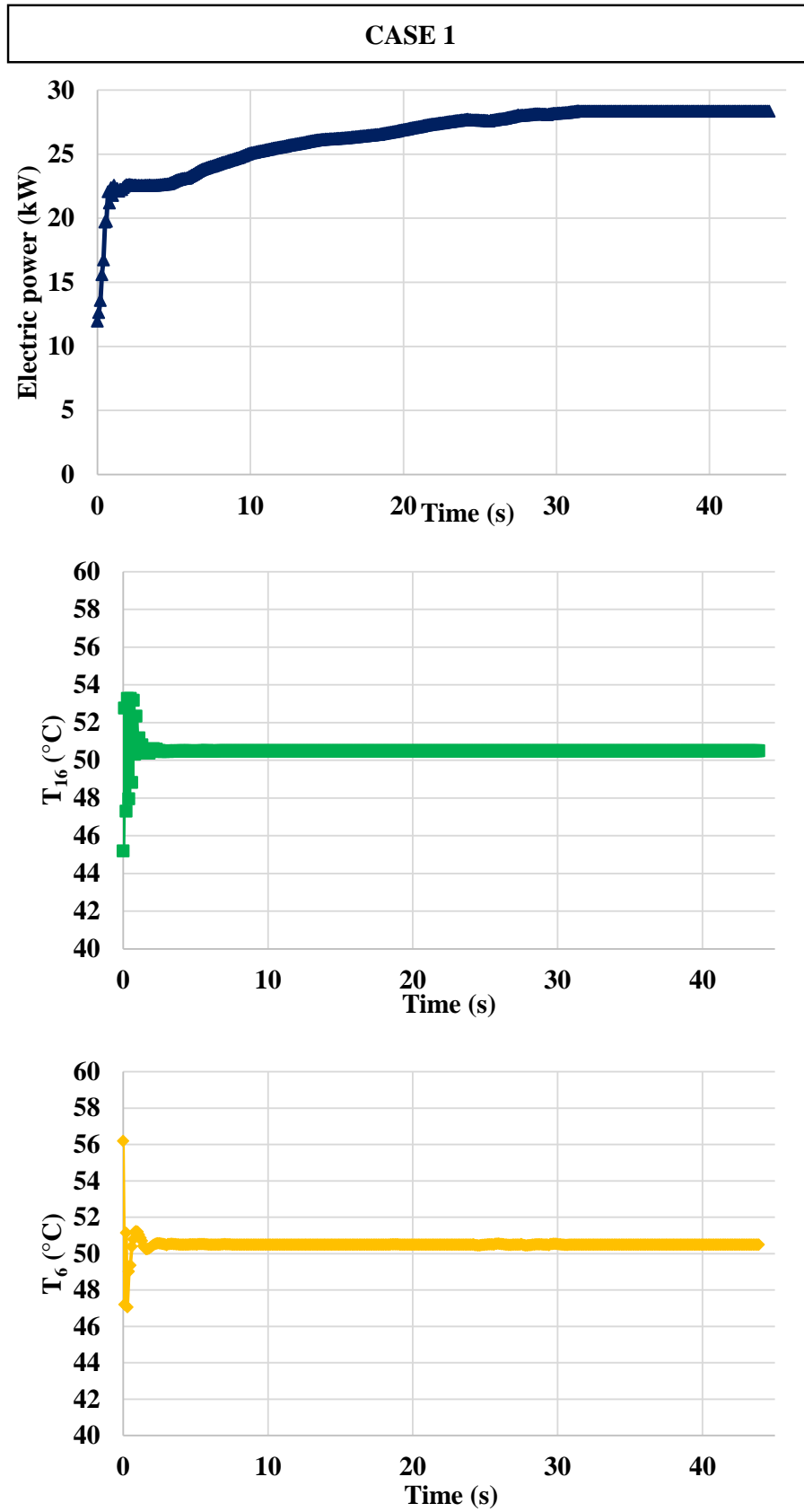
Source: Author.

Smooth transient data were used to validate the PID parameters obtained in the calibration of the control system. As the transient in the calibration dataset manifests itself primarily in the mass flow rate and discharge pressure, the results in terms of power output can be considered as quasi-steady state. However, even with the smooth transient input, it is noteworthy that one of the ORC designs could not withstand this off-design condition.

Subsequently, the ORC designs were evaluated under an intense transient scenario experienced by the compression train. Unlike the previously analyzed interval (0 - 2 s), this time interval spans 0 to 44 s. Additionally, during most of the load-up observed in this dataset, the compressor inlet temperature control is not active. Therefore, the ORC designs and the PID control were subjected to a situation representative of the load characteristics encountered on oil platforms. The response of the ORC designs to this transient, presenting the power output and temperatures of the gas stream after passing through the heat exchangers 1 and 2 is shown from Figure 91 to Figure 96.

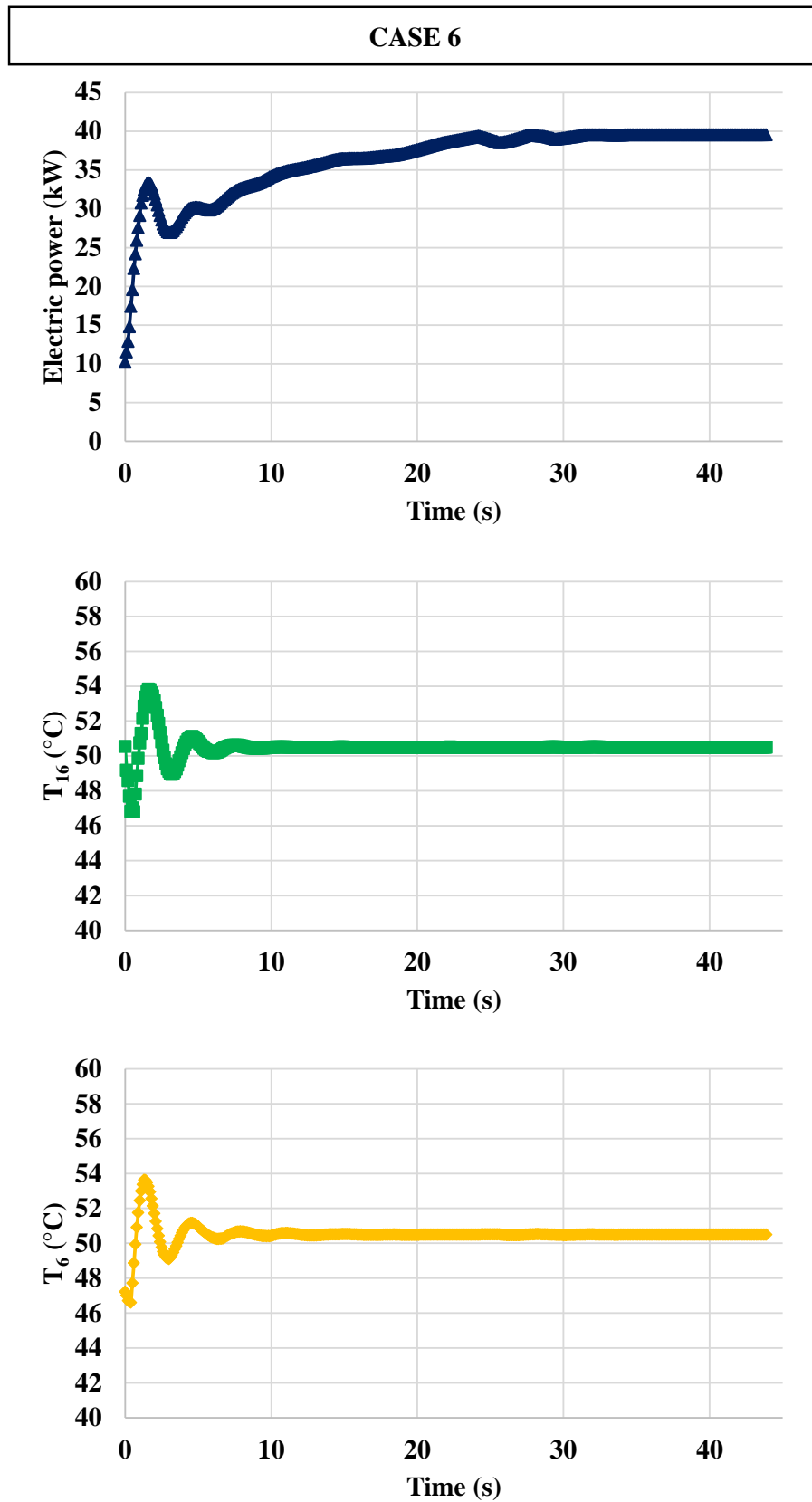


Figure 91 – Case 1: transient response and temperature control results.



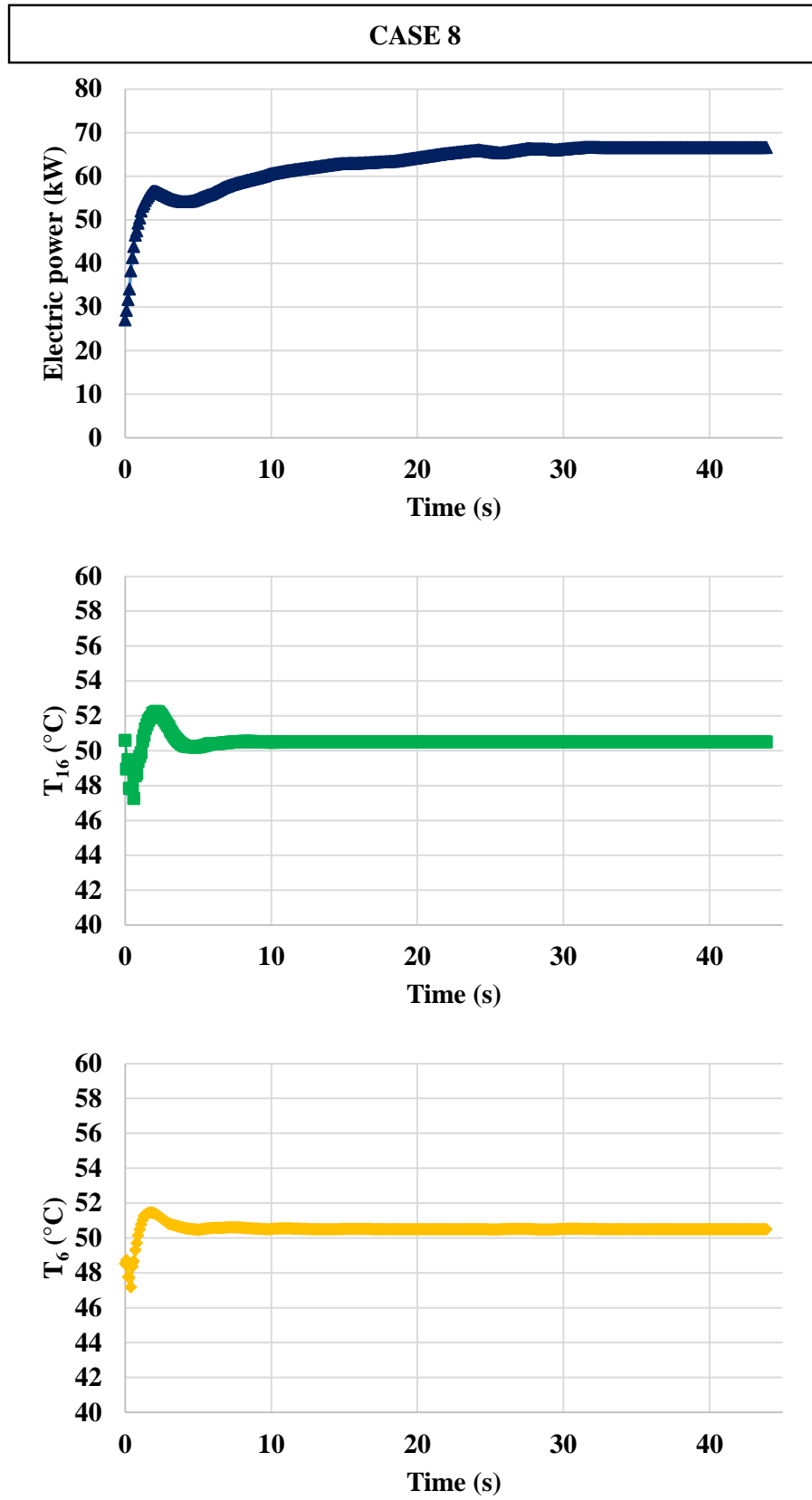
Source: Author.

Figure 92 – Case 6: transient response and temperature control results.



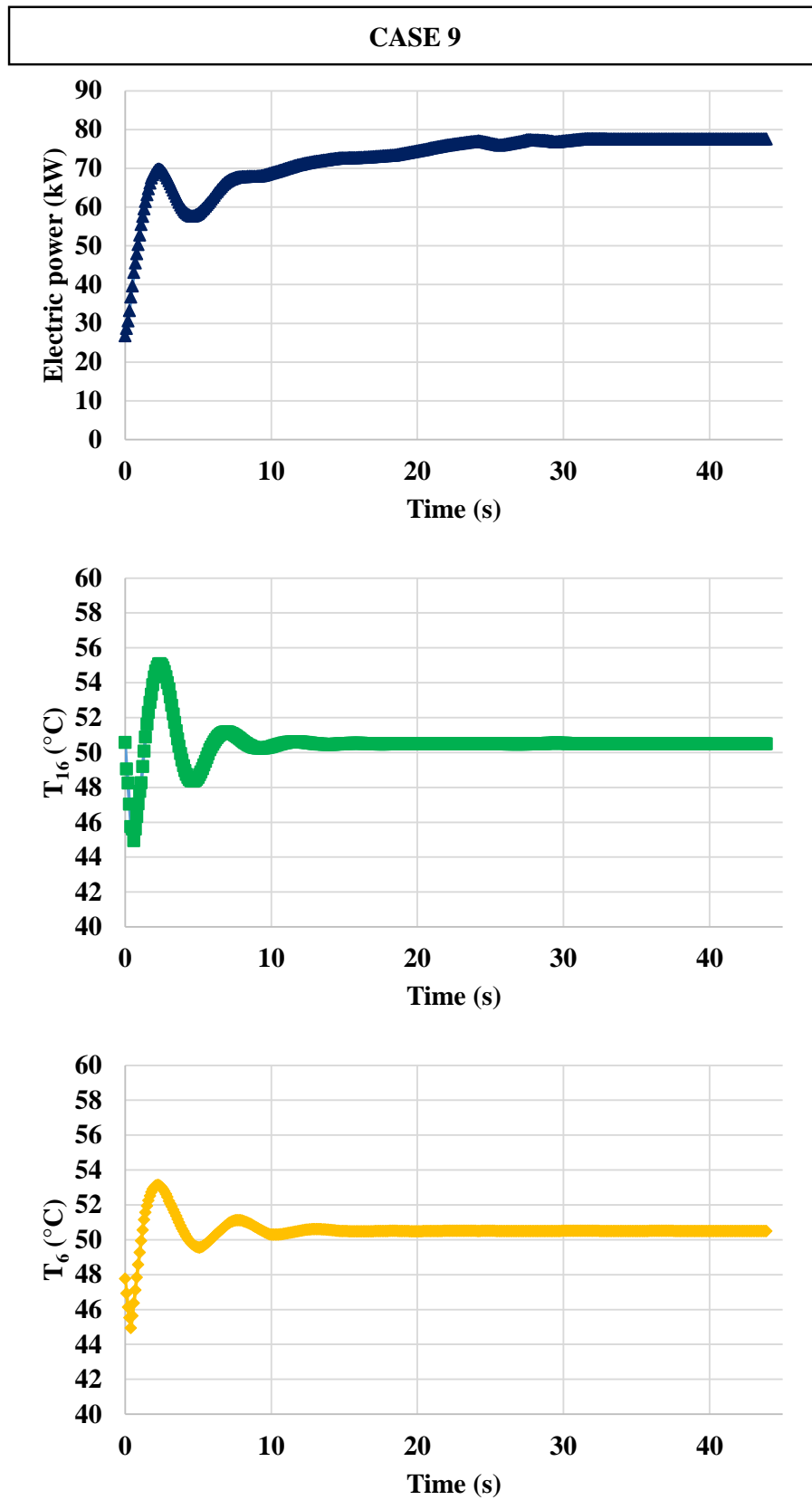
Source: Author.

Figure 93 – Case 8: transient response and temperature control results.



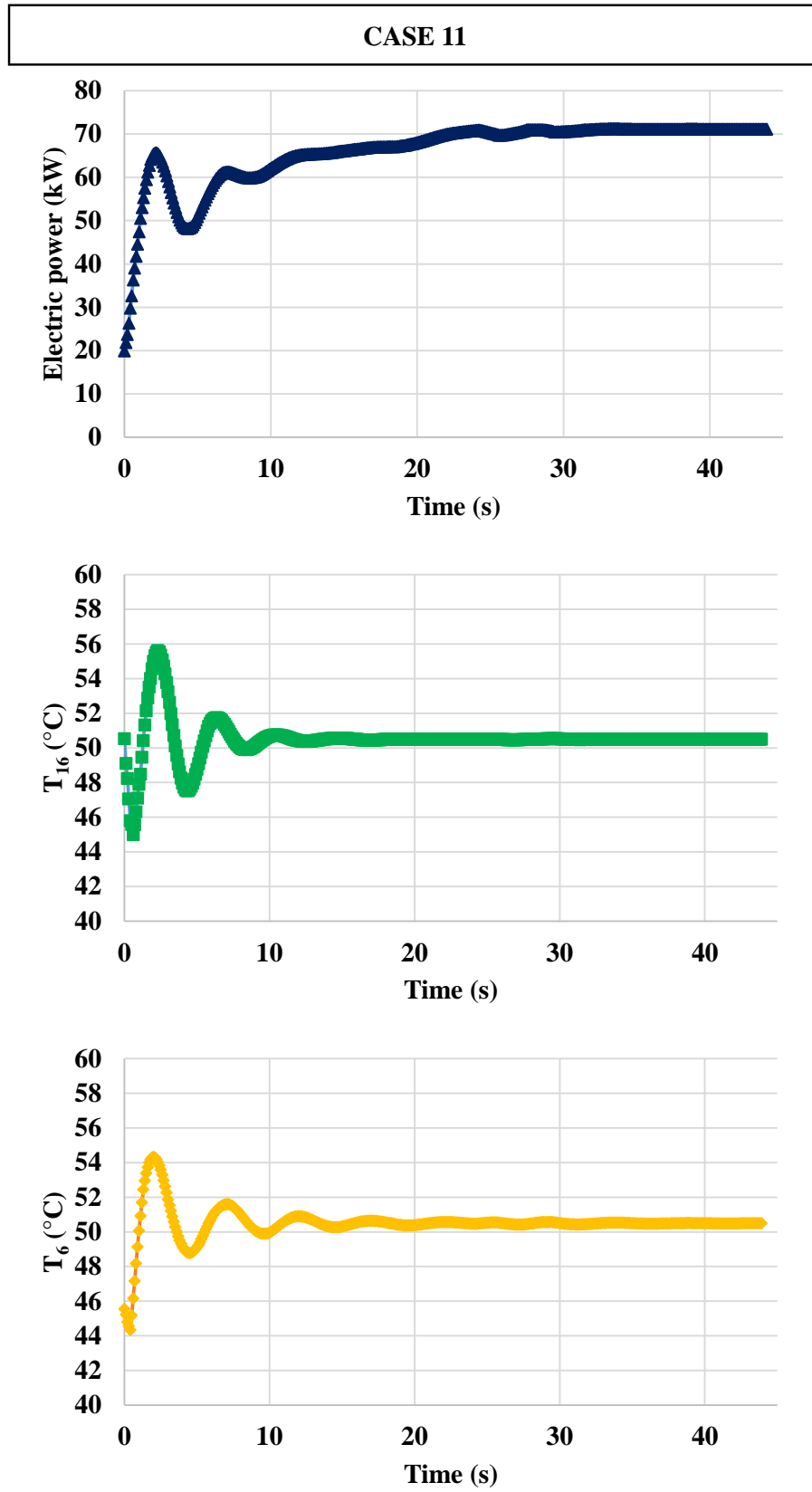
Source: Author.

Figure 94 – Case 9: transient response and temperature control results.



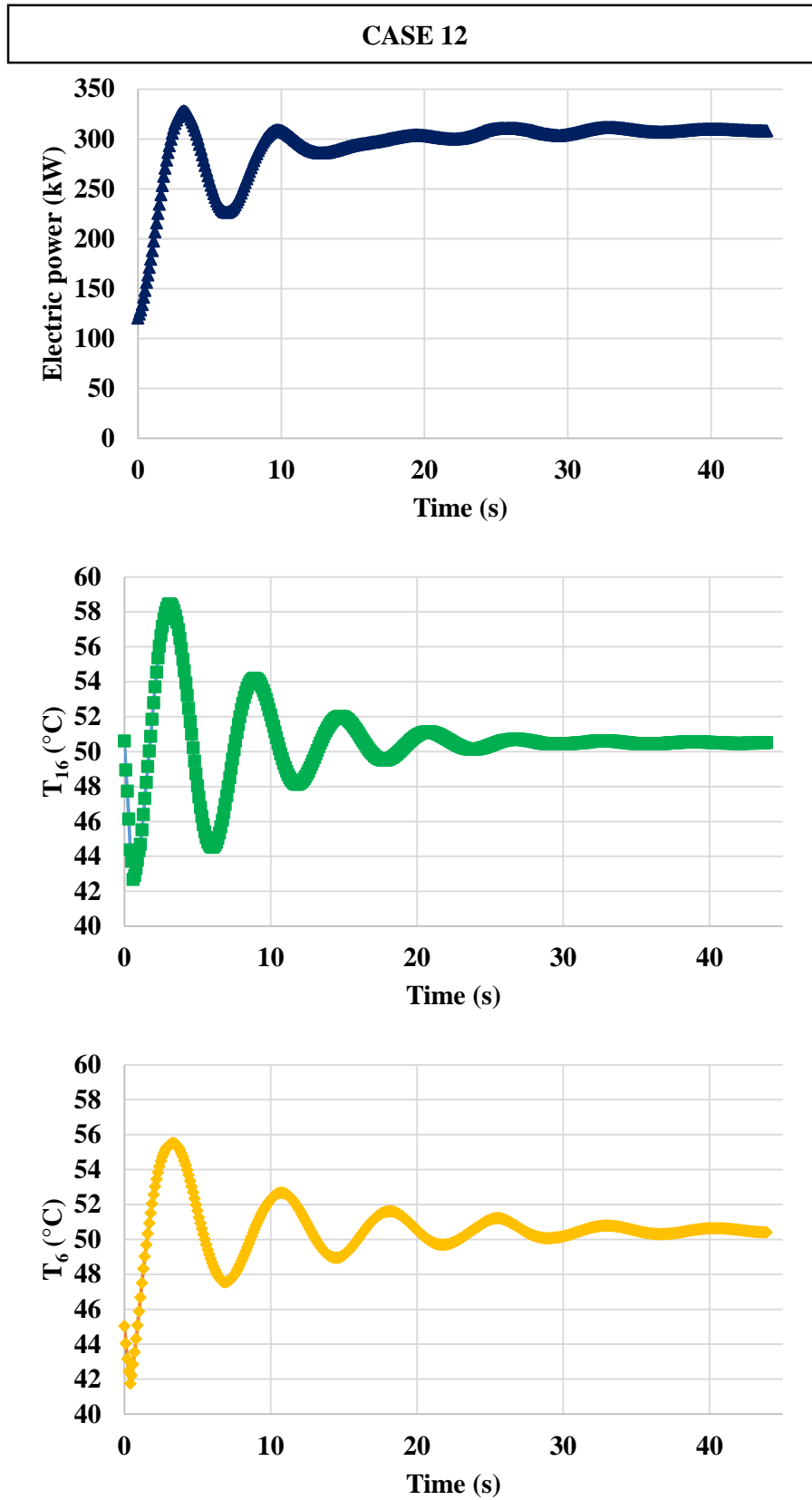
Source: Author.

Figure 95 – Case 11: transient response and temperature control results.



Source: Author.

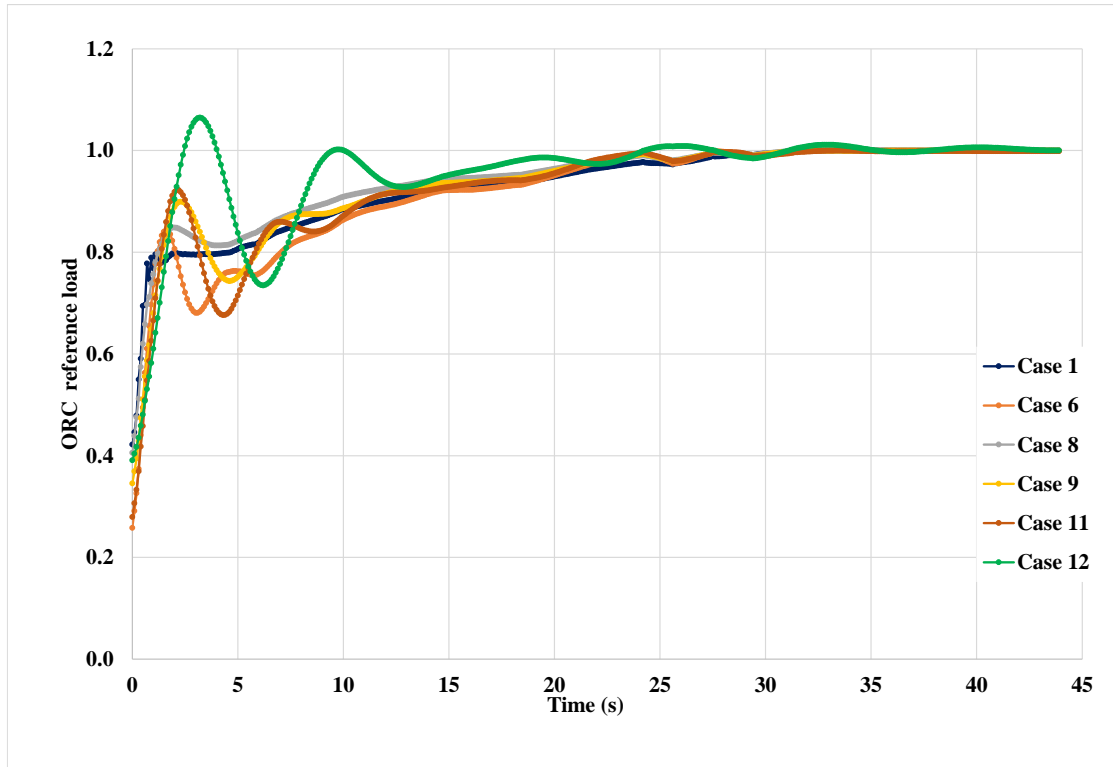
Figure 96 – Case 12: transient response and temperature control results.



Source: Author.

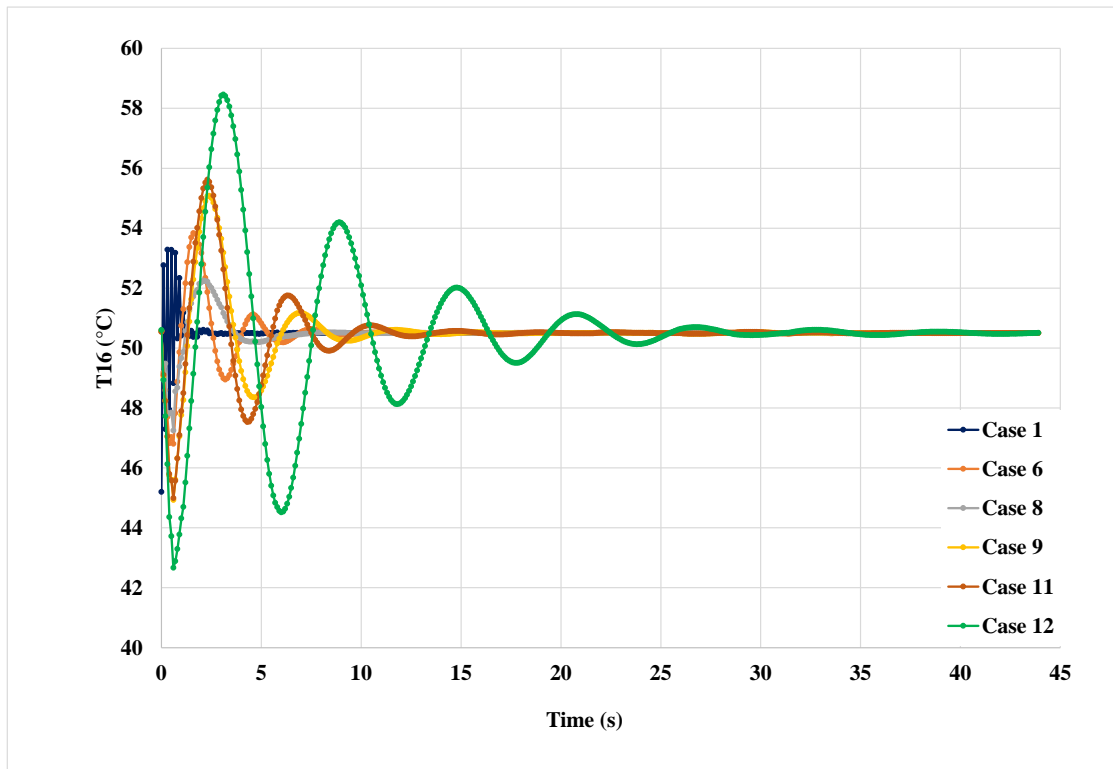
In addition to these charts, Figure 97, Figure 98 and Figure 99 allow a comparative analysis of the responses for the normalized load, T6 and T16. In these graphs, the overshoot and the stabilization period among the cases can be evaluated.

Figure 97 – ORC normalized load as a result of the transient input from the compressor. In this chart, the load is normalized against the maximum output power observed during this specific maneuver.



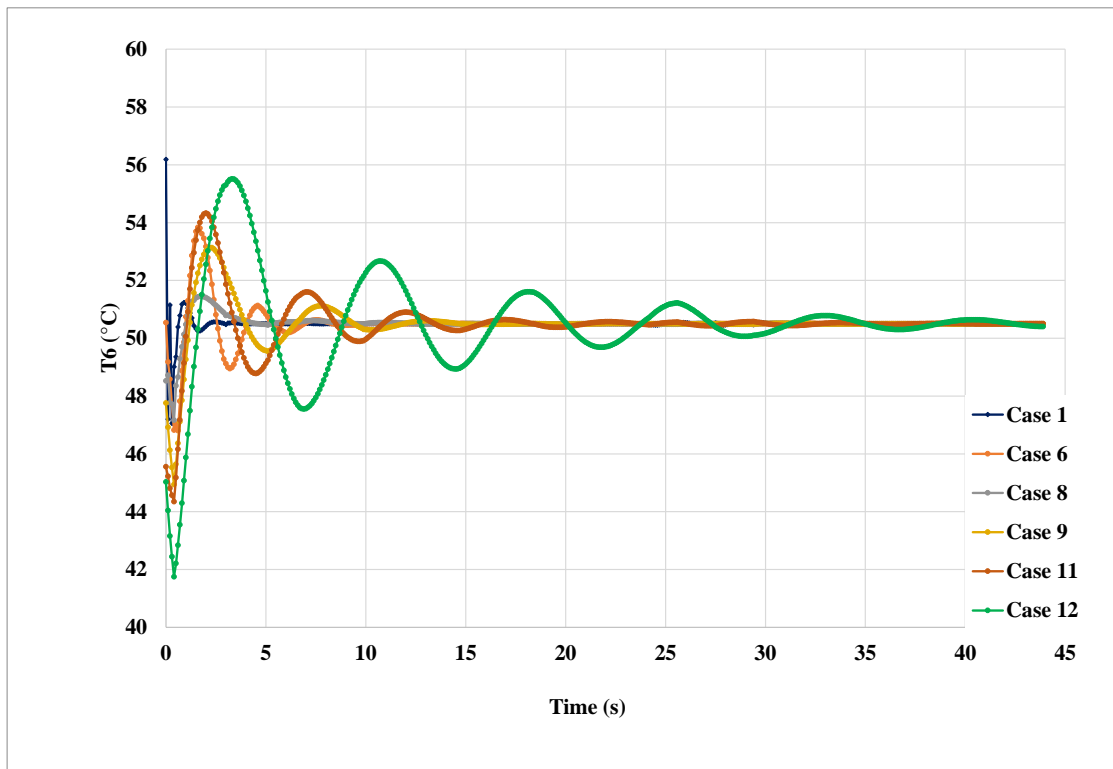
Source: Author.

Figure 98 – Controlled temperature at the discharge of the first stage of the compressor.



Source: Author.

Figure 99 – Controlled temperature at the discharge of the second stage of the compressor.



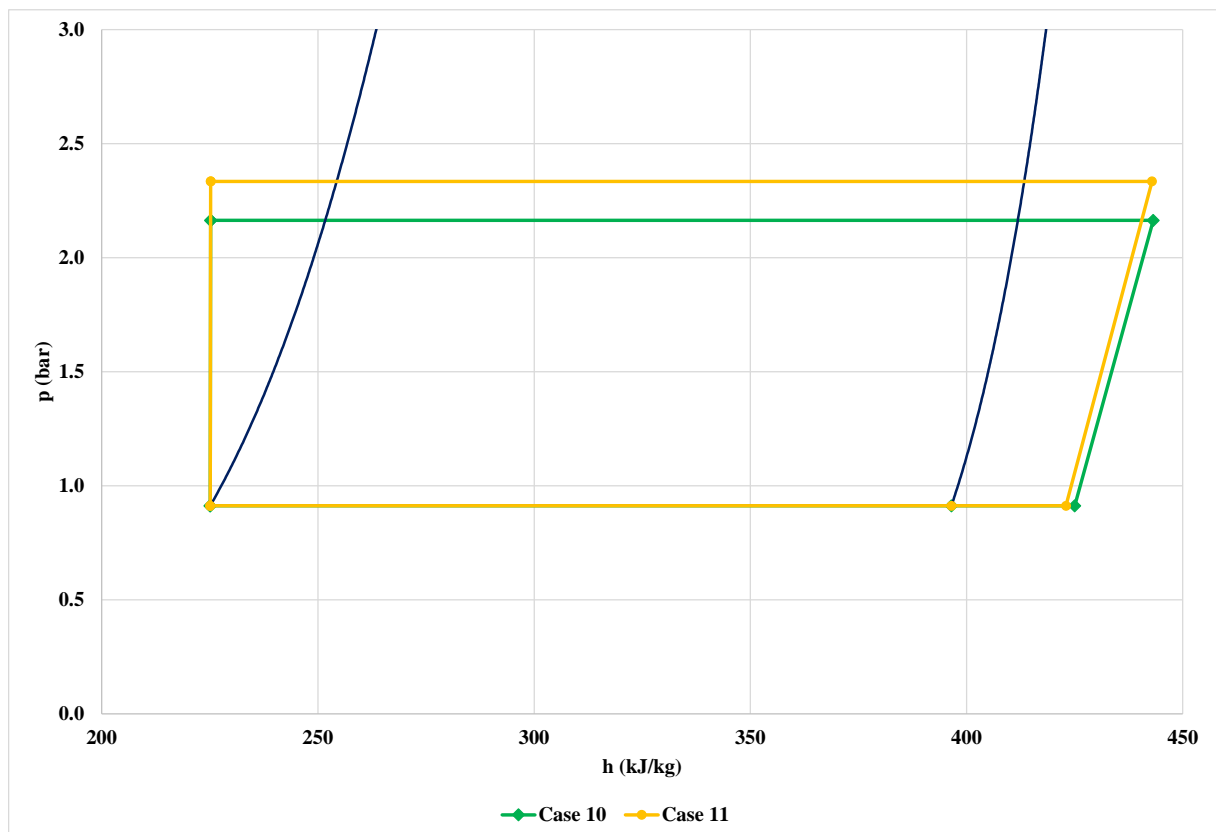
Source: Author.



In a general overview, the number of valid designs decreased from 12, considering the outputs from the smooth transient analysis, to 6. As observed in the gas turbine analysis, designs optimized for full load conditions may not necessarily be applicable to transient conditions, even with dedicated control tuning for each design, as demonstrated in this study. Notably, four of the non-valid designs utilized R141b (lower volumes and output power) as the working fluid.

It is worth to evaluate in more details the impact of the dynamic conditions over the generated designs. Considering design cases 10 (failed) and 11 (successful), it is possible to see in the pressure-enthalpy diagram shown in Figure 100 that the designs are thermodynamically very similar, with the main difference seen in the equipment size to the higher mass flow rate for case 11. However, the steep increase in temperature and mass flow rate on the hot side exceeded the heat exchangers capacity and made the design unfeasible for such severe conditions.

Figure 100 – Pressure enthalpy diagram at design point – cases 10 (failed) and 11 (successful). The saturation lines of the working fluid (R123) are shown in blue.



Source: Author.

The critical period of the transient is particularly notable between 0 and 10 s. Within this interval, cases 6, 9, and 12 exhibit significant overshoot, which is expected due to their

larger volumes and thermal inertia, in addition to the typical behavior of the control tuning given by the Ziegler-Nichols method. Although this underdamped response is not critical, presenting a maximum overshoot of 15,8%, and the systems remain stable, having more data available for PID calibration under intense transient conditions could potentially mitigate this specific behavior.

Specifically on the transient behavior of the ORC systems, the power output in this case is a consequence of the temperature control, and not the main goal of the controller. Even in this case, the electric power provided by the designed ORCs is in the range of 28.4 to 308.4 kW.

The dynamic behavior of the gas temperature after heat exchanger 1 (T16) indicates a stabilization after 15 s for most cases. A remnant oscillatory behavior is observed for cases 9 and 11, with stabilization after 35 s. This behavior indicates the successful control for all cases and an overshoot under the natural features related to the Ziegler-Nichols tuning method.

For the heat exchanger 2, the dynamic input from the second stage is not as steep as the input given in the first stage. This feature enabled faster temperature (T6) stabilization within 20 seconds for all cases except Case 12. While Case 12 stabilizes after 43 seconds, its overshoot is smaller than the first heat exchanger.

It is also worth noting that even with limited data for the PID calibration, it was possible to generate stable controls for such a complex system. In addition, temperature control for the compressor was possible and power generation was relevant considering the typical power demand.

Similarly to what was observed for the gas turbine case, the maximum thermal efficiency found at full load was 18% and fell to 7% at the minimum load. Again, the off-design conditions proved to be necessary to evaluate the feasibility of such designs; however, in this case, since the compressor plays an additional role to the heat recovery, it is important to mention that temperature control is performed with an advantage to the overall installation, which is power generation.

## 7. CONCLUSION AND RECOMMENDATIONS

### 7.1 Conclusion

In this thesis a novel Organic Rankine Cycle (ORC) design methodology is presented for waste heat recovery, employing a fuzzy-PSO algorithm within the HORCAT optimization framework for multi-objective optimization. This algorithm was implemented by combining the particle swarm and fuzzy logic approaches for the design of ORCs for offshore applications.

Since HORCAT is a new development, before using it for the design, the algorithm was validated against benchmark functions and demonstrated its robustness and adaptability to the specific characteristics of the ORC model under optimization. The effect of FLS decision-making becomes evident, showing that this implementation can achieve better results with fewer iterations.

Once the efficacy of HORCAT was established, it was employed to generate ORC designs for two significant cases relevant to thermal efficiency and power generation on oil platforms:

- (i) Gas turbine exhaust heat recovery (Brazilian FPSOs): HORCAT generated 16 designs, which underwent evaluation under part load and dynamic conditions. All solutions proved feasible for both full and partial loads, demonstrating the robustness of free optimization in producing reliable ORC designs. The electrical power range of the solutions at full load for this scenario ranged from 489 kW to 1.97 MW. Under dynamic conditions, the number of feasible solutions decreased from 16 to 12, aligning well with the response of the power output to the exhaust temperature of the gas turbine, under the control of a simple proportional mass flow rate regulator. In this case, feasible ORC designs offered an interesting opportunity to improve power production onboard along with an increase in the overall thermal efficiency. Although ORC designs can achieve high efficiency at full load (peaking 29%), they plummet sharply under realistic half-load scenarios (22% drop in this case). This underscores the importance of considering varied platform loads in feasibility analysis to avoid misleading conclusions based solely on ideal full-load conditions.
- (ii) Compressor Train Temperature Control and Heat Recovery (Norwegian Sea Platform): The innovative approach, facilitated by HORCAT, dynamic conditions validation, and optimized tuning of the PID controller, provided insights for real-world applications. First, as noted in the gas turbine application case, this approach led to designs with a

relevant power output and a suitable volume footprint for a potential real-world implementation. Noteworthy were the response of these designs under transient conditions, with a 50% reduction in the number of valid designs during intense transient simulations. This emphasized that steady-state conditions alone are inadequate to assess the suitability of the equipment. However, despite efficiency dropping from 18% at full load to 7% (Case 12) at minimum, the temperature control enhanced power generation. The application of PID controllers to manage transient conditions revealed nuances in performance, including a minor overshoot observed in larger ORCs. These controllers, while exhibiting effective setpoint tracking, also exemplify the complexity of tuning control systems. In addition, the use of ORCs for temperature control at compressor discharge demonstrated a clear increase in thermal efficiency, aligned with precise fluid temperature control for downstream applications.

It is important to highlight the capability to simulate harsh dynamic conditions demonstrated by the gas turbine and ORC models. Both systems were able to simulate the steady-state, part load, and dynamic conditions, as well as support the calibration of the control models and the ORC design.

In conclusion, this work highlights the importance of considering part-load and transient conditions in equipment design and control. Designs solely based on full-load scenarios may offer unfeasible ORC solutions to oil rigs, especially given the prevalent part and unsteady load conditions in upstream systems. The proposed approach underscores the need to address both near-optimal and part-load scenarios in order to correctly address the operational conditions on platforms.

### *7.2 Recommendations for future works*

The achievements of this work open some direct alternatives for improvements, further research, and other applications. Below, there is a list with the most straightforward recommendations for future works:

- Detailed design of the ORC, improving the geometric parameters, mainly those of the steam turbine and the heat exchangers.
- Application of the dynamic optimization capability of HORCAT, i.e., considering the objective function as  $f(\bar{x}, t)$ . This approach allows the calibration of both the design and the control parameters in a single optimization run.

- Evaluate the application of a regenerator to take advantage of the still superheated fluid downstream the steam turbine.
- Develop ORC designs for a typical Main Compression Unit operating in a Pre-salt FPSO, accounting for high-quality operational data.
- Apply constraints related to the commercial ORC, such as using an intermediary fluid, preheating, regenerator, limited power range, and fluids. The aim would be to conduct a feasibility analysis given the limitations of current technology.
- With the aim of reducing the volume footprint, evaluate the integration of hot streams and the application for combined heat and power.
- Assess integration into cutting-edge technologies such as subsea separation and all-electric FPSOs.
- Define an integrated control system for the compressor temperature control case, including the control of the pump speed and condenser pressure to increase the efficiency of the cycle.

**BIBLIOGRAPHY**

AGÊNCIA NACIONAL DO PETRÓLEO. **Safety Alert 001 -ANP/SSM CO2 Stress Corrosion Cracking (SCC-CO2)**. 2017.

AGÊNCIA NACIONAL DO PETRÓLEO. **Boletim da produção de petróleo e gás natural - Novembro/2023**. 159. ed. 2023.

ALLAHYARZADEH-BIDGOLI, A.; SALVIANO, L. O.; DEZAN, D. J.; OLIVEIRA JUNIOR, S.; YANAGIHARA, J. I. Energy optimization of an FPSO operating in the Brazilian Pre-salt region. **Energy**, 2018. DOI doi.org/10.1016/j.energy.2018.08.203.

ALLAHYARZADEH-BIDGOLI, A.; YANAGIHARA, J. I. Energy efficiency, sustainability, and operating cost optimization of an FPSO with CCUS: An innovation in CO2 compression and injection systems. **Energy**, 2023. DOI doi.org/10.1016/j.energy.2022.126493.

ANDRADE, A. et al. Offshore production units for Pre-salt projects. In: OFFSHORE TECHNOLOGY CONFERENCE. Houston. **Proceedings** [...]. 2015. DOI doi.org/10.4043/25691-MS.

ASTROM, K.; MURRAY, R. **Feedback Systems: An Introduction for Scientists and Engineers**. Princeton University Press, 2020. ISBN: 0691135762.

BADEER, G. H. **GE aeroderivative gas turbines - design and operating features**. General Electric, 2000.

BELL, I. H.; WRONSKI, J.; QUOILIN, S.; LEMORT, V. Pure and Pseudo-pure Fluid Thermophysical Property Evaluation and the Open-Source Thermophysical Property Library CoolProp. **Industrial Engineering Chemistry Research**, 2014. DOI doi.org/10.1021/ie4033999

BINH, T. T.; KORN, U. An evolution strategy for the multi-objective optimization. In: SECOND INTERNATIONAL CONFERENCE ON GENETIC ALGORITHMS. **Proceedings** [...]. 1996.

BOYCE, M. **Gas turbine engineering handbook**. 3rd. ed. Oxford: Gulf professional publishing, 2006. ISBN 978-0750678469

CAMPOREALE, S. M.; FORTUNATO, B.; MASTROVITO, M. A modular code for real time dynamic simulation of gas turbines in Simulink. **Journal of Engineering for Gas Turbines and Power**, 2006. DOI doi.org/10.1115/1.2132383.

CASATI, E. **New concepts for organic Rankine cycle power systems**. 2014. ISBN 978-94-6259-330-5.

CASELLA, F.; MATHIJSEN, T.; COLONNA, P.; VAN BUIJTENEN, J. Dynamic Modeling of Organic Rankine Cycle Power Systems. **Journal of Engineering for Gas Turbines and Power**. 2013. DOI doi:10.1115/1.4023120.

CASELLA, F.; LEVA, A. Modelica open library for power plant simulation: design and experimental validation. In: 3<sup>RD</sup> INTERNATIONAL MODELICA CONFERENCE. **Proceedings [...]**. 2003.

COHEN, H.; ROGERS, G. F. C.; SARAVANAMUTTOO, H. I. H. **Gas turbine theory**. 4<sup>th</sup>. ed. Longman, 1996. ISBN 978-0582236325

COLAÇO, M. J.; DULIKRAVICH, G. A survey of basic deterministic, heuristic and hybrid methods for single objective optimization and response surface generation. In: ORLANDE, H. R. B.; FUDYM, O.; MAILLET, D.; COTTA, R. M. **Thermal measurements and inverse techniques**. Rio de Janeiro. 2009. ISBN 978-0429110719.

COLONNA, P.; PUTTEN, H. Dynamic modeling of steam power cycles: Part I—Modeling paradigm and validation. **Applied Thermal Engineering**. 2007. DOI doi.org/10.1016/j.applthermaleng.2006.06.011.

CORREIA, R. et al. Decarbonization strategies to reduce GHG emissions on the all-electric FPSO. In: OFFSHORE TECHNOLOGY CONFERENCE. Houston. **Proceedings [...]**. 2023. DOI doi.org/10.4043/32402-MS.

CRUZ, M.; ARAUJO, O.; DE MEDEIROS, J. Deep seawater intake for primary cooling in tropical offshore processing of natural gas with high carbon dioxide content: Energy, emissions and economic assessments. **Journal of Natural Gas Science and Engineering**. 2018. DOI doi.org/10.1016/j.jngse.2018.06.011.

CRUZ, M.; ARAUJO, O.; DE MEDEIROS, J. Exergy Comparison of Single-Shaft and Multiple-Paralleled Compressor Schemes in Offshore Processing of CO<sub>2</sub>-Rich Natural Gas. **Journal of Natural Gas Science and Engineering**. 2020. DOI doi.org/10.1016/j.jngse.2020.103390.

EBERHART, J.; KENNEDY, R. Particle swarm optimization. In: ICNN'95 - INTERNATIONAL CONFERENCE ON NEURAL NETWORKS. **Proceedings** [...]. 1995. DOI 10.1109/ICNN.1995.488968.

ELMEGAARD, B. **Simulation of Boiler Dynamics: Development, Evaluation and Application of a General Energy System Simulation Tool**. 1999. ISBN 978-8774752226.

EMPRESA DE PESQUISA ENERGÉTICA. **Brazilian energy balance**. 2023.

ESMIN, A. A.; COELHO, R. A.; MATWIN, S. A review on particle swarm optimization algorithm and its variants to clustering high-dimensional data. **Artificial Intelligence Review**. 2015. DOI doi.org/10.1007/s10462-013-9400-4.

EYNI, L.; STANKO, M.; SCHÜMANN, H.; QURESHI, A. H. Dynamic process modeling of topside systems for evaluating power consumption and possibilities of using wind power. **Energies**. 2022. DOI doi.org/10.3390/en15249482.

FELLET, M.; NYBORG, R. Understanding corrosion of flexible pipes at subsea oil and gas wells. **MRS Bulletin**. 2018. DOI doi.org/10.1557/mrs.2018.214.

FORESTI, A.; ARCHETTI, D. **Waste heat recovery valorization with ORC technology**, 2020. <https://www.tasio-h2020.eu/index.php/public-documents/papers/>.

GALLO, W.; GALLEGO, A.; ACEVEDO, V.; DIAS, R.; ORTIZ, H.; VALENTE, B. Exergy analysis of the compression systems and its prime movers for a FPSO unit. **Journal of Natural Gas Science and Engineering**. 2017. DOI doi.org/10.1016/j.jngse.2017.04.023.

GENERAL ELECTRIC. **GE expands distributed power presence in Brazil's offshore sector**. 2014. Available in: <https://www.ge.com/news/press-releases/ge-expands-distributed-power-presence-brazils-offshore-sector>.

HAGLIND, F.; ELMEGAARD, B. Methodologies for predicting the part-load performance of aero-derivative gas turbines. **Energy**, 2009. DOI doi.org/10.1016/j.energy.2009.06.042.

HEIDARI, A. A.; MIRJALILI, S.; FARIS, H.; ALJARAH, I.; MAFARJA, M.; CHEN, H. Harris hawks optimization: Algorithm and applications. **Future Generation Computer Systems**. 2019. DOI doi.org/10.1016/j.future.2019.02.028.

HESTENES, M.; STIEFEL, E. Methods of conjugate gradients for solving linear systems. **Journal of research of the National Bureau of Standards**. 1952. DOI doi.org/10.6028/jres.049.044.



HOWELL, M.; HARTSHORN, B. Rapid design, integration and test of improved digital fuel control for the LM2500 gas turbine engine. In: ASME INTERNATIONAL GAS TURBINE AND AEROENGINE CONGRESS AND EXPOSITION. Houston. **Proceedings** [...]. 1995.

INTERNATIONAL ENERGY AGENCY. **Net Zero by 2050: a roadmap for the global energy sector**. 2021.

JALURIA, Y. **Design and Optimization of Thermal Systems**. 3rd. ed. CRC Press, 2019. ISBN 978-1498778244.

KAKAÇ, S.; LIU, H.; PRAMUANJAROENKIJ, A. **Heat Exchangers: selection, rating, and thermal design**. 2<sup>nd</sup> Edition. Taylor & Francis, 2002. ISBN: 978-0849309021.

KLAPPROTH, J.; MILLER, M.; PARKER, D. Aerodynamic development and performance of the CF6-6/LM2500 compressor. In: 4<sup>TH</sup> INTERNATIONAL SYMPOSIUM ON AIR BREATHING ENGINES. **Proceedings** [...]. 1979.

KOUKA, N.; FDHILA, R.; HUSSAIN, A.; ALIMI, A. M. Dynamic Multi Objective Particle Swarm optimization with Cooperative Agents. IN: IEEE CONGRESS ON EVOLUTIONARY COMPUTATION (CEC). **Proceedings** [...]. 2020. DOI 10.1109/CEC48606.2020.9285979.

KURZ, R. Gas turbine performance. In: 34<sup>TH</sup> TURBOMACHINERY SYMPOSIUM. **Proceedings** [...]. 2005.

LEE, C. C. Fuzzy logic in control systems: fuzzy logic controller. In: IEEE TRANSACTIONS ON SYSTEMS, MAN, AND CYBERNETICS, **Proceedings** [...]. 1990.

LEMMON, E. W.; JACOBSEN, R. T.; PENONCELLO, S. G.; FRIEND, D. G. Thermodynamic properties of air and mixtures of nitrogen, argon, and oxygen from 60 to 2000 K at pressures to 2000 MPa. **Journal of Physical and Chemical Reference Data**. 2000. DOI doi.org/10.1063/1.1285884.

LEVINE, W. S. **The Control Handbook**. Taylor & Francis, 1999. ISBN 81-7224-785-0.

LIEDMAN, J.; MAANSSON, R. **Dynamic simulation of a centrifugal compressor system**. Chalmers University of Technology, 2013.

LIU, R.; LI, J.; FAN, J.; MU, C.; JIAO, L. A coevolutionary technique based on multi-swarm particle swarm optimization for dynamic multi-objective optimization. **European Journal of Operational Research**. 2017. DOI doi.org/10.1016/j.ejor.2017.03.048

- MACCHI, E.; ASTOLFI, M. **Organic Rankine cycle (ORC) power systems**. Woodhead Publishing, 2017. ISBN 978-0-08-100510-1.
- MAGHAWRY, A.; HODHOD, R.; OMAR, Y.; KHOLIEF, M. An approach for optimizing multi-objective problems using hybrid genetic algorithms. **Soft Computing**. 2021. DOI doi.org/10.1007/s00500-020-05149-3.
- MARCHANDISE, S. **Cahier Technique n°16**. Organic Rankine cycle - Récupération de chaleur fatale pour la production d'électricité dans l'industrie et applications en Energie Renouvelable. Service Public de Wallonie, 2014.
- MENEZES PASSARELLI, F. et al. HISEP: A game changer to boost the oil production of high GOR and high CO<sub>2</sub> content reservoirs. In: OFFSHORE TECHNOLOGY CONFERENCE BRASIL, Rio de Janeiro. **Proceedings** [...]. 2019. DOI doi.org/10.4043/29762-MS.
- MEYER, R.; DECARLO, R.; PEKAREK, S.; DOKTORCIK, C. **Gas turbine engine behavioral modeling**. Purdue University. 2014.
- MORAIS, J. M. D. **Petróleo em águas profundas: uma história tecnológica da Petrobras na exploração e produção offshore**. IPEA/Petrobras, 2013.
- MOSAVI, A. A multicriteria decision making environment for engineering design and production decision-making. **International Journal of Computer Applications**. 2013.
- NATIONAL AERONAUTICS AND SPACE ADMINISTRATION. **NASA Systems Engineering Handbook**. U.S. Government Printing Office, 2017. ISBN 978-1680920901.
- NGUYEN, T.-V. et al. Modelling and analysis of offshore energy systems on North Sea oil and gas platforms. In: 53<sup>rd</sup> SIMS CONFERENCE ON SIMULATION AND MODELLING. **Proceedings** [...]. 2012.
- NGUYEN, T.-V.; PIEROBON, L.; ELMEGAARD, B.; HAGLIND, F.; BREUHAUS, P.; VOLDSUND, M. Exergetic assessment of energy systems on North Sea oil and gas platforms. **Energy**. 2013. DOI doi.org/10.1016/j.energy.2013.03.011.
- NGUYEN, T.-V.; VOLDSUND, M.; BREUHAUS, P.; ELMEGAARD, B. Energy efficiency measures for offshore oil and gas platforms. **Energy**. 2016. DOI 10.1016/j.energy.2016.03.061
- NOCEDAL, J.; WRIGHT, S. **Numerical Optimization**. 2nd ed. Springer, 2006. ISBN 978-0387-30303-1.

NONDY, J.; GOGOI, J. K. Exergoeconomic investigation and multi-objective optimization of different ORC configurations for waste heat recovery: A comparative study. **Energy Conversion and Management**. 2021. DOI doi.org/10.1016/j.enconman.2021.114593.

OFFSHORE MAGAZINE. **Petrobras contracts gas turbines from GE for four FPSOs**. 2013. Available in: <https://www.offshore-mag.com/home/article/16773348/petrobras-contracts-gas-turbines-from-ge-for-four-fpsos>.

OLIVEIRA JUNIOR, S.; VAN HOMBEECK, M. Exergy analysis of petroleum separation processes in offshore platforms. **Energy Conversion and Management**. 1997.

DE OLIVEIRA NETO, R.; SOTOMONTE, C. A. R.; CORONADO, C. J. R. Off-design model of an ORC system for waste heat recovery of an internal combustion engine. **Applied Thermal Engineering**. 2021. DOI doi.org/10.1016/j.applthermaleng.2021.117188.

DE OLIVEIRA, et al. Challenges and Opportunities for Subsea Electrical Power Systems for High Power Subsea Processing and Boosting: HISEP Study Case. In: OFFSHORE TECHNOLOGY CONFERENCE. Houston. Proceedings [...]. 2022. DOI doi.org/10.4043/31929-MS.

ORDYS, A.; PIKE, A. W.; JOHNSON, M. A.; KATEBI, R. M.; GRIMBLE, M. J. **Modelling and Simulation of Power Generation Plants**. Springer, 1994. ISBN: 978-1-4471-2114-5.

PEREIRA, J. L. J.; OLIVER, G. A.; FRANCISCO, M. B.; JR, S. S.; GOMES, G. F. Multi-objective Lichtenberg algorithm: A hybrid physics-based meta-heuristic for solving engineering problems. **Expert systems with applications**. 2022. DOI doi.org/10.1016/j.eswa.2021.115939.

PEREIRA, L. A. G.; YANAGIHARA, J. I. Sensitivity analysis and optimization to reduce dry weight and footprint of FPSO processing plants in a high CO<sub>2</sub> oil field. **Computers and Chemical Engineering**. 2022. DOI doi.org/10.1016/j.compchemeng.2021.107576.

PETROBRAS. **FPSO P-74**. 2023. Available in <https://comunicabaciadesantos.petrobras.com.br/p-74>.

PIEROBON, L.; NGUYEN, T.-V.; LARSEN, U.; HAGLIND, F.; ELMEGAARD, B. Multi-objective optimization of organic Rankine cycles for waste heat recovery: Application in an offshore platform. **Energy**. 2013. DOI doi.org/10.1016/j.energy.2013.05.039.

PIEROBON, L.; CASATI, E.; CASELLA, F.; HAGLIND, F.; COLONNA, P. Design methodology for flexible energy conversion systems accounting for dynamic performance. **Energy**. 2014. DOI 10.1016/j.energy.2014.03.010.

PIEROBON, L.; BENATO, A.; SCOLARI, E.; HAGLIND, F.; STOPPATO, A. Waste heat recovery technologies for offshore platforms. **Applied Energy**. 2014. DOI 10.1016/j.apenergy.2014.08.109

PILI, R.; JØRGENSEN, S. B.; HAGLIND, F. Multi-objective optimization of organic Rankine cycle systems considering their dynamic performance. **Energy**. 2022. DOI doi.org/10.1016/j.energy.2022.123345.

PING, X.; YANG, F.; ZHANG, H.; XING, C.; ZHANG, W.; WANG, Y.; YAO, B. Dynamic response assessment and multi-objective optimization of organic Rankine cycle (ORC) under vehicle driving cycle conditions. **Energy**. 2023. DOI doi.org/10.1016/j.energy.2022.125551.

PUTTEN, H.; COLONNA, P. Dynamic modeling of steam power cycles: Part II – Simulation of a small simple Rankine cycle system. **Applied Thermal Engineering**, 2007. DOI doi.org/10.1016/j.applthermaleng.2007.01.035.

QUOILIN, S. **Sustainable energy conversion through the use of organic Rankine cycles for waste heat recovery and solar applications**. Université de Liège. 2011.

QUOILIN, S.; Aumann, R.; Grill, A.; Schuster, A.; Lemort, V.; Hartmut, S. Dynamic modeling and optimal control strategy of waste heat recovery Organic Rankine Cycles. **Applied Energy**. 2011. DOI doi.org/10.1016/j.apenergy.2011.01.015.

REIS, M.; GUILLEN, J.; GALLO, W. Off-design performance analysis and optimization of the power production by an organic Rankine cycle coupled with a gas turbine in an offshore oil platform. **Energy Conversion and Management**. 2019. DOI doi.org/10.1016/j.enconman.2019.06.051.

ROHDE, D.; WALNUM, H.; ANDRESEN, T.; NEKSÅ, P. Heat recovery from export gas compression: Analyzing power cycles with detailed heat exchanger models. **Applied Thermal Engineering**. 2013. DOI 10.1016/j.applthermaleng.2013.06.027.

SABOIA, R. **The offshore O&G sector in Brazil**. Agência Nacional do Petróleo. 2023.

SANDANA, D. **Stress corrosion cracking of pipeline steels in contaminated aqueous CO<sub>2</sub> environments**. Newcastle University. 2016.

SBM OFFSHORE. **Floating production storage and offloading**. 2016.

SHI, Y.; ZHANG, Z.; CHEN, X.; XIE, L.; LIU, X.;SU, H. Data-Driven model identification and efficient MPC via quasi-linear parameter varying representation for ORC waste heat recovery system. **Energy**. 2023. DOI doi.org/10.1016/j.energy.2023.126959.

SIEMENS ENERGY. **SGT-A35 (Industrial RB211) aeroderivative gas turbine**. 2020. Available in: <https://www.siemens-energy.com/global/en/offerings/power-generation/gas-turbines/sgt-a30-a35-rb.html>.

SLEITI, A. K.; KAPAT, J. S.; VESELY, L. Digital twin in energy industry: Proposed robust digital twin for power plant and other complex capital-intensive large engineering systems. **Energy Reports**. 2022. DOI doi.org/10.1016/j.egy.2022.02.305.

SPECTOR, R. B.; CIMINO, L. S. Offshore Experience of the LM2500 Gas Turbine. In: ASME 1990 INTERNATIONAL GAS TURBINE AND AEROENGINE CONGRESS AND EXPOSITION. **Proceedings** [...]. 1990. DOI <https://doi.org/10.1115/90-GT-288>.

SVALHEIM, S.; KING, D. Life of Field Energy Performance. In: SPE OFFSHORE EUROPE OIL AND GAS EXHIBITION AND CONFERENCE. **Proceedings** [...]. 2003.

TOUMA, S. et al. Innovative Gas Treatment Solutions for Offshore Systems. In: OFFSHORE TECHNOLOGY CONFERENCE BRASIL. Rio de Janeiro. **Proceedings** [...]. 2019.

VELOSO, T.; SOTOMONTE, C.; CORONADO, C. J.; NASCIMENTO, M. Multi-objective optimization and exergetic analysis of a low-grade waste heat recovery ORC application on a Brazilian FPSO. **Energy Conversion and Management**. 2018. DOI 10.1016/j.enconman.2018.08.042.

WALSH, P.; FLETCHER, P. **Gas turbine performance**. 2nd. ed. Blackwell Science, 2004.

WANG, L.; BU, X.; LI, H. Multi-objective optimization and off-design evaluation of organic Rankine cycle (ORC) for low-grade waste heat recovery. **Energy**. 2020. DOI doi.org/10.1016/j.energy.2020.117809.

WANG, S.; LI, Q.; LIU, L.; HUO, E.; ZHANG, C. Selection principle of working fluid for organic Rankine cycle based on environmental benefits and economic performance. **Applied Thermal Engineering**. 2020. DOI 10.1016/j.applthermaleng.2020.115598.

YU, R.; CHEN, Y., HAN, B., & ZHAO, H. A Hierarchical control design framework for fuzzy mechanical systems with high-order uncertainty bound. **IEEE Transactions on Fuzzy Systems**. 2020. DOI 10.1109/TFUZZ.2020.2965913

ZADEH, L. A. Is there a need for fuzzy logic? **Information Sciences**. 2008. DOI 10.1016/j.ins.2008.02.012.

ZITZLER, E.; DEB, K.; THIELE, L. Comparison of multi-objective evolutionary algorithms: Empirical results. **Evolutionary computation**. 2000. DOI 10.1162/106365600568202.